High-viscosity biphasic flow characterization in a pipeline: Application to flow pattern classification and leak detection

Jose Fernando Noguera Polania

Supervisors: Ph.D. Marco Sanjuán
Ph.D. Lizeth Torres

Department of Mechanical Engineering
Universidad del Norte

This dissertation is submitted for the degree of
Doctor en Ingeniería Mecánica

Universidad del Norte June 2021

"Somos los pensamientos mas ilustres de un Ser Superior dentro de un gran experimento llamado ... vida"

Jose Fernando Noguera Polania

To my family; Altagracia Polania, Euclides Noguera, Maria Victoria Noguera, Luz Angela Noguera, Juan Carlos Noguera y Bárbara Alvarez.

Declaration

I hereby declare that, except where specific reference is made to others work, the contents of this dissertation are original and have not been submitted in whole or in part for consideration for any other degree or qualification in this, or any other university. This dissertation is my own work and contains nothing which is the outcome of work done in collaboration with others, except as specified in the text and Acknowledgements.

Jose Fernando Noguera Polania
June 2021

Acknowledgements

I would like to thank GOD and my family: my parents, my brother, and sisters for supporting me emotionally throughout writing this thesis and in my life in general.

I would like to express my sincere gratitude to my advisors Dr. Marco Sanjúan and Dr. Lizeth Torres for the continuous support of my Ph.D study and related research, for their patience, motivation, and immense knowledge. Their guidance helped me in all the time of research and writing of this thesis. I could not have imagined having a better advisors and mentors for my Ph.D study.

Besides my advisors, I would like to thank the rest of my thesis committee: Dr. Enrique Guzman, Dr. Alirio Acuña, Dra. Rita Peña-Baena and Dr. Lesme Corredor, for their insightful comments and encouragement.

My sincere thanks also goes to Dr. Cristina Verde, Jonathan Hernandez and Fernando Aragon, for their collaboration in this research from the Instituto de Ingeniería of the Universidad Autónoma de México.

I thank my doctoral studies friends; David Acosta, Adriana Rincón and Blanca Foliaco, Also I thank the classmates and labmates for the stimulating discussions and for all the fun we have had in the last four years.

Abstract

Pipeline systems play an essential role in the oil industry. These systems connect ports, oil fields, refineries, and consumer markets[104]. Pipelines covering long distances require pumping stations, where products are propelled to the next pumping station, refinery, or deposit terminal, thus traveling through most of the country. The product considered in this research work is crude oil. It is usually transported with a combination of crude oil with viscosity reducers (DRA, drag reducer agent) and oil with gas in onshore/offshore pipelines. This mode of transport is efficient for large quantities and large product shipment distances. Problems may arrive when a leak occurs. In major incidents, large scale damage to humans and the environment is possible. Then, this research addresses the problem of how to detect the leak earlier to reduce the impact in the surrounding areas and economic losses, considering five research topics taking into account that the products inside the pipeline are water-glycerol and gas-glycerol mixtures (simulating oil-DRA and oil-gas in the laboratory test apparatus).

The first research topic presents a mathematical model to describe the flow of a mixture of water and glycerol in pressurized horizontal pipelines, which emulates the mixture of heavy oil and a viscosity reducer. The model is based on the mass and momentum conservation principles and empirical correlations for the mixture's density and viscosity. The set of partial differential equations is solved using finite differences. These equations were implemented in a computer platform to be able to simulate a system. This simulation platform is a tool to simulate leak cases for different fractions of water and glycerol to evaluate algorithms for leak detection and localization before their implementation in a laboratory setting.

In the literature, mathematical models for detecting leaks in pipes are observed. Still, considering a single working fluid [101] [155] [75] [158], water [82], a viscous fluid [96], gas [96], [120], or even the transport of product in a pipeline in batches [22], [113], work has also been carried out to determine the volume and length of contamination between products in the case of batch shipping in a pipeline [1], [96]. However a mixture of a highly viscous fluid with a low viscosity fluid (which represents the multiphase behavior of crude oil in pipelines

[60]) has not been taken into account when developing the mathematical model focused on leak detection.

Today, several leak detection and localization methods are based on the calculation of the pressure gradient [79]. The second research topic presents an experimental methodology to calculate the leak in a pipe with a curved section making a pressure gradient adjustment, simulating leak cases for different fractions of water and glycerol, in order to improve the model prediction (from the first research topic) for the case when there is a pipeline with a U-shaped segment.

The second research topic also includes additional work on air-glycerol mixtures. The pressure gradient for the air-glycerol mixture along the laboratory piping system was analyzed, taking into account different combinations of liquid and air mass flow rates, which were experimentally tested.

The third research topic considers only air-glycerol mixture (with different mass flow rate combinations) because the gas-oil behavior can damage the pipe integrity due to vibrations, chronic fatigue, corrosion processes, and enhanced by high intermittent pressures, severe slugging. In this way, it is important to develop slug prediction models and characterization of dynamic behavior from gas-oil mixtures to achieve better leak detection systems and more reliable pumping systems. Then, pressure signals from a high-viscosity, air-glycerol mixture were characterized using statistical analysis and a slug prediction model was developed.

The fifth research topic shows a brief account of leak detection systems (with a taxonomy organization which gives us a better comprehension of how works the different methods to detect and locate pipeline leaks) and develops two leak diagnosis algorithms; one based on the pressure gradient method (using the pressure levels and gradient angles measurements of the sensors installed in the pipeline and trigonometric calculus to find the distance of the leak from a determined sensor) and one based on the Kalman filter method (this algorithm uses only four steps to estimate the real position of the leak with less than 0.1% of relative error), concluding in this way all the research work.

Table of contents

List of figures

List of tables

Chapter 1

Introduction

This chapter presents an introduction to allow for understanding the research background and motivation. First, Colombia's crude oil transportation context is addressed, showing the oil infrastructure, comparing the world energy consumption by energy source and costs associated with different means of oil transport. It additional illustrates Colombian operative oil transport infrastructure and spills (section 1.1). Second, the statement of the problem is presented. This includes negative impacts like damage to physical integrity and loss of human life, environmental damage, and economic losses (showing some PHMSA statistics). These negative impacts can be reduced by using early leak detection and location methods (section 1.2). Third, the state of the art in section 1.3 covers some works on early detection and location of leaks methods (also showing a PHMSA data on pipeline leak detection form), high viscosity liquid-liquid flow, and high viscosity liquid-gas flow. Fourth, the research groups or institutions that support this doctoral thesis work are presented in section 1.4. Fifth, the research gap presented in section 1.5 emphasizes the case for liquid-liquid flow analysis, the case for the gas-liquid flow analysis, and finally addresses a pipeline maintenance mechanism developed by Ecopetrol S.A. in Colombia. Also, it shows the research question regarding leak detection and location systems. Next, the research work objectives are presented in section 1.6 and the research methodology in section 1.7 through seven phases.

1.1 Context

Ecopetrol S.A. is the main and largest petroleum company in Colombia and was ranked as the 313^{th} from 2000 largest public companies in the world by Forbes 2020 Global 2000 [51],

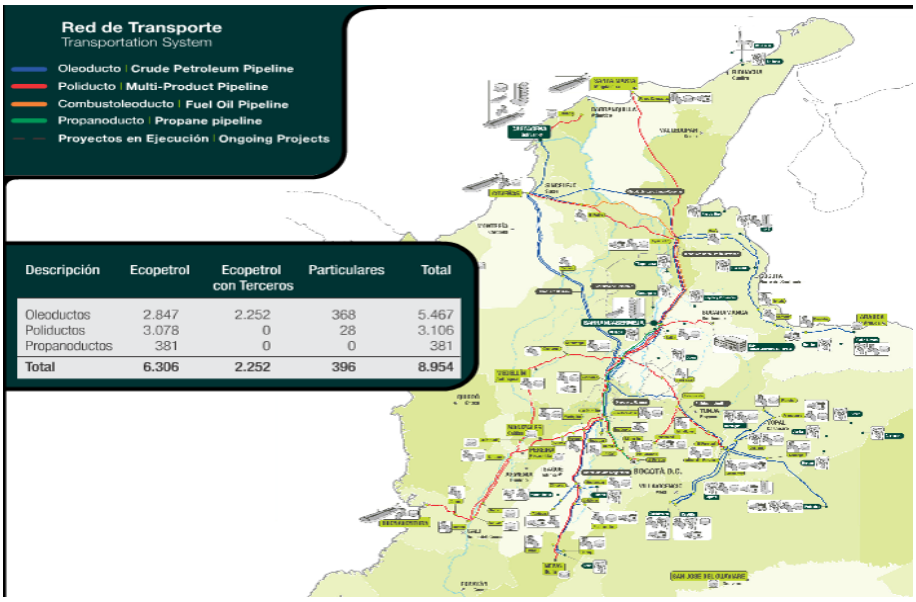

Fig. 1.1 Ecopetrol infraestructure

and it was ranked in 2012 as one of the four principal petroleum companies in America [119]. Ecopetrol's oil infrastructure, as shown on its website [40] (Figure 1.1), has 5,476 km of pipeline throughout the Colombian territory. However, problems may arrive when incidents occur. On December 23, 2011, an explosion of a section of the Puerto Salgar-Cartago pipeline of Ecopetrol S.A. left 32 dead and more than 80 injured in Dosquebradas (Risaralda). The causes were attributed to lack of maintenance, which caused a leak that ended in tragedy [44]. In the same way, there are more examples in the country and the world. The negative impacts of these incidents are damage to physical integrity, loss of human life, environmental damage, and economic losses (explained in section 1.2). Therefore, pipeline integrity is critical, and the oil companies are aware of it.

However, the negative impacts will persist because oil is one of the main energy sources, as presented [28] in Figure 1.2 and pipeline infrastructure will remain a massive active. Even in 2040, the projection of energy consumption is still dominated by hydrocarbons. This further reinforces the need to provide a safe and reliable means of transportation. However, the oil industry uses different means of transport (maritime and land) for shipping hydrocarbons such as; tankers, barges, rail cars, and pipelines [74]. It is worth mentioning that pipes are the preferred means of transporting these products because they have a low cost of transport (Figure 1.3), low energy consumption, do not produce road congestion, do not produce noise, do not produce atmospheric pollution, they are safe for humans. Pipeline transmission has a high

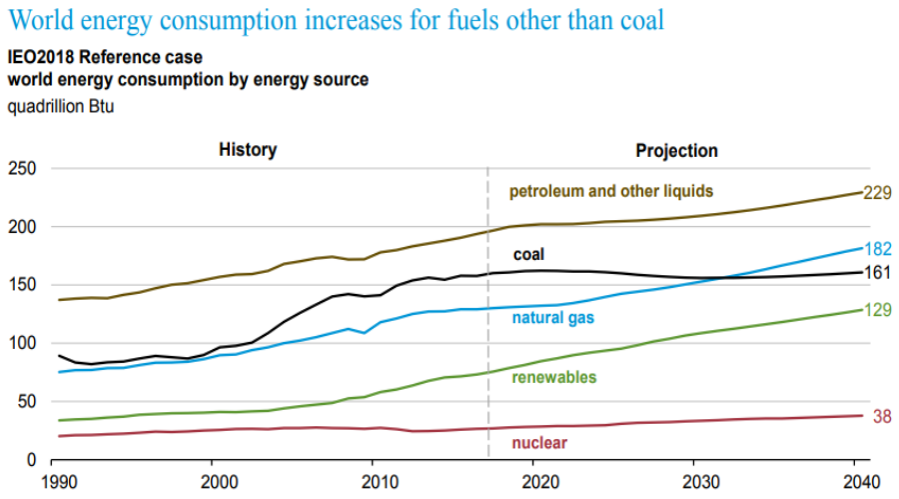

Fig. 1.2 Energy consumption

degree of reliability and automation because its operation is continuous and not affected by the weather [94].

1.1.1 Oil transport

Crude oil is formed from organic matter; phytoplankton, zooplankton, plant, and animal remains deposited millions of years on layers of clay, mud, and sand inside the so-called "mother rocks" [147], [41].

In Colombia, crude oil is classified as light, intermediate and heavy depending on API (American Petroleum Institute) grades. Light crudes have more than 26 API degrees; intermediate crudes have between 20 and 26 API degrees, and heavy crudes with less than 20 degrees API. Crude oil is also said to be "sweet" if it has less than 0.5 % sulfur and is said to be "sour" if it has more than 1 % sulfur. Therefore, sweet and light crudes generate more products called “whites” (for example, gasoline) and cause less pollution since less refining is required [41]. Oil extraction also generates sediments, water, and natural gas, so the construction of production, separation, and storage facilities is necessary. When the oil is separated from the sediments, water, and gas, it is ready to be sent to the storage tanks, and pipelines [41]. For heavy crude oil transmission, it is necessary to use a thinner to improve its viscosity condition and facilitate its pumping in the pipeline [26], Therefore, a flow of two different liquid phases will occur. According to the Colombian Ministry of Energy and Mine, resolution 72145 of 2014, crude oil suitable for transportation is defined as:

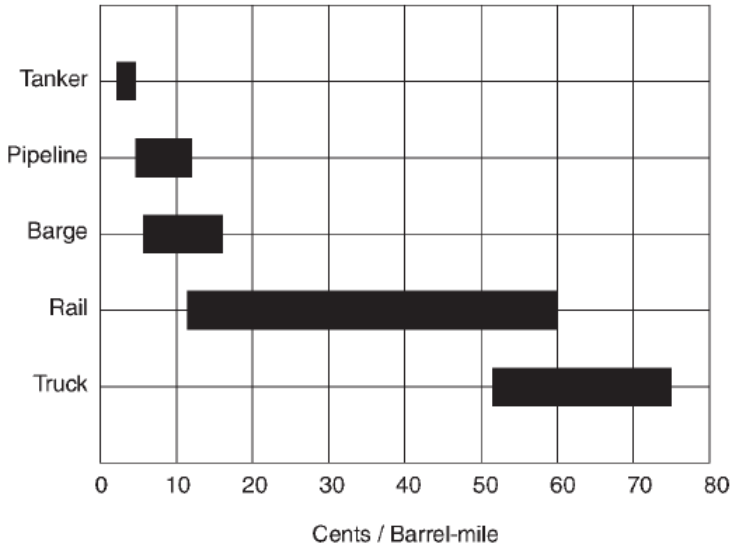

Fig. 1.3 Costs associated with different means of transport, taken from [94]

"It is understood that the hydrocarbon being transported must be inspected crude[1] in specifications for refining and free of external contaminants or chemical additives. However, the carrier may accept thinners' presence according to the characteristics of the mixture being transported. The transporter will not be obliged to provide the transport service when the crude oil presents characteristics that, under normal operating conditions, can significantly affect the transport equipment or the efficiency of the operation, induce unsafe conditions or decrease the quality of other crude oils that are transported by pipeline. The transporter will have the right to refuse the transport of crude oil when it does not satisfy the minimum quality conditions in:

1. Salt boundary conditions, pour point, water, and sediments that may cause damage to transport equipment or affect its operation.

2. Boundary conditions of density, viscosity, and water content that cause inefficiency in operation.

3. Boundary conditions of temperature and vapor pressure that jeopardize the operation of transportation through the pipeline.

4. Boundary conditions of content of metallic contaminants or sulfur that decrease the mixture's commercial value. "

[1]The inspected crude oil is that which has been separated from water, gas, and sediment, has been treated, rested, measured in inspection facilities and approved by Ministry of Mines and Energy.

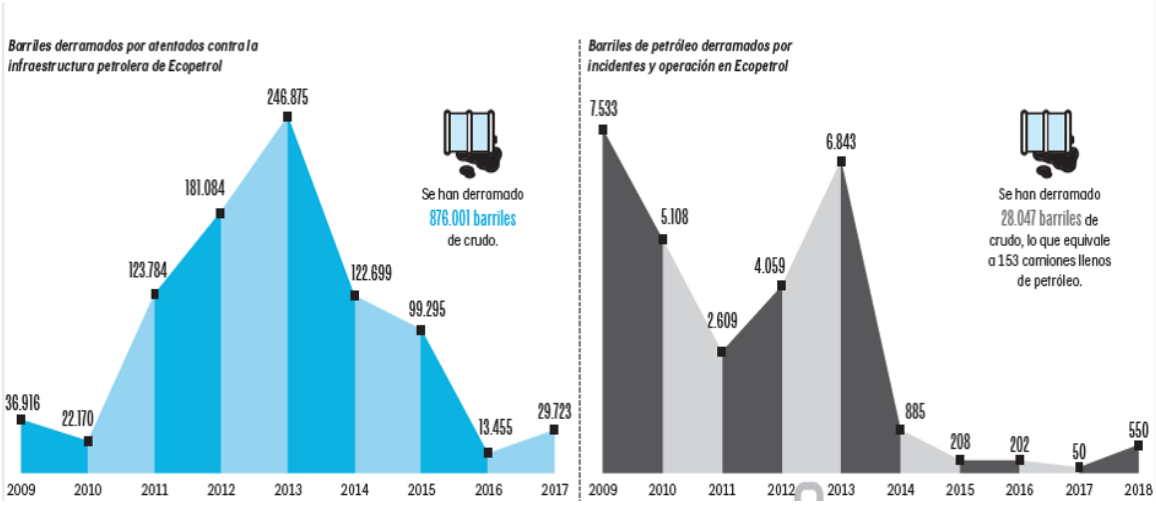

Fig. 1.4 Colombia's oil spills

Therefore, the previous resolution allows the transport of crude oil with a thinner. In the case of oil fields or product extraction, there will also be gas in the pipeline, which indicates that there will be two phases in the products to be transported through pipes. Either liquid-liquid flow or gas-liquid flow. But even with all the normative, problems may arrive when a leak occurs.

1.1.2 Oil spills

In Colombia, 3.7 million barrels of crude oil (equivalent to 20,182 trucks) have been spilled in the last 38 years due to attacks (2,745 attacks), and incidents in Ecopetrol's operation. On March 2nd, 2018, 550 barrels of oil were spilled in the Lizama, and Caño Muerto streams, approximately 3 trucks, 6,001 trees were contaminated, 2,442 animals died, and most of the fish [69]. The streams of crude oil and mud affected the township of La Fortuna in Barrancabermeja, since the bad smells and headache it caused to its inhabitants made it uninhabitable. The National Agency for Environmental Licenses said that the ecosystem will take more than 20 years to recovered according to expert estimates [14]. Figure 1.4 shows that between 2009 and 2017, the number of spills due to attacks was greater. However, the amount of 28,047 barrels of oil (153 trucks full of oil) spilled due to incidents and operation is considerably large. The environmental damage, whatever the cause, will always be an invaluable loss.

1.2 Impact of leaks on pipes

This section addresses the negative impacts of early detection and location of leaks. The Table 1.1 summarizes the possible causes of pipeline oil spills and the negative effects associated with this problem. Pipeline integrity plays an important role in the spill causes related to aging of the pipe, installation failures (Here can be associated the pumping systems), landslides, and even the clandestine shots and terrorist attacks. All they have a very negative impact, and this section focuses on it. Early detection and location of leaks are briefly addressed in the section 1.3 and a more detailed review of leak detection systems is developed in the chapter 5.

Table 1.1 Pipeline issues

Possible causes of spills	Negative impacts	Problem
Aging of the pipes	Damage to physical integrity	
Installation failures	and loss of human life	
Landslide	Environmental damage	Early detection and location of leaks
Clandestine shots		
Terrorist attacks	Economic losses	

1.2.1 Damage to physical integrity and loss of human life

From the point of view of the human health, it is necessary to observe the components of oil that directly affect human health to understand its seriousness. Four hydrocarbon molecules are established called hydrocarbon series [34]. Each molecule in the series can vary from one crude oil to another, thus modifying the physical properties of each crude oil. For this reason the extracted oil differs from one place to another. Table 1.2 below, showing the common percentage by weight of each hydrocarbon molecule type.

Table 1.2 Hydrocarbon molecules types

Hydrocarbon	Percentage by Weight	Percentage Rank
Paraffin	30	15 to 60
Cycloalkanes	49	30 to 60
Aromatic	15	3 to 30
Asphaltenes	6	The rest

As mentioned previously, the various crudes have different chemical compounds; however, the main part may have polycyclic aromatic hydrocarbons (PAH), which are much more toxic than the other components. Benzene is formed from these components, and it is carcinogenic;

there [117]. According to the Agency for Toxic Substances and Disease Registry (ATSDR) [142] there are more than 100 different classes of PAH's. Table 1.3 shows that these substances can be found in crude oil, coal, tar or pitch, creosote, plastics, inks, pesticides. They can also form with incomplete incineration of coal, oil, gas, wood, garbage, and organic substances such as tobacco and charcoal-grilled meat. These substances exist as colorless, white, or pale yellow-green solids and have a slight pleasant odor. They can also be found in the air attached to dust particles or as solids in soils or sediments and also in water and cause tumors, cancer, reproductive problems, congenital disabilities, decreased bodyweight, harmful effects on the skin, body fluids, and immune system when breathed, eaten or in contact with the skin. For this reason, they are on the list of national priorities (NLP) of the Environmental Protection Agency (EPA) and the U.S. Department of Health and Human Services. This is way petroleum products transported in pipelines are very harmful to humans.

Table 1.3 Damage to physical integrity

Cause	It can be found in
Cancer	crude oil, coal, tar, pitch, creosote, plastics, inks, pesticides
reproductive problems	incomplete incineration of coal, oil, gas, wood, garbage.
congenital disabilities	Tobacco and charcoal-grilled meat
decreased body weight	Colorless, white, or pale yellow-green solids with a mild, pleasant odor
harmful effects on the skin, body fluids and the immune system	dust particles or as solids in soils or sediments and also in water

1.2.2 Environmental damage

Crude oil and its by-products can be released into the environment due to ship transport, offshore/onshore exploration, production, and pipeline transportation, as reported in [2] and shown in the Figure 1.5. According to [57], oil spills are among the most serious environmental damages, affecting soils, rivers, seas, flora, fauna, and all biodiversity. The impacts of crude oil have an effect of decades or even centuries. If the ecosystem is dynamic and the spill is not huge, it may take 10-20 years for the ecosystem to recover; in other cases, it may take up to a century [117].

When an oil spill occurs, many animals die, aquatic, terrestrial and aerial, and even the microorganisms that fertilize the soil die. It is necessary to remove the vegetation and the part of the soil that came into contact to decontaminate. The surrounding communities that live from hunting, fishing, or agriculture are affected [43]. In general terms, these pollutants affect the soil's chemical and physical composition, causing loss of fertility, contaminating

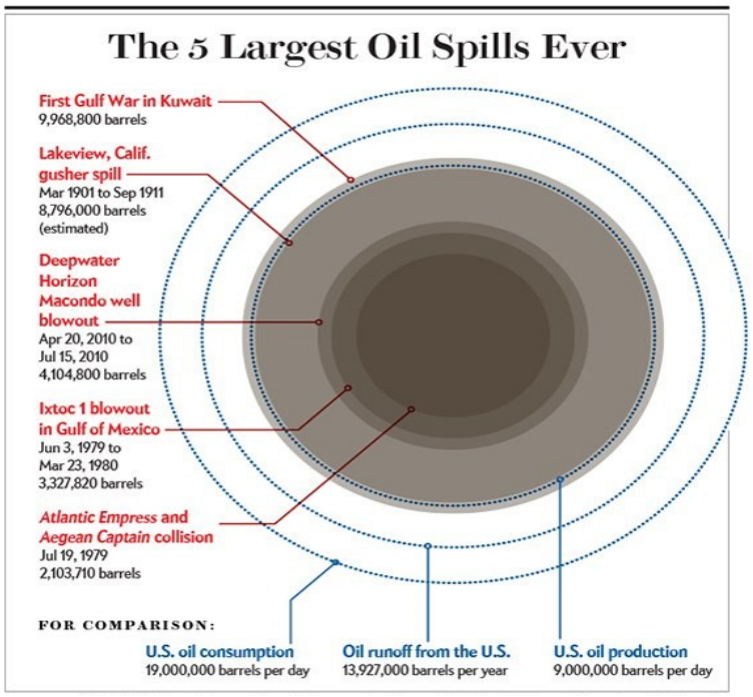

Fig. 1.5 World oil spills

groundwater or aquifers, contaminating the air due to the effect of evaporation and odors that it emits, changing the entire ecosystem and generating displacement of communities [2], [102], [48].

In marine ecosystems, algae are affected, thus affecting herbivorous species that feed from them. When herbivorous are affected carnivorous species that feed on such herbivorous will also be affected. For this reason species such as salmon, tuna, and sharks accumulate the largest amount of toxic substances, and hence such contamination is transmitted to humans [117]. Ten years after the Exxon Valdez spill, it was discovered in a study that fish and clams marketed in the sector were still exposed to residual hydrocarbons in the environment [76]. A subsequent study, seventeen years after the spill in question, showed that there is still residual contamination from the incident [8]. As popular as the Exxon Valdez spill is, it is not in the top five of global oil spills. Therefore we can only imagine how long the impact from oil spills during the Gulf War (Figure 1.5) will be present in nature.

1.2.3 Economic losses

The U.S. Department of Transportation Pipeline and Hazardous Materials Safety Administration (PHMSA) [144] presents some useful data;

Table 1.4 Pipeline incidents PHMSA

Year	Incident number	Fatalities	Injuries	Total cost reported
2000	380	38	81	$191.822.840
2001	341	7	61	$63.092.462
2002	642	12	49	$102.167.588
2003	670	12	71	$139.044.004
2004	671	23	60	$267.836.502
2005	719	17	47	$1.245.463.189
2006	639	21	36	$151.983.767
2007	610	15	49	$153.772.432
2008	659	8	56	$564.830.840
2009	627	13	64	$179.070.183
2010	586	22	108	$1.081.366.995
2011	588	13	55	$275.055.391
2012	571	12	57	$146.330.914
2013	617	9	44	$279.510.525
2014	706	19	95	$189.056.111
2015	712	11	48	$257.235.089
2016	632	16	87	$213.775.998
2017	647	20	36	$165.211.124
2018	634	7	79	$213.891.948
2019	657	11	36	$160.610.942
Total	**12.308**	**306**	**1.219**	**$6.041.128.844**

Table 1.4 shows the number of incidents, including damage and deaths, from 2000 to 2019, considering the transport of dangerous liquids and gas. In total, 306 fatalities, 1.219 injuries, and a total cost in dollars of $6.041.128.844 are observed, which lead's to an average cost by incident of $490.829. The costs and incidents in the Table 1.4 are detailed by year in the Figure 1.6 where the incident count remains at an average between 500 and 600 per year. The annual total cost associated with the spills remains at an average of $300.000.000 million dollars per year.

Considering now only hazardous liquids, the PHMSA reports in Table 1.5 a total of 7.314 incidents with 29 fatalities, 81 damages, $3.988.888,501 in associated costs, and 1.850.083 barrels spilled, which are close to 2.103.710 barrels of the fifth largest spill (Figure 1.5) of the collision of the SS Atlantic Empress tanker with the Aegean Captain tanker near the island of Tobago on July 19, 1979. Also, the property damage and barrels spilled by year are shown in

Table 1.5 Pipeline incidents with dangerous liquids PHMSA

Year	Incident number	Fatalities	Injuries	Total cost reported	Barrels Spilled
2000	146	1	4	$150.555.745	108.652
2001	130	0	10	$25.346.751	98.348
2002	458	1	0	$51.648.517	97.253
2003	432	0	5	$67.403.035	81.300
2004	377	5	16	$166.021.004	89.311
2005	369	2	2	$306.454.691	138.095
2006	354	0	2	$75.120.324	137.693
2007	332	4	10	$60.493.450	95.600
2008	376	2	2	$148.290.329	102.388
2009	342	4	4	$74.169.877	55.014
2010	350	1	3	$1.075.193.990	100.558
2011	344	0	1	$273.527.447	89.110
2012	366	3	4	$145.477.426	45.884
2013	400	1	6	$278.605.240	117.464
2014	455	0	0	$141.021.610	48.383
2015	460	1	0	$256.251.180	102.226
2016	420	3	9	$212.131.607	86.135
2017	415	1	1	$163.284.351	89.700
2018	405	0	2	$159.478.761	108.300
2019	383	0	0	$158.413.166	58.668
Total	**7.314**	**29**	**81**	**$3.988.888.501**	**1.850.083**

the Figure 1.7 where the property damage remains on average less than $200.000.000, except for the year 2010, the data reported by PHMSA does not include the incident of Deepwater horizon (the year 2010) because it was a dynamically positioned, semi-submersible offshore drilling rig, there was no transportation of crude by pipeline, but the problem was directly on the extraction work, due to this the data of barrels spilled in Table 1.5 and Figure 1.7 do not show the big spill of Deepwater horizon in the Figure 1.5. The spilled barrels remain on average between 80.000 and 100.000 approximately. In this way, taking all the information about the economic losses, it is possible to understand that human health and the environment are affected. Still, the total cost associated with spills and even property damage is huge.

1.3 State of art

This section presents a review for three components relevant to the research work: detection and location of pipeline leaks, high viscosity liquid-liquid flow, and high viscosity liquid-gas flow. It will briefly describe the detection and location of pipeline leak methods, and show statistical information about pipeline leak detection mechanisms. It will also show some works

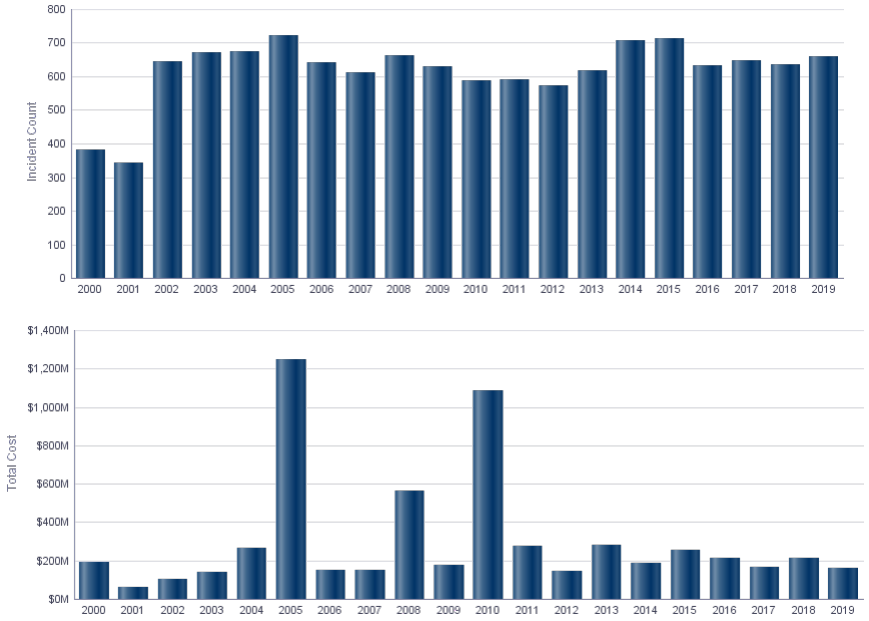

Fig. 1.6 Pipeline incidents

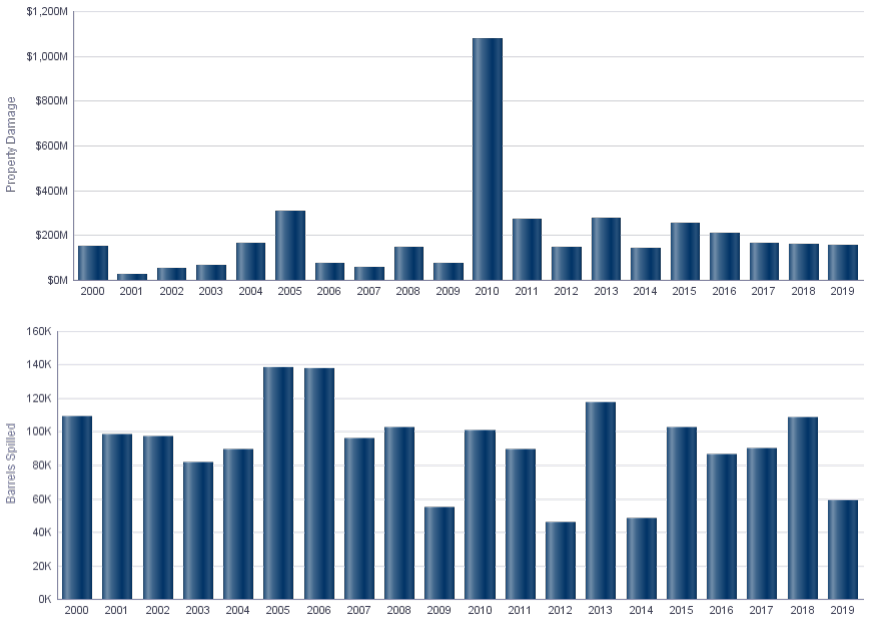

Fig. 1.7 Pipeline incidents with dangerous liquids

on liquid-liquid flow topics taking into account glycerol in laboratory experiments. Finally, this section ends with a brief review of the literature on high viscosity liquid-gas flow of some recent works from 2017 to 2020.

1.3.1 Early detection and location of leaks

Leak detection has two related approaches in the literature; the internal focus and the external focus [62]. However, literature also reports a third approach that combines the previous two in a hybrid design [121], [143];

Internal approach: It is based on volume or mass balance methods, pressure point analysis, statistical systems, real-time transient model (RTTM), and extended RTTM.

External Focus: It is based on external implementation hardware such as impedance change sensors, capacitive volume sensor, fiber optic, acoustic sensor, infrared sensors for image processing.

Mixed approach: It results from a combination of the previous two, so there could be an acoustic sensor and it relates its analysis to pressure and volume or mass balance.

However, given current technological and scientific progress, it has not been possible to increase the remote detection rates, as identified in the Figure 1.8. Data gathered from the U.S. Department of Transportation Pipeline and Hazardous Materials Safety Administration (PHMSA) [144] shows that only 8.7 % pipeline spills between the years 2010 to 2019 were identified with a leak detection system, while 63.6 % and 9.1 % of the spills were detected by workers at the site or notification from public. This research work aims to reduce (in a future) the gap that exists in terms of pipeline leak detection systems (specifically described in section 1.5) because it can be used to design better pipeline leak detection systems for two phase flow like liquid-liquid flow or air-liquid flow or it can be used to design better pumping systems taking into account the behavior of the two phase flow described here.

1.3.2 High viscosity liquid-liquid flow

Glycerol is used in many applications, such as in the textile, food, and chemical industries [106]; but the most popular use of glycerol is in the fabrication of personal care products. Glycerol is also used in laboratory research because it is cheap and non-toxic [151]. In particular, glycerol-water mixtures are commonly used for experimental investigation of flows within a wide range of Reynolds numbers because their viscosity can be adapted by changing the mixture's glycerol fraction [32]. Also, the similarity of the viscosity of pure glycerol ($\sim$ 1.5 Pa.s) and extra-heavy

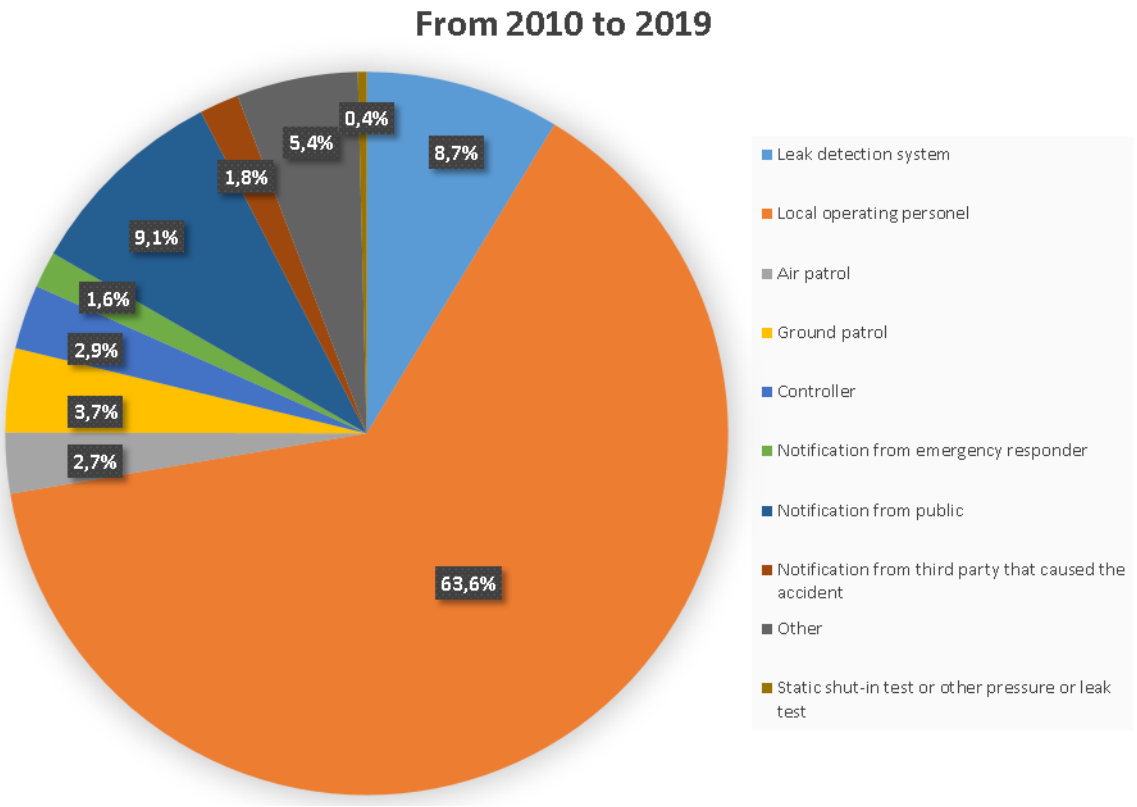

Fig. 1.8 Pipeline leak identifiers

crude ($\sim$ 1 Pa.s) provides the possibility to perform laboratory experiments for the study of extra-heavy oils safely.

The study of extra-heavy oils is significant in the petroleum industry because of the enormous increase in oil demand and the progressive exhaustion of low-viscosity oil reservoirs. Nevertheless, production, distribution, transport, blending, and the conditioning process of such crude oils are technological challenges due to their very high viscosity [35]. In particular, heavy and extra-heavy crude oils through pipelines from the head-well to the refinery are difficult to transport due to the crude's low mobility and fluency.

An alternative to improve the heavy crude oils' mobility consists of reducing friction between the pipeline and the heavy oil using substances that reduce drag inside the pipe [26]. The quantities required to reduce pipeline transportation viscosity depend on several factors such as the pipeline facilities' energy consumption capabilities or the pipeline design specifications. Therefore, these quantities are different for each case.

Once a viscosity reducer is used, and the oil can be transported through pipelines, it is subject to the same hazards and disturbances as light and medium oils during transport: leaks, blockages, or thefts. For this reason, it is important to develop algorithms to detect and localize faults in pipelines that transport heavy oils with the viscosity altered by drag reducing agents (DRA). In this respect, various contributions have been presented to numerically study oil flows in pipelines with a leak (e.g. [84, 131, 37, 105]). These contributions provide a great insight into the overall leak detection and permit the development of leak detection techniques and their evaluation before an experimental validation.

1.3.3 High viscosity liquid-gas flow

The offshore pipelines transport heavy-oil and natural gas. Then, the study of high viscosity liquid-gas flow is essential because this affects the pipelines due to pressure drop, intermittent flow, chronic fatigue, internal corrosion, vibrations, etc. This oil-gas behavior can damage the pipeline integrity leading to a pipeline failure or leak, affecting the general transport operation. This research work presents an additional topic on air-glycerin characterization and slugs prediction to achieve better pipeline operation and leak detection systems.

A brief survey of the literature review shows some recent works from 2017 to 2020. The authors [157] make a critical review from 157 papers, and 3947 published experimental data points for gas-liquid flow maps taking into account only vertical pipes and annuli. They consider the pipe geometry and measurement techniques (identifying flow regimes like; annular, slug,

bubble, and churn), the authors presents an outlook of research needs and developments in the prediction of gas-liquid flow only in vertical geometries. The authors also [114] developed a review on slug dynamical modeling, detection, analysis, and elimination in offshore Oil and Gas Exploration and Production(E&P) processes. The authors state the actual anti-slug methods have robustness problems, there is a risk of reducing the production, and the slug challenges will be more severe for a longer vertical riser in the future of deepwater E&P.

In [12] the authors show that liquid viscosity has a high impact on slug length. They carried out an experiment with air-water and air-oil mixtures with nominal viscosities ranging from 1.0 to 5.5Pa.s. They took measurements with two fast sampling gamma densitometers with a frequency of 250 Hz and developed a slug length correlation using dimensional analysis.

A model for slug bubble velocity in high viscosity slug flow was developed by [17]. The authors consider 241 experiments developed in a horizontal pipe of 15m length with 57 mm of diameter with three different liquids with viscosities from 240 to 730 cP. The measured parameters were pressure drop, slug length, liquid holdup, and bubble velocities.

In [10] the authors carried out an experimental investigation estimating the slug liquid holdup and concluded that it varies directly with viscosity and inversely with the gas input fraction. The experiments were performed in two pipelines of 5.5m and 17m with diameters of 0.0254m and 0.0762m. The viscosities of the liquid varies from 0.189 to 8.0 Pa.s. The measurements were performed by Electrical Capacitance Tomography. The authors in [154] calculated the wavelength, height, and speed of propagation in a gas-liquid flow in horizontal pipe with high pressure (2MPa). Also, they calculated the gas-wall, liquid-wall, and interfacial friction factors making some correlations, they analyzed the pressure drop too.

The more recent experiments were developed by [85] identifying bubble entrainment mechanism, bubble trajectories, and bubble loss from slug body using a high-speed camera (HSC) and particle image velocimetry (PIV) in an 18.9 m long with 50.8mm diameter pipe. The experiment takes into account High viscosity liquid-air two flow. The authors state the slug aeration mechanism proposed can be used to develop proper slug liquid holdup models.

1.4 Research background

The UREMA research group from Universidad del Norte supports this Doctoral work. This group intends to create a structure that allows production and service companies to carry out various energy studies, such as eco-audits, joint research projects, and evaluations. These are reflected in an increase in energy efficiency and, consequently, in an increase in productivity. It

also seeks to design energy-environmental training plans for the region's inhabitants, due to the large percentage of energy consumption in the commercial, residential sector in Colombia, and to emphasize and disseminate alternative energies like wind, solar, and biomass. The group research lines are;

- Biofuels
- Bioprocesses
- Industrial process control
- Energy conversion

The following works that support the research experience in piping systems are reported at the Universidad del Norte, as shown in the Table 1.6.

Table 1.6 Related research at Universidad del Norte

Thesis Name	Type of Thesis – Year
Diseño de una arquitectura de supervisión de tuberías de transporte de gases no condensables para el diagnóstico de fugas	Master Thesis – 2019
Liquid Transport Pipeline Monitoring Architecture Based on State Estimators for Leak Detection and Location	Doctoral thesis – 2018
Detección de fallas en líneas de transporte de gas natural mediante redundancia analítica de modelos	Doctoral thesis - 2015

This work is also supported by the Universidad Nacional Autónoma de México (UNAM) engineering institute in Mexico City, founded in 1956. The Engineering Institute of UNAM (IIUNAM) is the engineering research center with the longest tradition and prestige in Mexico. It has generated knowledge and has developed quality, original, useful and competitive procedures and technologies applied in large part of Mexico's infrastructure. He is also committed to training high-quality engineers and researchers in engineering. IIUNAM is a community made up of approximately 950 people, of which more than 200 are academics, with a similar number of workers and administrative personnel.

On the other hand, the Institute receives about 550 scholarship holders each semester who carry out thesis work for bachelor's, master's, and / or doctorates. Its facilities within Ciudad Universitaria in Mexico City occupy 18 buildings distributed along 20,000 square meters built between laboratories, classrooms, cubicles, offices, workshops, and outdoor spaces.

IIUNAM has two academic units in the province, one in Juriquilla, Querétaro, and another, in Sisal, Yucatán. The Engineering Institute is a high-level specialist engineering consultant

for the public and private sectors. It maintains a solid relationship and holds agreements of great importance every year. In the Hydrocarbons' context, special attention has been paid to the training of human resources in petroleum engineering and disseminating the results of their research, contributing to the development of the country and society's well-being.

The university has undergraduate, master, and doctoral programs in petroleum engineering, electronic engineering, electrical engineering, mechanical engineering, and other professional programs that enrich the multidisciplinary work. With research lines related to this work as shown in the Table 1.7

Table 1.7 UNAM research lines

Research line	Professor
· Fluid dynamics · Multiphase flows	Ph.D. Arturo Palacio Pérez
· Automatic fault diagnosis in dynamic systems · Fault-tolerant control of dynamic processes · Automatic location of leaks in pipelines	Ph.D. Cristina Verde Rodarte
· Automatic fault diagnosis · Structural monitoring of pipelines · Supervision of fluid transport and distribution systems	Ph.D. Lizeth Torres Ortíz
· Computational fluid dynamics · Turbulence	Ph.D. William Vicente Rodríguez
· Crude characterization	Ph.D. Edgar Ramírez Jaramillo
· Multiphase flows in transport systems · Heat transfer in transport systems	Ph.D. José Enrique Guzmán Vázquez

1.5 Research gap and problem statement

In the liquid-liquid flow case, there is a dynamic of the flows in the pipeline (where one will be the liquid phase of heavy crude oil and the other liquid phase will be the thinner) that to date remains not entirely understood [68]. There is a complex interaction between two liquid phases where there is a wide range of possible flow regimes due to interfacial forces, wetting characteristics, phase inversion and turbulence and which depend on the properties of the fluid (density, viscosity, interfacial tension), velocities flow and pipe characteristics. Two liquid phase flow can also be classified into two categories; separate flows and mixed flows. Separate flows are associated with the existence of two continuous fluid layers on each side of an interface that can be smooth or wavy, while mixed flows are more complex due to the appearance of drops from one phase to another [68]. As observed in Figure 1.9, for the case of water and oil there

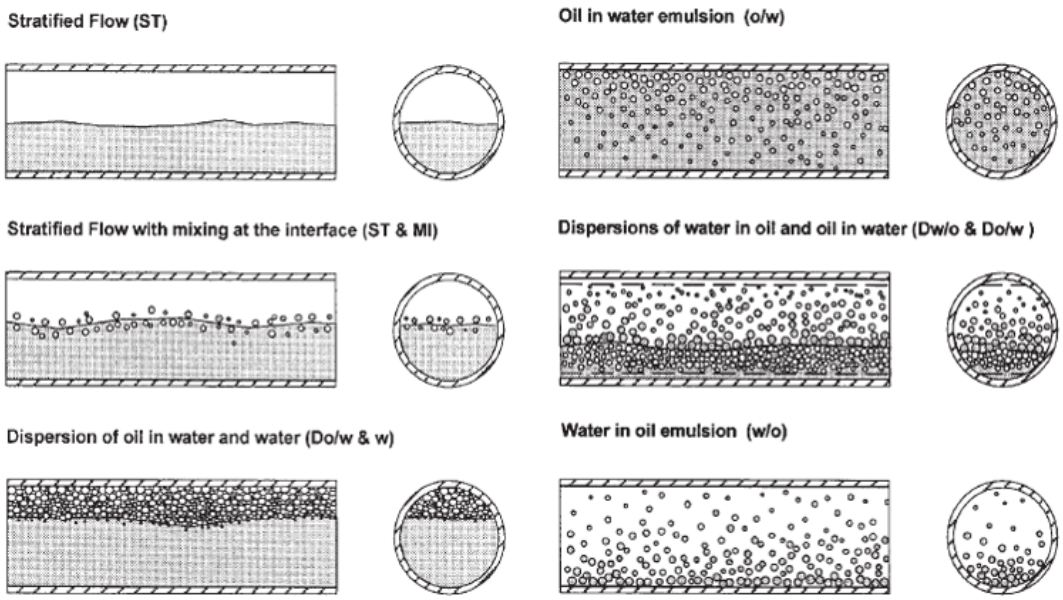

Fig. 1.9 Flow pattern in horizontal pipes, taken from [140]

are six flow patterns in horizontal pipes as established by the authors in [140]: (1) stratified flow, (2) stratified flow with mixing at the interface, (3) dispersion of oil in water and water, (4) oil-in-water emulsion, (5) water-in-oil and oil-in-water dispersions and (6) water emulsion in oil. In the framework of such dynamics between two liquids of different viscosity, this doctoral thesis work intends to integrate such behavior into a leak detection system based, taking into account the work carried out in [79] where the working fluid was only water.

In the context of gas-liquid flow, this phenomenon occurs in many stages of oil and gas production systems. It can be found, for example, in offshore and onshore pipelines [42]. This two-phase flow class is susceptible to damages such as pressure drops greater than in single-phase flow, erosion, and corrosion because of high velocities and other mechanical problems. Therefore, the study of two-phase flows is essential to develop cutting-edge technology that helps keep pipelines safe. A careful investigation of the world's oil reserves data reveals that heavy oils represent 70% of the world's existing reserves. They frequently come with gas in production, distribution, and transport, so it is crucial to know the oil-gas flow behavior to develop better processes [127]. The authors also state the conclusions of experimental results obtained from most of the literature review are: (1) the transitions of flow pattern depend on liquid viscosity and (2) the models have a poor performance when the liquid phase has a high viscosity fluid, such as 100mPa.s to 10,000 mPa.s.

In particular, some problems occur during the heavy oil management: severe slugging, pressure pulses, and pipe vibrations causing fatigue and damage, taking into account failure in pipe structure, gas leak, oil spill, equipment failure, stop operations, negative impact on the environment and economy. Such problems require then characterizations and models that improve the prediction of flow regimes, pressure drops, and dynamical patterns of the flow [23].

The predominant gas-heavy oil flow pattern found in most oil fields is intermittent flow, which can be defined as a liquid slugs and gas bubbles sequence [64]. This sequence leads to an intrinsically unsteady flow condition, even in steady-state, which poses difficult problems for its characterization and prediction. The intermittent flow regime is usually divided into two sub-regimes: the plug flow or flow with elongated bubbles, in which the slugs do not carry gas, and the slug flow, in which the slugs carry many gas bubbles [19]. The intermittent flow parameters usually investigated are the slug body liquid holdup, the slug frequency, and the slug length, particularly for high-viscosity flows. It has been found, for instance, that the slug frequency increases, and the slug length decrease when the viscosity increases [24, 55, 56]. In the same way, other features are particular of high-viscosity slugs. However, even when there is an obvious necessity for extensive investigation on the intermittent flow of high-viscosity fluids, the number of publications dealing with mixtures where the liquid phase has a dynamic viscosity above 1 Pa.s is still minimal [13].

At present in Colombia context, as a result of the tragedy that occurred in Dosquebradas (Risaralda), Ecopetrol has implemented a system of visual and geotechnical inspection of the pipelines, as the main part of its pipeline maintenance mechanism, and has a system for the detection of leaks in its pipelines. Still, the concern remains if it is adapted for mixtures of fluids, types of crude oil, or emulsions, the margin of error in terms of leak location, location time, and sensitivity to the level of leakage is unknown. Then, the real research problem is the early pipeline leak detection. Given the negative impact generated by an oil spill, we must ask ourselves the following research question:

How is it possible to remotely detect leaks earlier, taking into account the two phase flow behavior in crude oil pipeline transmission, to reduce the spill's negative impact in the surrounding areas?

1.6 Objectives

Taking into account the research question in previous section, then, this research work have the following objectives;

Fig. 1.10 pipeline inspection

1.6.1 Main objective

- Design a supervision architecture for pipelines transporting a binary liquid mixture composed of a high-viscosity liquid and a low-viscosity liquid that incorporates a state estimator for system's characterization and early detection and location of leaks.

1.6.2 Specific objectives

- Define a model for transporting a liquid-liquid mixture (low - high viscosity) through pipelines. Taking into account the particular behavior of each fluid.
- Develop a parametric identification algorithm based on a state estimator that allows characterizing the transportation system.
- Develop a strategy based on a state estimator for detecting leaks in pipelines that transport a binary liquid mixture composed of a high-viscosity liquid and a low-viscosity liquid.
- Design experiment plans to detect and locate leaks, taking into account the particular and joint characteristics of each substance.
- Validate the algorithm developed in relevant transport environments of a binary liquid mixture composed of a high-viscosity liquid and a low-viscosity liquid.

1.7 Methodology

To achieve the correct achievement of the objectives, the work has been divided into phases according to the work breakdown methodology [70] WBS (Work Breakdown Structure) and

basing the constitution and development of activities in project management, which is the discipline that allows the organization and administration of resources in such a way that objectives can be met within the defined scope, time and costs. In this sense, and as stated by [115], the type of research is mixed because it collects, analyzes, and links qualitative and quantitative data in a single research project.

In this sense, the proposed phases to achieve the satisfactory execution of the project are presented below:

Phase I. State of the art: in this first stage, a study and bibliographic research were carried out on high viscosity liquid-liquid flow in pipes, as well as for high-viscosity liquid-gas flow in pipes. First, it was investigated the liquid-liquid flow and the characteristics of the glycerin-water mixture, to lay the foundations for pressures and flow predictions. Next, it was investigated air-liquid flow to understand the flow characteristics which affect the pump operation and pipe integrity. This can be found in the chapter 1 and chapter 2 of this document.

Phase II. Analysis: the hypotheses were determined by applying the mass and momentum conservation equations from [31] the mixture model [151] for water and glycerine in different proportions. Next, an experimental program was designed to test pressures and flow from algorithms considering the mixture case. This can be found in the chapter 2.

Phase III. Experimentation: once the second phase of the project has concluded, experiments were carried out in the laboratory of multiphase flows to validate the algorithms. This phase can be found in chapter 2. Within the doctoral internship, experiments were carried out in the laboratory of the National Autonomous University of Mexico (UNAM) The laboratory has the following characteristics. [33]

- Experimental testing section 60 m long with 8 in. Internal diameter pipe. Pumping system for real crudes with a pumping capacity of 17 m3/h.
- Three systems of impedance computed tomography ERT and ECT for measuring volumetric fractions with real-time sampling. The system is 3 in. (0.076 m) internal diameter, and allows the measurement of flows of two-phase or three-phase mixtures with gases, liquids, and solids.
- Anton Paar PVT system for thermodynamic envelope measurement and SARA characterization of crude oils.
- Rheometer, chromatographs, surface tension gauges, and shear stress gauges.

- Dehydrated and refrigerated air compression system, for continuous volumetric flows of 2,800 L/min at 21 bar.
- Back-up of compressed air with an independent 2 m3 tank, to produce flow peaks above 6,000 L/min at 21 bar.
- 3 m3 tanks for storage and handling of real crudes. Air regulation system for high and low expenses.

Phase IV. Testing and adjustment stage: in this phase, tests, and adjustments were carried out as follows:

- Obtain empirical relationships from the experimental results.
- Design leak diagnosis algorithms in liquid-liquid mixture flow in pipes.

This phase can be found developed through chapters 3, 4 and 5.

Phase V. Results and Conclusions: in this phase all the results obtained from the investigative and experimental work were organized. Analysis and conclusions were developed to establish the dynamic behavior of high viscosity two phase flow (liquid-liquid, air-liquid). Future work considers investigative continuity to positively impact Colombia, related to risk and environmental management associated with spills caused by hydrocarbon leaks in pipelines or a positive impact related to better operation systems in oil pipeline transport. This phase can be found from chapter 2 to chapter 5, but there is a global revision of all the research work in this document in the chapter 6.

Phase VI. Article and conference presentation: this is the phase where the work was organized, and the research results were shown to the academic community. This phase was organized according to the previous phases' results, and it was worked in parallel, from the tests carried out in phase three. The published articles are organized from each chapter; there are two articles from chapter 2 and one article from chapter 3 and 4. Also, there is a conference presentation from the chapter 2.

Phase VII. Final Report: all the results obtained were organized and the final report was developed. This phase was fed with the results from previous phases, and the result is the present document.

Chapter 2

Model for homogeneous mixtures

2.1 Introduction

This chapter proposes a model for the flow of a mixture of water and glycerol, emulating the mix of heavy oil and DRA. The model's principal goal is to run numerical simulations of several leak cases for different water and glycerol fractions. Such numerical simulations will permit: (a) the formulation of algorithms based on control and/or artificial intelligence for localizing leaks in pipelines that transport fluids with high viscosity, (b) the evaluation of such algorithms in a simulation environment before their evaluation in the laboratory tests, (c) the design of experimental tests to assure their successful implementation and (d) the study of how the DRA affect the detection and localization of leaks in pipelines that transport heavy oils.

The model is constituted by a couple of partial differential equations obtained from mass and momentum balances, which are approximated by finite differences to get a numerical solution. Moreover, the model is constituted by experimental formulas to compute the density and the mixture's dynamic viscosity. The model's equations were programmed in MATLAB for obtaining a numerical solution, which was compared with observations obtained from a laboratory test.

Section 2.2 describes the apparatus used to perform experimental tests and how the data was acquired. Section 2.3 presents the formulation of the mathematical model. Section 2.4 presents the formulation of the computational model (numerical simulator). Section 2.5 presents the results of a comparison between experimental data and the predictions provided by the numerical simulator. Section 2.6 presents some simulation results for three study cases, and Section 2.7 provides some conclusions.

2.2 Test apparatus and data acquisition

To evaluate the accuracy of the proposed mathematical model and program a simulator (a computational model) from it, the characteristics of the flow loop shown in Figure 2.1 are considered. Such a pipeline is located at Instituto de Ingeniería-UNAM, and it was built to investigate the flow properties of liquid-liquid and liquid-air mixtures produced by high-viscosity liquids such as heavy and extra heavy crude oils. The test section's overall length is 54 m, which was constructed with schedule 80 steel tubes with an internal diameter of 0.0762 m (3 in) and absolute roughness around 4.6×10^{-5}. A progressive cavity pump (Seepex Mod. BN35-24, 40 HP) was installed to supply the liquid's necessary flow rate into the test section. This pump can deliver constant volume flow rates in the interval $[0, 4.7 \times 10^{-3}]$ m^3/s. The test section's outlet is connected to a separator tank with an internal capacity of 1.5 m^3 (Figure 2.2). This separator tank is connected to the pump's inlet to close the flow circuit.

The liquid inflow rate can be measured with an Endress-Hauser Coriolis meter: the Promass 83F80DN80 3" model, with an accuracy of 0.1% across the entire measuring range. Besides, all the pressures can be measured with an array of conventional MEAS U5300 transducers whose accuracy errors are less than 0.1% across the measuring range. Five pressure transducers were placed along the experimental duct, labeled P_1, P_2, P_3, P_4, and P_5. The distance between each sensor is indicated at the bottom of Figure 2.1. The experiments developed in chapter 3 and chapter 4 use the twin-scroll Kaeser Aircenter SK.2 compressor, which supplied a dry air constant mass for pressures within the interval [0.0 Pa, 1.6×10^6 Pa](Figure 2.3), this compressor was used for the glycerin-air mixtures. Also for chapter 4, the pressure sensor configuration is shown in Figure 2.4

The dataset presented in this section was collected in a laboratory flow circuit designed to investigate high-viscosity flows. The data set comprises 12000 samples (20 minutes of measurements at 100 ms sampling time) of mass flow and pressure measurements taken at five points along the pipeline. The first 3000 samples were recorded when the flow in the loop was composed only of glycerol. The remaining data were acquired when the flow was composed of a water–glycerol mixture. During data acquisition, two extractions were produced. The research reported [111] uses 1600 samples of the data provided here. This section explains in detail the experimental set-up and the principal instruments used for obtaining the dataset. The dataset is in the form of seven columns: Time, Mass Flow, Pressure 1, Pressure 2, Pressure 3, Pressure 4, Pressure 5, in supplementary Excel and Matlab files, which can be found in [112].

Table 2.1 Specifications table

Subject	Mechanical Engineering
Specific subject area	Fluid mechanics
Type of data	Excel files-Matlab files
How data were acquired	20 min of measurements (100 ms sampling time) per data using: (1) Mass Flow Transducer (Endress-Hauser Coriolis mass flowmeter, Promass 83F80DN80 3, ±0.1% Full-Scale error) (5) Pressure Transducers (MEAS U5300, ±1% error)
Data format	Raw
Parameters for data collection	Before any preliminary test, electrical wires connections were checked
Description of data collection	A progressive cavity pump provides the energy necessary to recirculate the liquid through the pipeline. The inlet mass flow is measured, as well as the pressure at five different points along the pipeline.
Data source location	Institution: Universidad Nacional Autónoma de México City: Mexico City Country: Mexico
Data accessibility	In this section
Related research article	Noguera, J. F., Torres, L., Verde, C., Guzmán, E., Sanjuan, M. Model for the flow of a water-glycerol mixture in horizontal pipelines. 2019 4th Conference on Control and Fault-Tolerant Systems (SysTol) (pp. 117–122).IEEExplore.

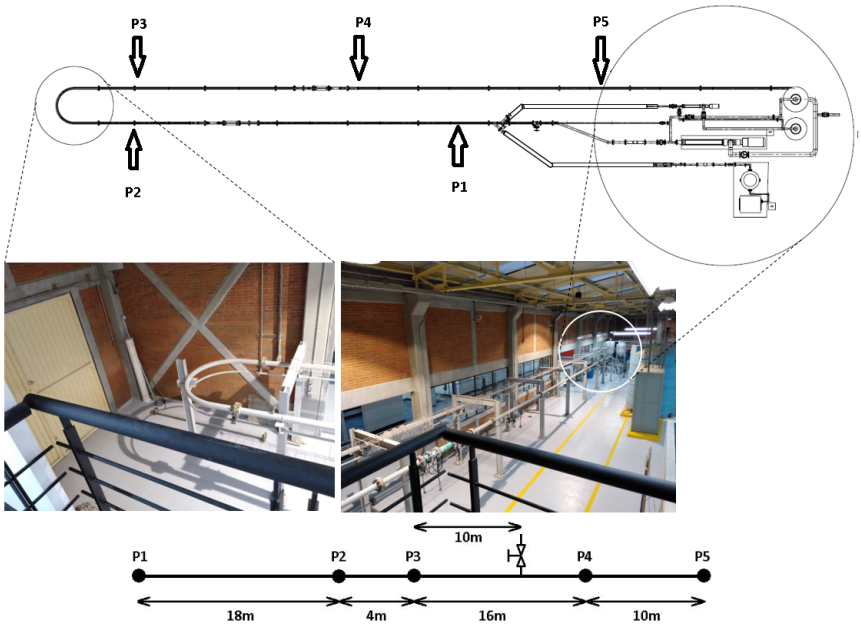

Fig. 2.1 Laboratory test apparatus

Value of data and importance of experiments

The academic community can use the data presented here (found in [112]). These data are valuable because the similarity in glycerol viscosity and extra-heavy crude allows researchers to use the data provided here to evaluate models that describe the flow of extra-heavy crude. The glycerol diluted with water emulates the mixture of extra-heavy oils with drag-reducing agents (DRA), which are usually employed to reduce the pressure during the transport of extra-heavy oils. For this reason, the data provided here can help researchers and practitioners to evaluate prediction models involving DRA.

Also, in the experiments, a valve was used to emulate the appearance of leaks. Hence, the data set can similarly validate leak diagnosis approaches, like [80], Because pressure and flow data are reporting the variation when the valve is opened.

The dataset and experiments can benefit pipeline owners, operators, and researchers since this can be used to validate pipeline dynamical models and improve the transport operation and the accuracy of leak detection systems. The data can be used as inputs and outputs to validate models that describe the flow of pure glycerol and the flow of water-glycerol in pressurized horizontal pipes. This can be done only by separating the portions of the time series recorded

Fig. 2.2 Discharge tanks

when only glycerol was flowing in the pipeline or when the aqueous glycerol was flowing. The pressures are also taken at the beginning and the end of the curve section to help analyze the glycerol flow behavior when circulating U-shaped sections.

Experimental design, materials, and methods

Figure 2.1 shows the pipeline utilized to perform experimental investigations. In the experiment, the viscosity of pure glycerol was 0.460 Pa.s, and the viscosity of diluted glycerol was 0.007 Pa.s. The experiment process is described here next:

- The progressive cavity pump turns on at time t = 63.37 s, and it reaches a mean mass flow of 6.26 kg/s of pure glycerol.
- Glycerol diluted with water was injected at time t = 321 s, in a proportion of 45% glycerol and 55% water. The mass flow of diluted glycerol injected was 5% of the mass flow of pure glycerin.

Fig. 2.3 Air compressor

- At time t = 567 s, a leak, with a mass flow Q l = 0.0126 kg/s, was induced by opening a valve located 10 m downstream from pressure sensor P_3 (Bottom of Figure 2.1). This valve was closed at time t = 668 s.
- At time t = 779 s, the diluted glycerol injection was stopped.
- At time t = 1045s, a second leak, with a mass flow Q l = 0.0127 kg/s, was induced. In this case, the valve was closed at time t = 1136s.

In Figure 2.5 are shown the measurements of the five pressure sensors (P_1 to P_5) and the mass flow sensor at the pipeline inlet (Q1). Also, the Matlab file to plot the Figure is shared in [112]

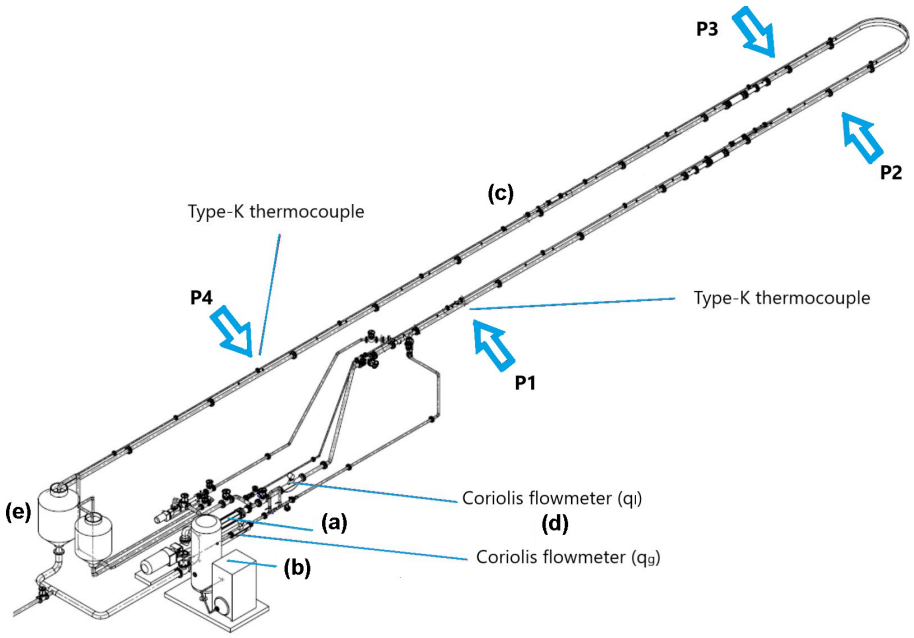

Fig. 2.4 Laboratory test apparatus

2.3 Model for a water-glycerol mixture flow

The assumptions to formulate the model are the following:

(A1) The flow is one-dimensional.

(A2) The two fluids are well mixed.

(A3) Both fluids are slightly compressible.

(A4) Convective changes in velocity are negligible.

(A5) The cross-sectional area of the pipeline is constant.

(A6) The walls and both fluids are linearly elastic.

2.3.1 Governing equations

Considering the assumptions (A1)-(A5), the model comprises the following mass and momentum conservation equations [81]:

$$P_t + \frac{\rho(T)b^2}{A_r} Q_z = 0 \tag{2.1}$$

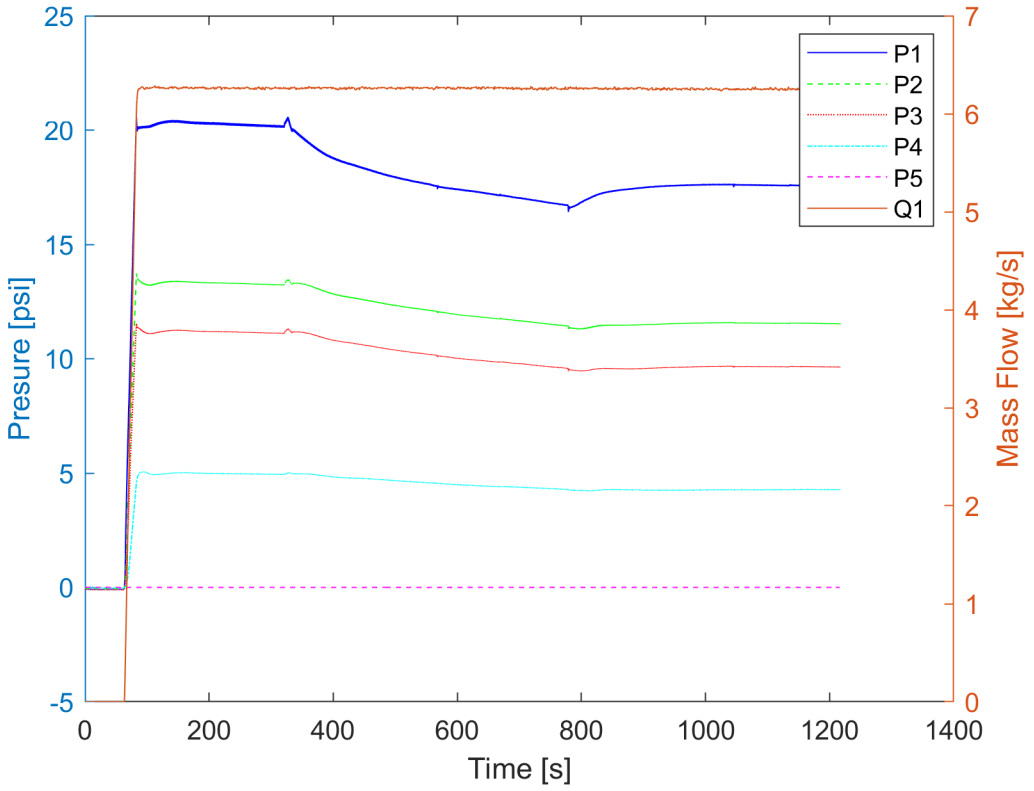

Fig. 2.5 Laboratory pipeline mass flow and pressures

$$Q_t + \frac{A_r}{\rho} P_z + \frac{f(Q,T)Q|Q|}{2A_r\phi} = 0 \tag{2.2}$$

where z and t are the spatial and time coordinates, respectively, P is static pressure (Pa), $P_z = \partial P/\partial z$, $P_t = \partial P/\partial t$, Q is flow rate (m^3/s), $Q_z = \partial Q/\partial z$, $Q_t = \partial Q/\partial t$, A_r is the cross-sectional area of the pipeline, b is the sound velocity in a mixture of water and glycerol (m/s), ϕ is the pipe internal diameter (m), g is the gravitational acceleration (m/s^2), ρ is the density of the mixture of water and glycerol (kg/m^3) and $f(Q,T)$ is the friction factor, which depends on Q and the mixture temperature T through the Reynolds number.

2.3.2 Friction computation

For calculating the friction factor, in the case of laminar flow, the model comprises the following expression derived from the Hagen-Poiseuille equation:

$$f(Q,T) = \frac{64}{Re(Q,T)} \tag{2.3}$$

In the turbulent flow case, the model uses the Swamee-Jain equation, which is expressed as follows [39], [78]:

$$f(Q,T) = \frac{0.25}{\left[\log\left(\frac{\varepsilon/\phi}{3.7} + \frac{5.74}{Re(Q,T)^{0.9}}\right)\right]^2} \tag{2.4}$$

where ε is the roughness of the internal pipeline wall, $Re(Q,T) = Q\phi/\nu(T)A_r$ is the Reynolds number, $\nu(T) = \mu(T)/\rho(T)$ is the mixture kinematic viscosity, $\rho(T)$ is the mixture density and $\mu(T)$ is the mixture dynamic viscosity. These later parameters are calculated by using two experimental formulas described in the following paragraphs.

Density of the water-glycerol mixture

To calculate the mixture density, the following experimental equation reported by [151] is used:

$$\rho(T) = \kappa(T)\left[\rho_w(T) + \frac{\rho_g(T) - \rho_w(T)}{1 + \frac{\rho_g(T)}{\rho_w(T)}\left(\frac{1}{w_g} - 1\right)}\right] \tag{2.5}$$

where $w_g \in [0,1]$ is the weight fraction of glycerol, T is the temperature (°C), $\rho_w(T)$ is the density of pure water (kg/m^3), $\rho_g(T)$ is the density of pure glycerol (kg/m^3), $\kappa(T)$ is the volume contraction coefficient. The density of pure water and pure glycerol can be calculated by using

the following formulas, respectively:

$$\rho_w(T) = 1000\left(1 - \left|\frac{T-3.98}{615}\right|^{1.71}\right) \tag{2.6}$$

$$\rho_g(T) = (1273 - 0.612T) \tag{2.7}$$

where

$$\kappa(T) = 1 + A(T)\sin\left(w_g^{1.31}\pi\right)^{0.81} \tag{2.8}$$

$$A(T) = 1.78\times10^{-6}T^2 - 1.82\times10^{-4}T + 1.41\times10^{-2} \tag{2.9}$$

Dynamic viscosity of a water-glycerol mixture

It is calculated by using the experimental formula proposed in [32], which is expressed as follows:

$$\mu(T) = \mu_g(T)e^{(A(T)\alpha(T))} \tag{2.10}$$

where $\mu_g(T)$ is the glycerol dynamic viscosity (Pa·s), $A(T)$ denotes the relation factor between the dynamic viscosities and $\alpha \in [0,1]$ is the weighting factor associated with the concentration of glycerol. Such terms can be obtained through the following expressions:

$$\mu_g(T) = 12100e^{\left(\frac{(-1233+T)T}{9900+70T}\right)} \tag{2.11}$$

$$A(T) = \ln\left(\frac{\mu_w(T)}{\mu_g(T)}\right) \tag{2.12}$$

$$\alpha(T) = 1 - w_g(T) + \frac{\gamma(T)\beta(T)w_g(T)(1-w_g(T))}{\gamma(T)w_g(T) + \beta(T)(1-w_g(T))} \tag{2.13}$$

where $\mu_w(T)$ is the water dynamic viscosity (Pa·s), $\gamma(T)$ and $\beta(T)$ are the coefficients of the weighting factor. These parameters are calculated with the following experimental formulas:

$$\begin{aligned} \mu_w(T) &= 1790e^{\left(\frac{(-1230-T)T}{36100+360T}\right)} \\ \gamma(T) &= 0.705 - 0.0017T \\ \beta(T) &= (4.9 + 0.036T)\gamma(T)^{2.5} \end{aligned} \tag{2.14}$$

2.4 Computational model

The computational model (or numerical simulator) presented in this work was implemented to predict the mixture's flow in a straight section of the pipeline shown in Figure 2.1 More precisely is the segment is limited by the transducers P_1 and P_2. It means that the boundaries of the spatial domain are the positions of these transducers: $z = 0$ (m) is P_1 and $z = L$ (m) is the position of P_2. The straight section's length is $L = 18$ (m), as shown at the bottom of Figure 2.1.

For implementing the computational model and obtaining its numerical solution, a time-varying flow rate, indicated as Q_{in}, is used as the boundary condition at $z = 0$ (m). In contrast, a pressure, denoted as P_{out}, is used as a boundary condition at $z = L$ (m).

The first step towards the simulator implementation is the approximation of the spatial derivatives (pressure and flow rate gradients) involved in equation (2.1) and equation (2.2) by different quotients as follows [86]:

$$(P_z)_i \approx \frac{\Delta P_i}{\Delta z} = \frac{P_{i+1} - P_i}{\Delta z} \tag{2.15}$$

$$(Q_z)_i \approx \frac{\Delta Q_i}{\Delta z}, = \frac{Q_{i+1} - Q_i}{\Delta z} \tag{2.16}$$

where Δz is the spatial step, which can be calculated as follows: $\Delta z = L/N$, where N is the total number of spatial steps (spatial differences).

By substituting the finite differences into equation (2.1) and equation (2.2), these become.

$$P_t + \frac{\rho(T)b^2}{A_r}\left(\frac{Q_{i+1} - Q_i}{\Delta z}\right) = 0 \tag{2.17}$$

$$Q_t + \frac{A_r}{\rho(T)}\left(\frac{P_{i+1} - P_i}{\Delta z}\right) + \frac{f(Q_i, T_i)Q_i|Q_i|}{2A_r\phi} = 0 \tag{2.18}$$

Since equation (2.17) and equation (2.18) involve only temporal derivatives, $P_t \approx dP_i/dt = \dot{P}_i$ and $Q_t \approx dQ_i/dt = \dot{Q}_i$, such that the following set of ordinary differential equations is obtained:

$$\dot{P}_i = -\frac{\rho(T)b^2}{A_r}\left(\frac{Q_{i+1} - Q_i}{\Delta z}\right) \tag{2.19}$$

$$\dot{Q}_i = -\frac{A_r}{\rho(T)}\left(\frac{P_{i+1} - P_i}{\Delta z}\right) - \frac{f(Q_i, T_i)Q_i|Q_i|}{2A_r\phi} \tag{2.20}$$

which can be solved by using a numerical method such as the Euler or the Runge-Kutta method.

By considering the defined boundary conditions, equation (2.1) can be solved $\forall i = 1,,...,N-1$ and equation (2.20) can be solved $\forall i = 2,3,...,N$ since $Q_1 = Q_{in}$ and $P_N = P_{out}$ [133].

The spatial and time steps must be chosen for satisfying the stability condition for the numerical solution, which is known as the condition of Courant Friedrich Lewy (CFL), [31] and expressed as follows:

$$\Delta z \geq b\Delta t = \frac{L}{N} \geq b\Delta t \tag{2.21}$$

To model the effect of a leak in the flow of the glycerol-water mixture, the continuity equation must be modified to include the flow rate of the leak in the flow rate balance:

$$\dot{P_i} = -\frac{\rho(T)b^2}{A_r}\left(\frac{Q_{i+1} - Q_i - Q_\ell}{\Delta z}\right) \tag{2.22}$$

where Q_ℓ is the flow rate of the leak, which is expressed by Torricelli's equation given as follows

$$Q_\ell = C_\ell A_\ell \sqrt{2gH_\ell} \tag{2.23}$$

where C_ℓ is the discharge factor, A_ℓ is the leak area, $H_\ell = P_\ell / g\rho(T)$ is the pressure head at the leak position z_ℓ, and P_ℓ is the pressure at z_ℓ.

The computational model was implemented in MATLAB and solved using the ODE3 solver, which is based on a third-order Runge-Kutta method. The total number of spatial steps was chosen $N = 8$ such that $\Delta z = 2.25$ (m). The time step for the numerical integration was $\Delta t = 0.001$ (s). Since the pressure wave velocity is $b = 1920$ (m/s), the CFL condition is satisfied.

2.5 Experimental test

The experimental test's goal described here was getting real data to validate the computational model, which was described in the previous section. The experiment started with pure glycerin injection into the test pipeline at the following flow rate: $Q_{in} = 5.95 \times 10^{-3}$ m^3/s. The temperature of the flow registered during the experiment was 33°C. At this temperature, the dynamic viscosity of the pure glycerol is approximately μ_g = 0.4723 Pa·s (472.3cP). The pressure recorded by the transducer P_2 during the experiment is the blue signal shown in Figure

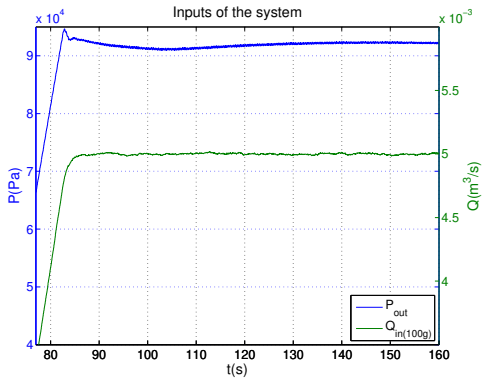

Fig. 2.6 Boundary conditions

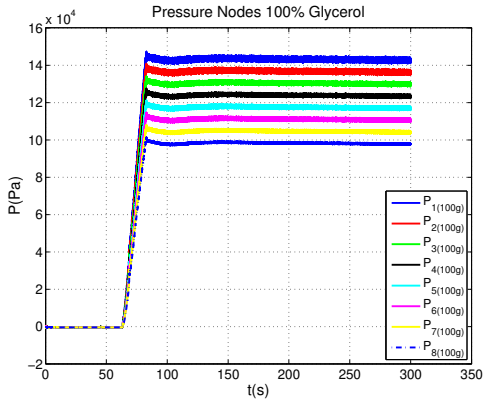

Fig. 2.7 Case 1: predicted pressures by the numerical simulator

2.6, whereas the flow rate recorded at the pipeline inlet is the green signal shown in the same Figure. Both recordings were introduced into the numerical simulator as boundary conditions to get a numerical solution. During the experimentation, no extraction was provoked. Therefore, the flow rate prediction along the spatial domain is equal to the steady-state flow rate used as a boundary condition.

The predicted pressures by the computational model for every spatial step are the signals shown in Figure 2.7, whereas in Figure 2.8 the predicted pressure at $z = 0$ m, denoted as P_{in}-Sim, is shown together with the pressure measured by the transducer P_1, indicated as P_{in}-Real. The relative error between both pressures in steady-state is around 2.5%, which can be due to uncertainties in the experimentally measured quantities used in the model. However, a rigorous experimental analysis of uncertainty must be performed to prove this conjecture.

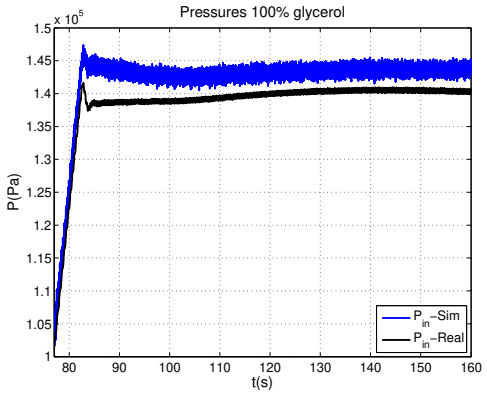

Fig. 2.8 Numerical solution for pressure at $z = 0$ m vs. pressure measured by sensor P_1

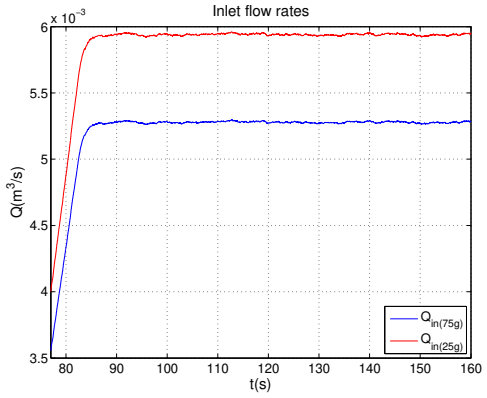

Fig. 2.9 Boundary conditions for the numerical solution of the model

2.6 Simulation tests

The simulation tests whose results are presented here below were performed by using the computational model. The goal of such tests was the study of the glycerol-water mixture flow when a leak occurs. Three study cases were considered: (1) flow of pure glycerol, (2) flow of a mixture with 75% of glycerol, and (3) flow of a mixture with 25% of glycerol. To find a numerical solution for the three cases, the flow rate used as a boundary condition at $z = 0$ m for the first case was the plotted one in Figure 2.6. In contrast, the flow rates used for the second and third cases are plotted in Figure 2.9. The pressure signal plotted in Figure 2.6 was used as a boundary condition at $z = L$ m for the three cases.

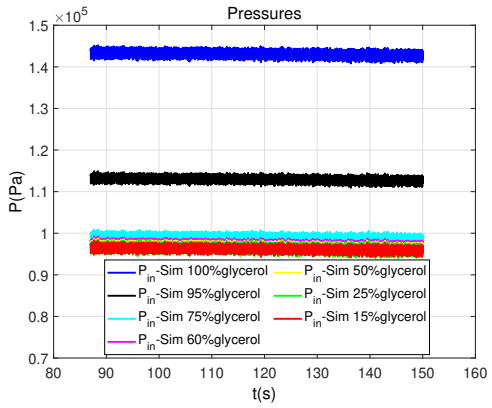

Fig. 2.10 Numerical solution for pressure at $z = 0$ m for different fractions of glycerol

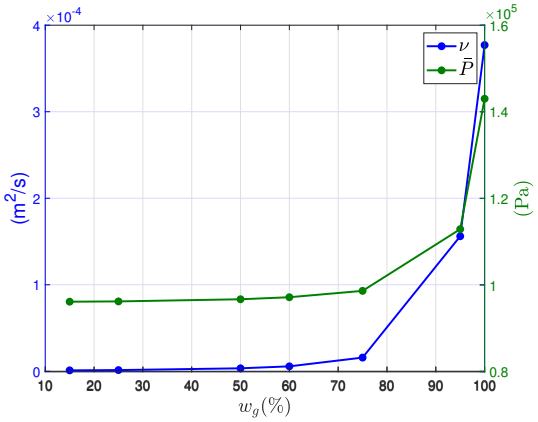

Fig. 2.11 Kinematic viscosity and pressure as functions of w_g

The predicted pressures at $z = 0$ m for the three study cases and additional weight fractions of glycerol are the signals shown in Figure 2.10. Notice that the difference between 100% and 75% fraction cases is about 0.5 bar approximately. In contrast, the difference between 75% and 25% fraction cases is less than 0.05 bar approximately. This fact is due to the mixture's dynamic viscosity, which has an exponential behavior for the glycerol fraction that affects the pressure; see Figure 2.11 for checking the correlation between the kinematic viscosity and the mean of the pressure in a steady state. The predicted pressures for each spatial step for the second case can be appreciated in Figure 2.12, whereas in Figure 2.13 the predicted pressures for the third case are displayed.

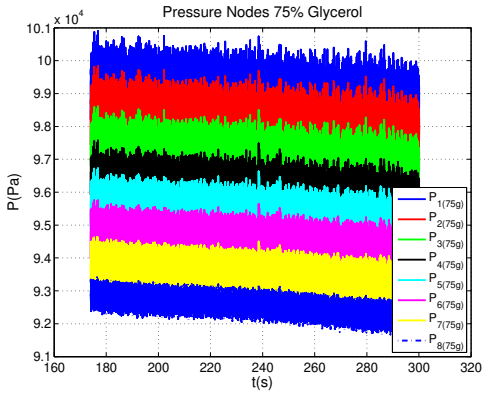

Fig. 2.12 Case 2: predicted pressures by the numerical simulator

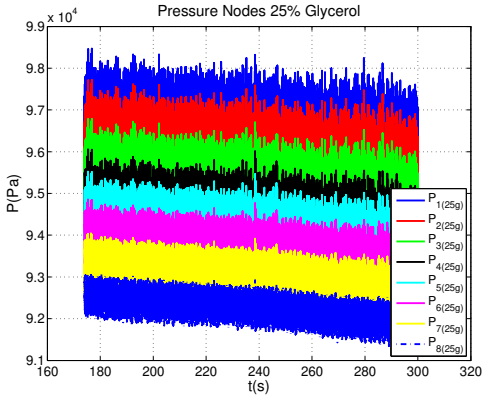

Fig. 2.13 Case 3: predicted pressures by the numerical simulator

Table 2.2 Leak discharge information

Leak	Case 1		Case 2		Case 3	
ϕ(")	$\frac{\bar{Q}_\ell}{\bar{Q}_{in}}$	$_\ell(m^3/\text{s})$	$\frac{\bar{Q}_\ell}{\bar{Q}_{in}}$	$_\ell(m^3/\text{s})$	$\frac{\bar{Q}_\ell}{\bar{Q}_{in}}$	$_\ell(m^3/\text{s})$
	%	$(\times 10^{-5})$	%	$(\times 10^{-5})$	%	$(\times 10^{-5})$
1/8	0.48	2.40503	0.39	2.19511	0.36	2.09209
1/4	1.89	9.44866	1.56	8.64048	1.45	8.23326
1/2	7.49	37.442	6.22	34.505	5.81	32.852

Three leaks with different discharge (i.e., with different flow rate) and located at $z_\ell = 4.5$ m were simulated for the three study cases. Since a leak can be emulated in the test apparatus using valves with orifices of different diameters, each leak's discharge was manipulated, in the numerical simulations, by changing the leak diameter in three standard valve orifice sizes: 1/8", 1/4" and 1/2".

In Figure 2.14 are illustrated the predicted flow rates at $z = L$ m for the three cases. In Table 2.2 are listed the means of the leak discharges in steady-state for the three different diameters and the three different cases, as well as the mean percentage ratio of these discharges for the mean of the inlet flow rate ($\bar{Q}_\ell/\bar{Q}_{in}$). The information of this Table is plotted in Figure 2.15, where it can be noticed that the percentage ratio, as a function of the glycerol fraction, has the same behavior of both the kinematic viscosity and pressure in Figure 2.11, which is because the leak discharge is a function of the pressure at the leak coordinate (as expressed in equation (3.10)). This situation must be considered in the development of leak diagnosis systems because a slight change in the kinematic viscosity, which can be due to temperature variations, or a small shift in the glycerol fraction, which can be due to the applied quantity of the viscosity reducer, affects the leak discharge behavior exponentially.

2.7 Conclusions

This chapter presented a simplified mathematical model based on physical principles for predicting the behavior of the flow of a mixture of glycerol and water in a horizontal pipeline when a leak occurs. The set of differential equations that constitute this model was programmed in MATLAB for being numerically solved and used as a simulator for different leak scenarios. Part of the numerical solution for a scenario was compared with real data obtained during

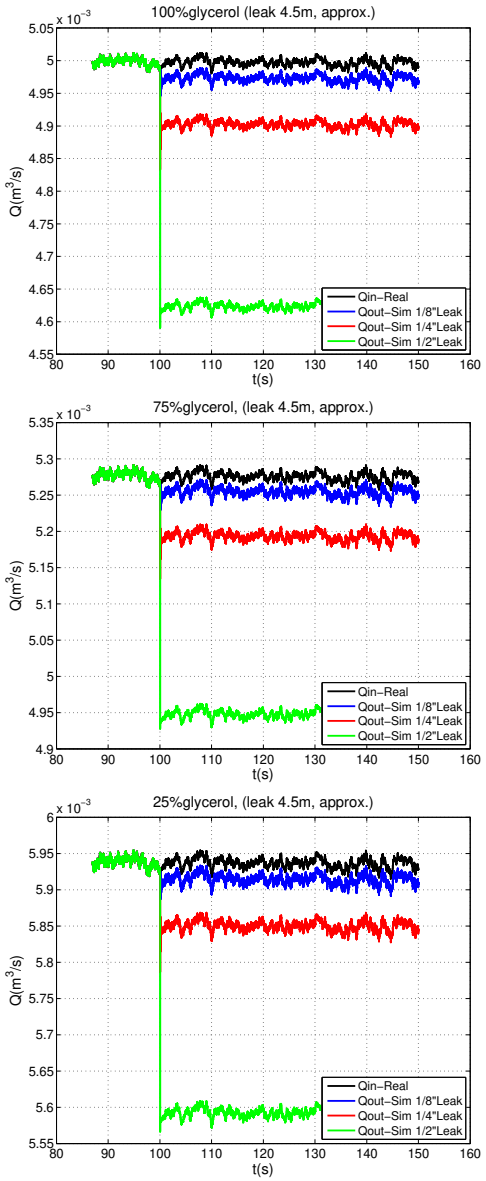

Fig. 2.14 Q at $z = L$ (m): (top) Case 1, (middle) Case 2 and (bottom) Case 3

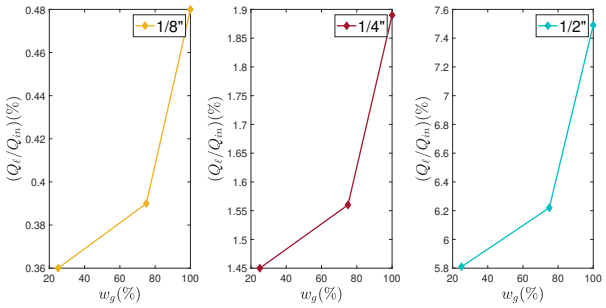

Fig. 2.15 Leak percentage ratio as function of w_g

the experimentation in a laboratory pipeline. The contribution presented in this work is the initial step for the conception and implementation of leak diagnosis algorithms for pipelines transporting fluids with high viscosity, taking into account their mixing with drag-reducing agents and the temperature effects on viscosity properties.

Chapter 3

Analysis of gradients for water-glycerol and air-glycerol mixtures

3.1 Introduction

Crude oil and its by-products can be released into the environment due to ship transport, offshore/onshore exploration, production, and pipeline transportation [2]. According to [57], oil spills are among the most serious environmental damages, affecting soils, rivers, seas, flora, fauna and all biodiversity. The impacts of crude oil have an effect of decades or even centuries. If the ecosystem is dynamic and the spill is not huge, it may take 10-20 years for the ecosystem to recover, in other cases it may take up to a century [117]. For this reason, the development of leak detection systems is important. One of the methods to detect leaks is using the calculation of the gradient, however in simulators such as the PipelineStudio® software, from Energy Solutions, which works with horizontal pipes. So it is far from the reality of pipe installations that have curved sections, elbows, etc. There are numerous works for use in horizontal pipes with single-phase flows, such as [139] and references therein.

As mentioned by the authors in [3], the pressure gradient is the most critical parameter in the liquid-liquid flow, since an accurate prediction is important to achieve an efficient operation. In the transportation of crude oil, there are studies regarding the use of a water-oil mixture to reduce pressure, but it is observed that it varies depending on the volumetric fraction of the water and varies from one system to another [161]. It is also important to characterize the flow pattern regime since one-phase models are not sufficient to correlate the pressure gradient data in all flow regimes [63]. In the history of liquid-liquid phase flow, several works has been

carried out with low-viscosity mix; [11], [140], for dispersions of the mixture; [18], [7], for stratified flow; [45], [29]. However, the emulsion viscosity is not predictable [160]. In [145] the author mention two possible causes: (1) flocculation and (2) non-uniform distribution of the phases. In general, numerous works on flow drag reducers and different models for calculating the pressure gradient are reported in the literature, as mentioned by the authors in [3].

Gas-liquid flow is a phenomenon that occurs in many stages of oil and gas production systems. It can be found, for example, in offshore and onshore pipelines [42], which, because of transporting this class of two-phase flow, are susceptible to damages such as pressure drops greater than in single-phase flow, erosion, and corrosion because of high velocities, and other mechanical problems. Therefore, the study of two-phase flows is essential to develop cutting-edge technology to keep subsea pipelines safe.

A careful investigation of the world's oil reserves data reveals that heavy oils represent many of its existing reserves. Notwithstanding, production, distribution, and transport of heavy oils, with associated gases, are technological challenges due to their high viscosity [35]. Some problems occur during heavy oil management: severe slugging, pressure pulses, and pipe vibrations. Such problems require then characterizations and models that improve the prediction of flow regimes, pressure drops, and dynamical patterns of the flow [50].

The predominant gas-heavy oil flow pattern found in most oil fields is intermittent flow, which can be defined as a liquid slugs and gas bubbles sequence [64]. This sequence leads to an intrinsically unsteady flow condition, even in a steady-state, which poses difficult problems for its characterization and prediction. The intermittent flow regime is usually divided into two sub-regimes: the plug flow or flow with elongated bubbles, in which the slugs do not carry gas, and the slug flow, in which the slugs carry many gas bubbles [19]. The intermittent flow parameters usually investigated are the slug body liquid holdup, the slug frequency, and the slug length, particularly for high-viscosity flows. It has been found, for instance, that the slug frequency increases and the slug length decrease when the viscosity increases [56], [55], [24]. In the same way, other features are particular of high-viscosity slugs. However, even when there is an obvious necessity for extensive investigation on the intermittent flow of high-viscosity fluids, the number of publications dealing with mixtures where the liquid phase has a dynamic viscosity above 1 Pa.s is still minimal [13].

The present chapter shows some introductory concepts on gradient calculus applied to leaks (section 3.2), the calculation of the pressure gradient experimentally, taking into account the equivalent length, considering a section of curved pipe and different variations in the speed of the pump for a single-phase flow (section 3.3) and coupling this calculation to a

pseudo-homogeneous mathematical model of two-phase flow (section 3.4). Also, this chapter's important contribution relies on the experimental characterization of the intermittent flow of glycerin-air through a horizontal pipeline (section 3.5). The characterization is based on the pressure gradients constructed from the pressure drops along three different flow circuit sections.

3.2 Brief theory behind gradient calculus

As mentioned by the authors in [139], there is a pressure gradient in a horizontal pipe that depends on the distance L, so when a branch or leak occurs in the pipe, the total pressure gradient (from P_{in} to P_{out}) changes with,(P_{f1}, P_{f2}) and it is possible to calculate the point where the following gradients intersect $\frac{P_{in}-P_{f1}}{\Delta Z_1}$, $\frac{P_{f1}-P_{f2}}{\Delta Z_2}$, $\frac{P_{f2}-P_{out}}{\Delta Z_3}$ and so locate the branch or leak as seen in Figure 3.1. However, when the pipeline has a curve, the continuity of the gradient is affected and this affects the leak calculations, such as those proposed in [139] or [82] among others. A review of the literature shows that to date, there is no method to correct the calculation of the pressure gradient throughout the entire pipeline when there is a curve with a single-phase flow or a two-phase flow and thus be able to implement leak detection algorithms based on pressure gradients.

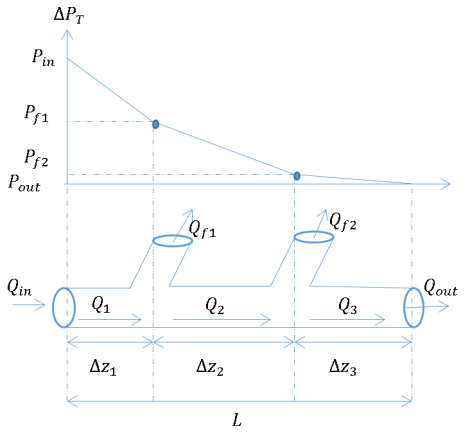

Fig. 3.1 Pressure gradients with leaks

3.3 Experimental gradient calculus for a water-glycerol mixture flow in the curve segment

This section addresses the gradient calculus developing an experiment in the test apparatus presented in chapter 2. Thus, this section shows briefly the pipe preparation before the experiment and the experimental procedure. Mext, this section presents a detailed analysis of the water-glycerol data to obtain a factor called equivalent length which is a correction to the calculus of pressure gradient in a curved section.

3.3.1 Pipe preparation:

Water is circulated through the pipe, and then compressed air is introduced for two minutes to clean the pipe; the storage tanks are washed with water and dried with compressed air for two minutes.

3.3.2 Experimental procedure:

- The pump's speed is adjusted
- The system is allowed to run for two minutes to eliminate the air trapped in the pipe and stabilize the pressure.
- Pressure, mass flow, density, and temperature data are recorded online for 3 minutes.

3.3.3 Analysis of liquid-liquid data

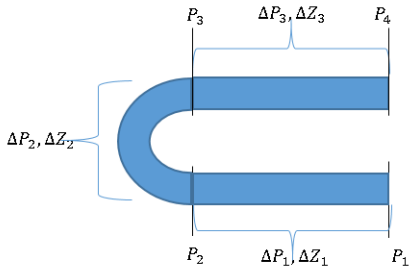

Fig. 3.2 Pipe sections analyzed

There are three pipe sections to be analyzed in the laboratory, those included between P_1, P_2, P_3, and P_4 as shown in Figure 3.2. It should be mentioned that P_5 is discarded since it is not necessary for the following analysis, so:

- $\Delta P_1 = P_1 - P_2$(Pa), is the first section.
- $\Delta P_2 = P_2 - P_3$(Pa), is the second section.
- $\Delta P_3 = P_3 - P_4$(Pa), is the third section.
- $\Delta Z_1 = 18$(m), is the first section distance.
- $\Delta Z_2 = 4$(m), is the second section distance.
- $\Delta Z_3 = 16$(m), is the third section distance.

If the pressure gradient of all pipe sections over the entire distance is graphed, it can be seen from the right section of Figure 3.3 (for pump velocity of 50Hz) that it does not behave the same as a completely horizontal pipe (this one has an almost imperceptible angle of inclination in the distance $\Delta Z = 18$ (m) different from the case of the horizontal pipe), in this way, the leak detection and location calculations based on the pressure gradient would not be correct. Therefore, it is necessary to find an equivalent length for the section of the curve so that the total gradient of all the pipe sections is not affected. Therefore, $P_3 - P_4 \approx P_1 - P_2$, so that ΔP_3 will be approximately equal to ΔP_1, following this relationship it is associated the pressure gradient of the third section with the second section as:

$$\frac{\Delta P_3}{\Delta Z_3} \approx \frac{\Delta P_2}{\lambda_2 \Delta Z_2} \tag{3.1}$$

Where the term λ_2 is the necessary adjustment to find the equivalent length over ΔZ_2. In the same way, the first pipe section is associated with the second curve section as:

$$\frac{\Delta P_1}{\Delta Z_1} \approx \frac{\Delta P_2}{\lambda_1 \Delta Z_2} \tag{3.2}$$

with these calculations two very close values are found for λ which result in two equivalent lengths. Solving for λ_1 in equation (3.2), then:

$$\lambda_1 \approx \frac{\Delta Z_1}{\Delta Z_2} \frac{\Delta P_2}{\Delta P_1} \tag{3.3}$$

in the same way, solving for λ_2 in equation (3.1):

$$\lambda_2 \approx \frac{\Delta Z_3}{\Delta Z_2}\frac{\Delta P_2}{\Delta P_3} \tag{3.4}$$

so two equivalent lengths are found:

$$Leq_1 = \lambda_1 \Delta Z_2 \tag{3.5}$$

$$Leq_2 = \lambda_2 \Delta Z_2 \tag{3.6}$$

from where:

$$LeqM = \frac{Leq1 + Leq2}{2} = \frac{\lambda_1 \Delta Z_2 + \lambda_2 \Delta Z_2}{2} = \frac{\Delta Z_2}{2}(\lambda_1 + \lambda_2) \tag{3.7}$$

Using these equations, the equivalent lengths and their average are calculated for each centrifugal pump speed, as shown in Table 3.1.

Table 3.1 Equivalent length

Hz	λ_1	λ_2	Leq_1	Leq_2	LeqM
10	1,1733	0,9158	4,6933	3,6632	4,1783
20	1,1625	0,9178	4,6500	3,6712	4,1606
30	1,1660	0,9177	4,6640	3,6709	4,1675
40	1,2110	0,9536	4,8438	3,8144	4,3291
50	1,2670	0,9988	5,0679	3,9953	4,5316

With these results, the pipe's total gradient is calculated again (for pump velocity of 50Hz), and a perfect alignment is observed, as shown in blue color line of Figure 3.3.

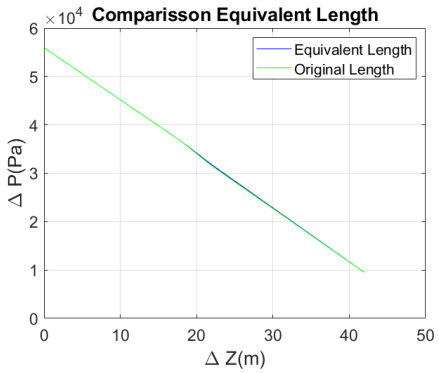

Fig. 3.3 Pressure gradient for the original length and for the equivalent length correction

The average equivalent length L_{eqM} for the different flow velocities changes as shown in Figure 3.4. In this way, there is an autotune factor for implementing the algorithm in [111] pipelines with curved sections.

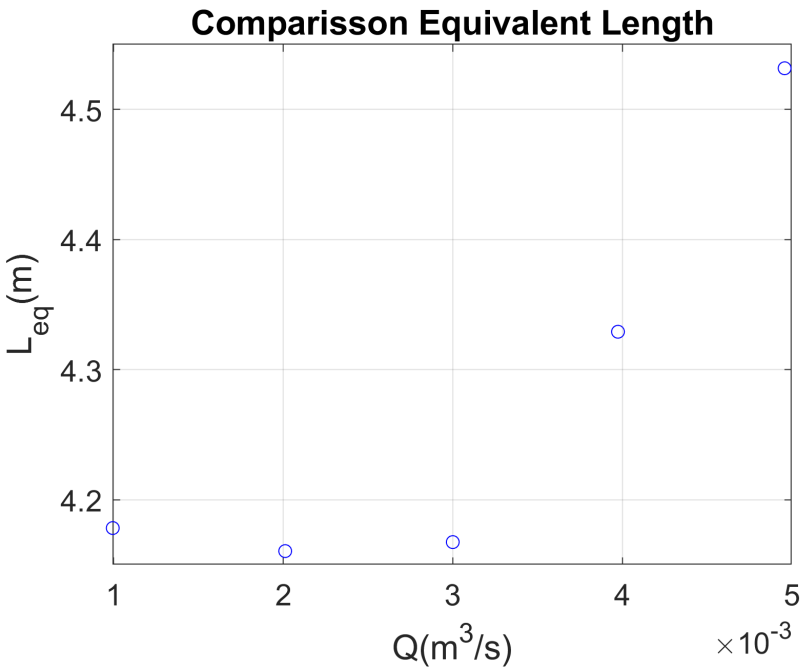

Fig. 3.4 L_{eq} for pump speed variations.

3.4 Results

The experimental test's goal described here below was getting real data to evaluate the computational model's accuracy described in chapter 2 with the equivalent length curve adjustment from previous section. The experimental data also can be found in [112] to reproduce the results presented in this work.

To begin the experiment, pure glycerin was injected into the test pipeline at the following flow rate: $Q_{in} = 5.95 \times 10^{-3}$ (m^3/s). The temperature registered during the experiment for the flow was 33°C. The dynamic viscosity of the pure glycerol is approximately $\mu_g = 0.4723$ Pa·s (472.3cP) at this temperature.

The transducer P_3 recorded the pressure at the end of the curve segment during the experiment, and it is the blue signal shown in Figure 3.5, whereas the recorded flow rate at the inlet of the pipe is colored green in the same figure. Both recordings correspond to the input to

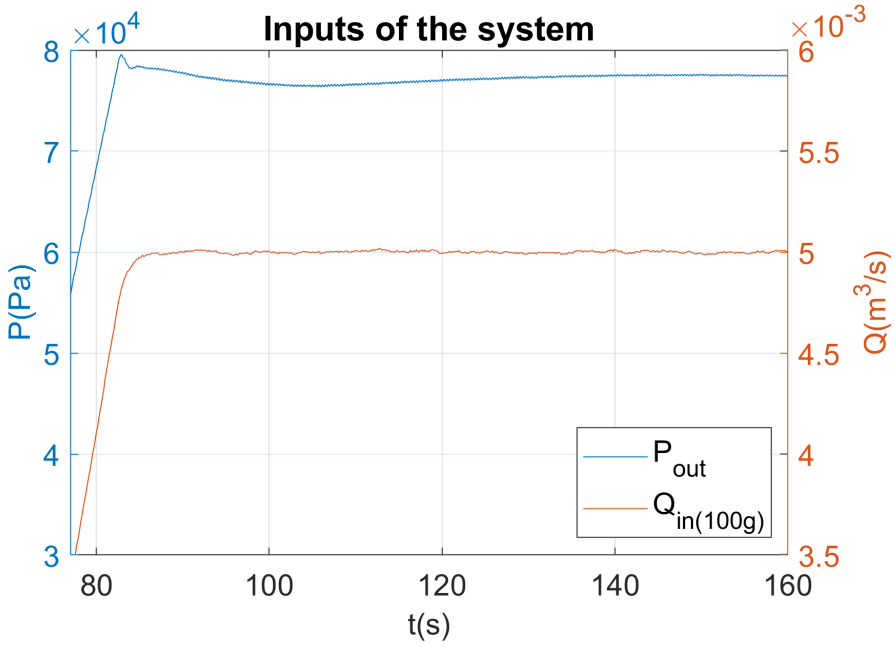

Fig. 3.5 Boundary conditions 100% glycerol

the numerical simulator as boundary conditions. Since no leak was simulated, the flow rate prediction in all of the steady-state spatial domains is the same as the flow rate in the boundary condition.

Using the equivalent length proposed in the previous section improves the inlet pressure prediction by 0.5 KPa approximately. As it is shown in Figure 3.6, the predicted pressure at the entrance of the curved segment $z = 0$, denoted as P_{in}-Sim, is shown together with the pressure measured by the transducer P_2, denoted as P_{in}-Real. The relative error between both pressures (Figure 3.7) is smaller when the length is adjusted using the proposed method.

3.4.1 Statistical t-test

In the Figure 3.6, the values of P_{in}-sim-Adjusted (renamed now $P_{in}Adj$ to avoid confusion later) can be compared with the values of P_{in}-Real (renamed now $P_{in}R$ to avoid confusion later) by mean of a T-test, so the model is robust with the adjustment for the calculus of the inlet pressure to the pipeline curved section. The T-test is defined like;

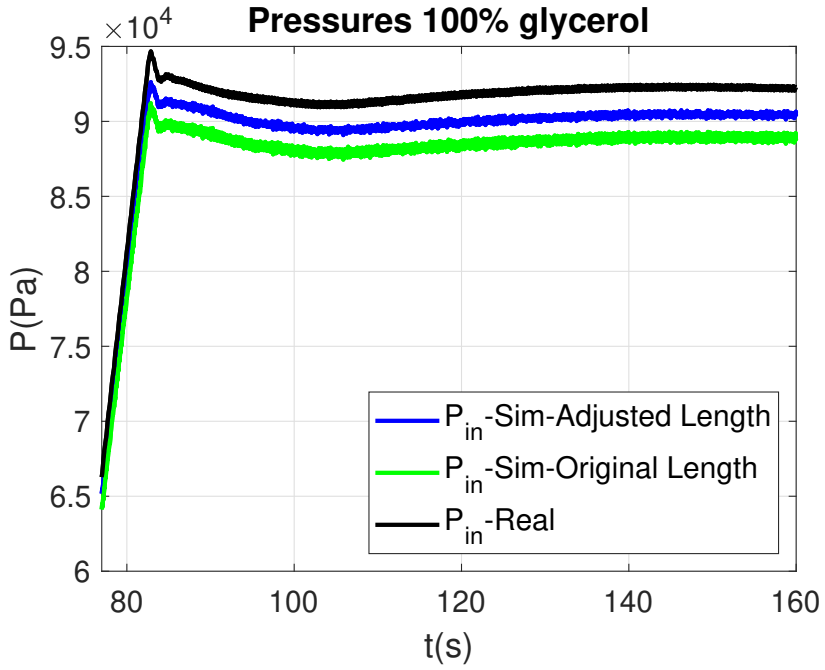

Fig. 3.6 Numerical solution for pressure at $z = 0$ vs. pressure measured by P_2 for the original and adjusted curved segment length

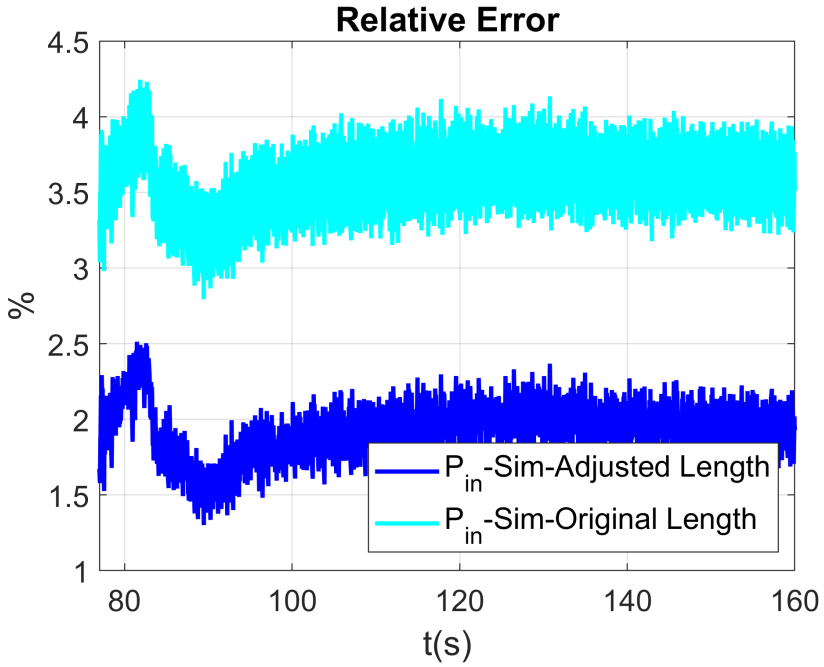

Fig. 3.7 Relative error

$$t_o = \frac{d}{S_d/\sqrt{n}} \tag{3.8}$$

where;

- $d = P_{in}R - P_{in}Adj$
- $S_d = \sqrt{\frac{d_i - \bar{d}}{n-1}}$ is the standard deviation
- n is the number of samples

First, the data from $P_{in}Adj$ and $P_{in}R$ are organized from time $t = 63.77$ (s) because before this time, the pipeline is empty and the data collected are noisy data from sensors. Table 3.2 was automatically obtained from an Excel file. The selected test is for two paired samples because the model must predict everything in steady-state and dynamics. The t-test tests the hypothesis that the mean of $P_{in}R - P_{in}Adj$ is equal to 0 ($H_0 : \mu_d = 0$) versus the alternate hypothesis that the mean of $P_{in}R - P_{in}Adj$ is not equal to 0 ($H_0 : \mu_d \neq 0$). Because the P-value in the Table 3.2 for this test is less than 0.05, the null hypothesis can be rejected with 95.0% confidence. This result shows that the difference between the means of $P_{in}Adj$ and $P_{in}R$ is not zero, then the results of the model adjusted for the curve is not statistically equal to the real values of the pressure inputs. But it is necessary to know if there is a threshold value in which it is possible to state that the model is accepted. So, the Table 3.2 shows that the T statistic is a negative value ($t_o = -206.0911$), which is above the critical value of t ($t_c = 1.961$) or above the minimal value of acceptance region, falling in this way in the region of rejection of H_0. Then, exist a value of D where T statistic is equal to the critical value of t ($t_o = t_c$). This value was found using the tool solver in Excel. So, $D = 1477.6$ (Pa) or $D = 0.21$ (psi). If this difference can be accepted inside the normal operating conditions, then a robust model is statistically equal to represent input pressure's real data.

3.4.2 The adjusted model

Using the pipe length adjustment for the curved segment, the following tests using the computational model were performed to study the glycerol-water mixture flow when a leak occurs. Three study cases were considered: (1) only glycerol, (2) mixture with 75% of glycerol, and (3) mixture with 25% of glycerol. The flow rate used as a boundary condition at the curved segment entrance $z = 0$ for the first case was the plotted one in Figure 3.5, whereas Figure 3.8

Table 3.2 T-test for means of two paired samples.

	$P_{in}Adj$	$P_{in}R$
Mean	86615.0867	88106.9111
Variance	217756001.2	224235314.2
Observations	2364	2364
Pearson's correlation coefficient	0.999827183	
Hypothetical difference of means	0	
Degrees of freedom	2363	
T statistic (t_o)	-206.0911	
P(T<=t) two tails	0	
Critical value of t (t_c, two-tailed)	1.961	

presents the flow rates for the second and third cases. The pressure signal shown in Figure 3.5 was used as a boundary condition at the curved segment exit $z = L$ for the three cases. A leak was modeled, modifying the continuity equation to include the leak's flow rate in the flow rate balance. The leak area's flow rate is found using Torricelli's equation, depending on the discharge factor, the leak area, and the pressure head at the leak position.

$$\dot{P}_i = -\frac{\rho(T)b^2}{A_r}\left(\frac{Q_{i+1} - Q_i - Q_\ell}{\Delta z_i}\right) \tag{3.9}$$

where Q_ℓ is the flow rate of the leak, which is expressed by the Torricelli's equation given as follows

$$Q_\ell = C_\ell A_\ell \sqrt{2gH_\ell} \tag{3.10}$$

where C_ℓ is the discharge factor, A_ℓ is the leak area, $H_\ell = P_\ell / g\rho(T)$ is the pressure head at the leak position z_ℓ, and P_ℓ is the pressure at z_ℓ.

Using the adjusted length proposed in this work, the numerical model can predict pressures for each spatial step of the curved segment in each simulated case. Three leaks with different flow rates located at $z = 1$ (m) were simulated. Only the results for the case with a mixture of 75% of glycerol is illustrated in Figure. 3.9

It is noteworthy to mention that the mixture's kinematic viscosity has exponential behavior concerning the glycerol fraction, which affects the pressure predicted by all study cases, as shown in Figure 3.10. In this way, the predicted pressure for pure glycerol is much higher than the predicted pressure when a fraction of glycerol is used, as seen on Figure 3.11.

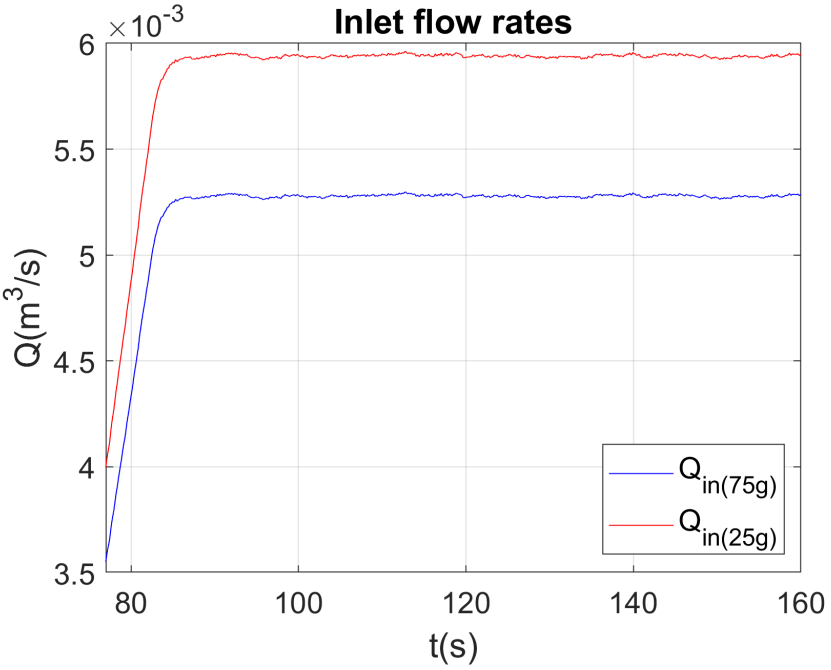

Fig. 3.8 Boundary conditions 75% glycerol and 25% glycerol

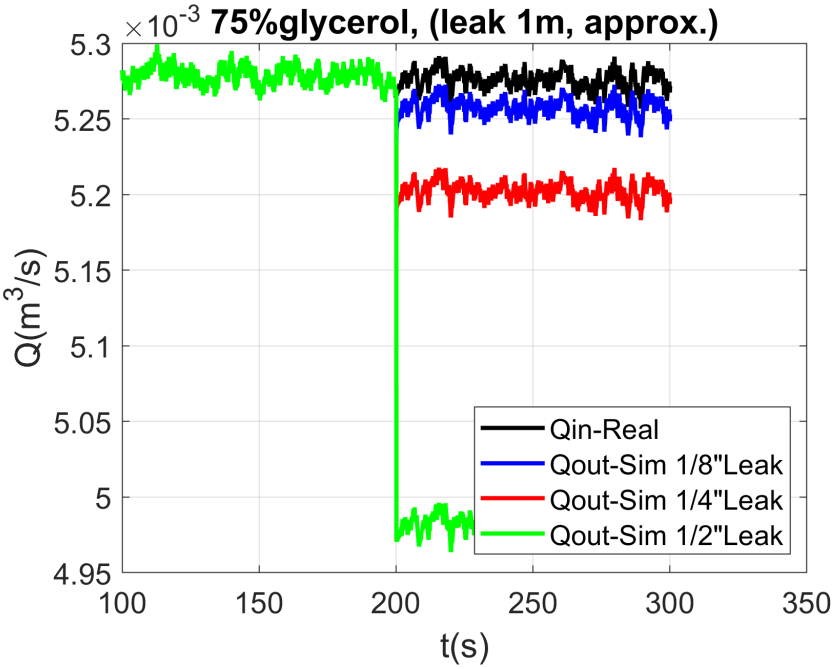

Fig. 3.9 Simulated flow rates at the end of the curved segment and leaks of different size using the adjusted length correction for case (2) mixture with 75% of glycerol

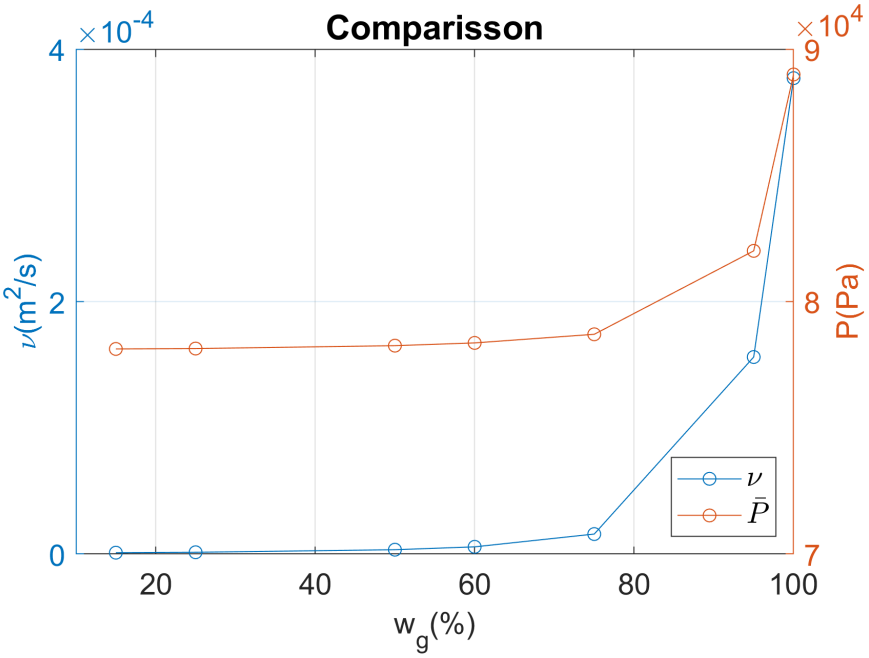

Fig. 3.10 Kinematic viscosity and pressure as functions of w_g

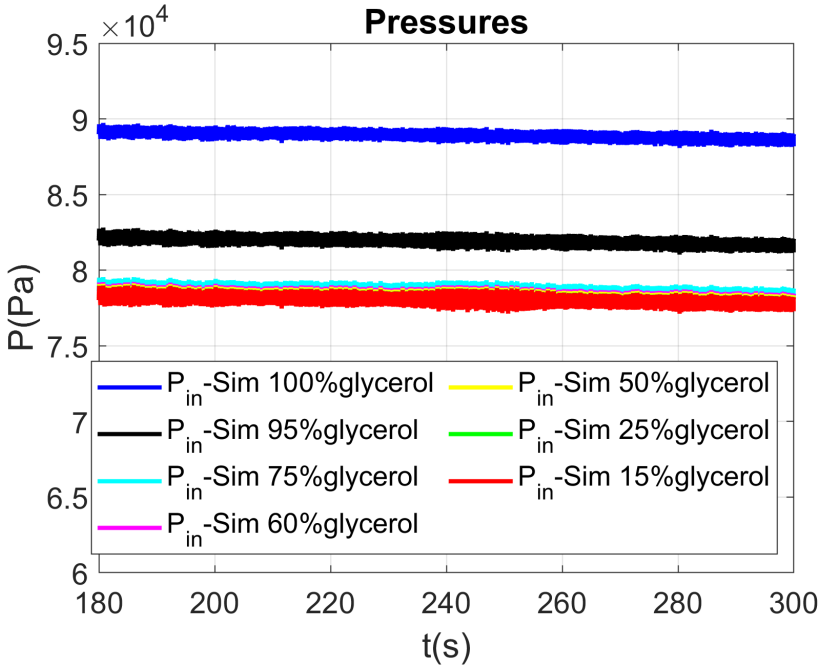

Fig. 3.11 Numerical solution for pressure at the input of the curved segment $z = 0$ for different fractions of glycerol

3.5 Experimental gradient calculus for the air-glycerol mixture flow in the horizontal segment

This section presents the experimental methods to gather the data from the pressure transducers with an special combination of different inlet mass flows for liquid and gas mixture. Also, this section presents a characterization of pressure gradients taking into account an root means square (RMS) Euler number weighted with the flow rates ratio.

3.5.1 Experimental methods

The experiments were produced following the (inlet) mass flow rates indicated in Table 3.3. Nine flow rate combinations (Q_l, Q_g) were considered. The resulting mixture was discharged into a separator tank. Care was taken to avoid recycling glycerin with gas bubbles that were entrained due to the mixing process.

Table 3.3 Liquid and gas mass-flow-rates (in kg/s) and superficial velocities (in m/s). v_{sg} varies within the indicated maximum and minimum values.

Q_l	v_{sl}	Q_g	v_{sg}	
			max	min
1.3	0.23	0.005	0.99	0.73
3.7	0.68	0.02	3.98	2.93
6.1	1.11	0.03	5.98	4.40

MEAS U5300 pressure transducers were installed at 0, 18, 22, and 43 m, downstream from the inlet (Figure 2.4). All pressures were measured with an accuracy of 0.1% within the 0.0 to 3.45×10^5 Pa interval. The mixture's temperature was simultaneously measured near the inlet and outlet planes of the pipe, employing type-K thermocouples with a resolution of 0.5 °C. Besides, samples of the mixtures were extracted during each test to verify their actual viscosity values with a Brookfield DV2T viscometer.

The experiments were carried out according to the following procedure: (a) the glycerin was pumped at the selected Q_l until a steady-state was reached, (b) the air was injected with the prescribed Q_g, (c) the mixture was allowed to evolve until the average pressure value registered at the inlet reached a stationary value, (d) the measurements were registered with the IMC Chronos-Flex CRFX-2000 acquisition system, and (e) the collected data was processed in a PC.

Table 3.4 shows the definitions required for the pressure gradients' computations reported in the results section. Obviously, the values of the pressure drop in each leg depending on the actual measurements.

Table 3.4 Length and pressure drop in each test section's leg.

Item	Definition	Value	Units
Δx_1	$x_{P2} - x_{P1}$	18	
Δx_2	$x_{P3} - x_{P2}$	4	m
Δx_3	$x_{P4} - x_{P3}$	21	
ΔP_{12}	$P_1 - P_2$	-	
ΔP_{23}	$P_2 - P_3$	-	Pa
ΔP_{34}	$P_3 - P_4$	-	

3.5.2 Characterization of pressure gradients

Various efforts have been made to obtain a unique correlation to predict the pressure gradient in a two-phase flow similar to single-phase flow. Any proposed correlation should preferably be expressed using dimensionless parameters and present data on a single graph. In particular, finding dimensionless parameters to simplify correlations is significant. Taking into account the work of Al-Sarkhi and Sarica [6], a new correlation with two dimensionless parameters is proposed: the Euler number Eu and the mass flow rate ratio Q_l/Q_g. Previously, the pressure gradients' behavior along Δx_1, Δx_2 and Δx_3 for the different combinations of Q_l and Q_g was considered, to provide the proper context.

Generally speaking, the average pressure gradients are different in each of the three sections of the pipeline. Figure 3.12 illustrates this situation with plots for ΔP_{12}, ΔP_{23} and ΔP_{34} for all combinations of glycerin and air mass flows rates.

The specific $\Delta P_i/\Delta x_i$ values summarized in Table 3.5 and Table 3.6 led to the following observation: the greatest differences between pressure gradients are produced with the highest liquid and gas mass flow rates.

Figure 3.13 shows the average pressure gradients as a function of the mixture velocity, $v_m = v_{sg} + v_{sl}$ (where $v_{sl} = 4Q_l/(\rho_l \pi D^2)$ and $v_{sg} = 4Q_g/(\rho_g \pi D^2)$ are the superficial liquid and gas velocities). The gradients are similar for low v_m values but exhibit substantial differences at higher velocities. In the latter case, the average pressure values cease to represent good estimates because the elevated number of fluctuations produces a wider statistical dispersion. Therefore, a more meaningful measure of the pressure drop may be defined in terms of a Root Mean Square (or RMS) value that considers the statistical dispersion. Then:

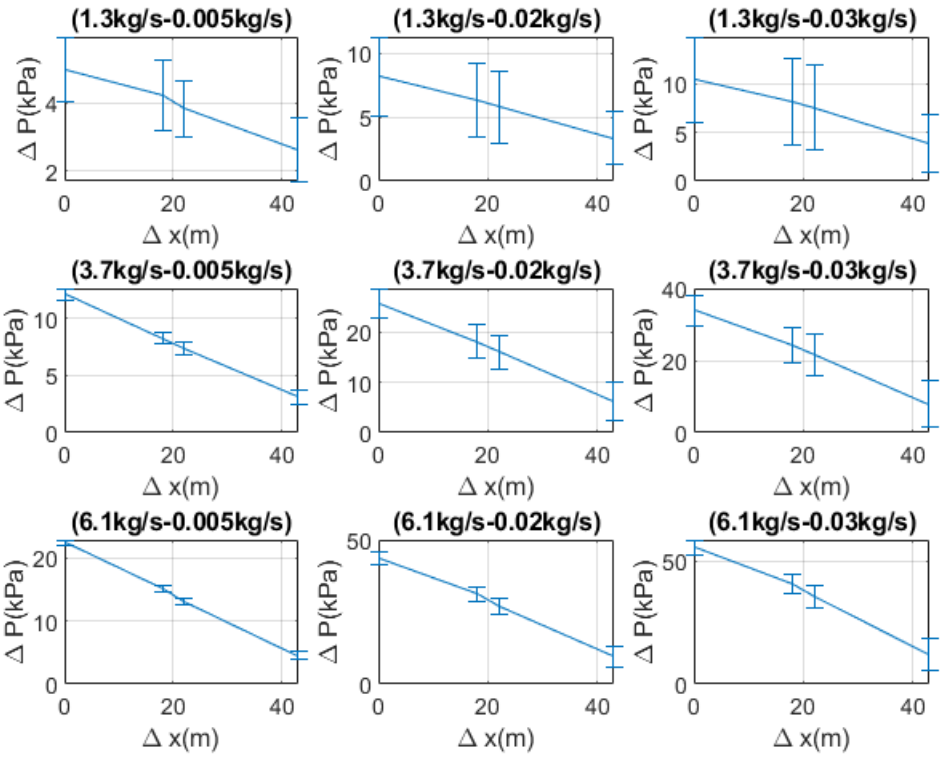

Fig. 3.12 Average pressure drop computed with the data from the set of experiments A.

Table 3.5 Pressure gradients along Δx_1 and Δx_3, in terms of Q_l and Q_g (in kg/s), for experiment A.

Q_g	0.005		0.02		0.03	
Q_l	$\Delta P_{12}/\Delta x_1$	$\Delta P_{34}/\Delta x_3$	$\Delta P_{12}/\Delta x_1$	$\Delta P_{34}/\Delta x_3$	$\Delta P_{12}/\Delta x_1$	$\Delta P_{34}/\Delta x_3$
1.3	0.04	0.06	0.1	0.12	0.12	0.17
3.7	0.21	0.2	0.42	0.47	0.53	0.64
6.1	0.4	0.41	0.69	0.84	0.83	1.11

$$\left(\frac{\Delta P_{ij}}{\Delta x_i}\right)_{RMS} = \sqrt{\overline{\Delta P_{ij}}^2 + \sigma^2_{\Delta P_{ij}}} \tag{3.11}$$

Here, $\overline{\Delta P_{ij}}$ is the arithmetic mean, and $\sigma_{\Delta P_{ij}}$ is the standard deviation of the data. As shown in Figure 3.14, this estimate underlines the significance of the fluctuations concerning the average pressure in each leg of the pipe.

Table 3.6 Pressure gradients along Δx_1 and Δx_3, in terms of Q_l and Q_g (in kg/s), for experiment B.

Q_g	0.005		0.02		0.03	
Q_l	$\Delta P_{12}/\Delta x_1$	$\Delta P_{34}/\Delta x_3$	$\Delta P_{12}/\Delta x_1$	$\Delta P_{34}/\Delta x_3$	$\Delta P_{12}/\Delta x_1$	$\Delta P_{34}/\Delta x_3$
1.3	0.04	0.06	0.11	0.12	0.13	0.17
3.7	0.21	0.2	0.42	0.46	0.52	0.64
6.1	0.41	0.41	0.69	0.84	0.83	1.1

In 1994 Wambsganss et al. considered RMS values of the pressure drop to identify intermittent flow pattern transitions [152]. They detected an increase of the RMS pressure drop in the plug-bubble flow regime, followed by a sharp increase during the transition to the slug flow pattern. More recently, in 2002, Wang and Shoji used the RMS value to investigate the fluctuation characteristics of a two-phase flow splitting at a T-junction [153] by analyzing the RMS differential pressures.

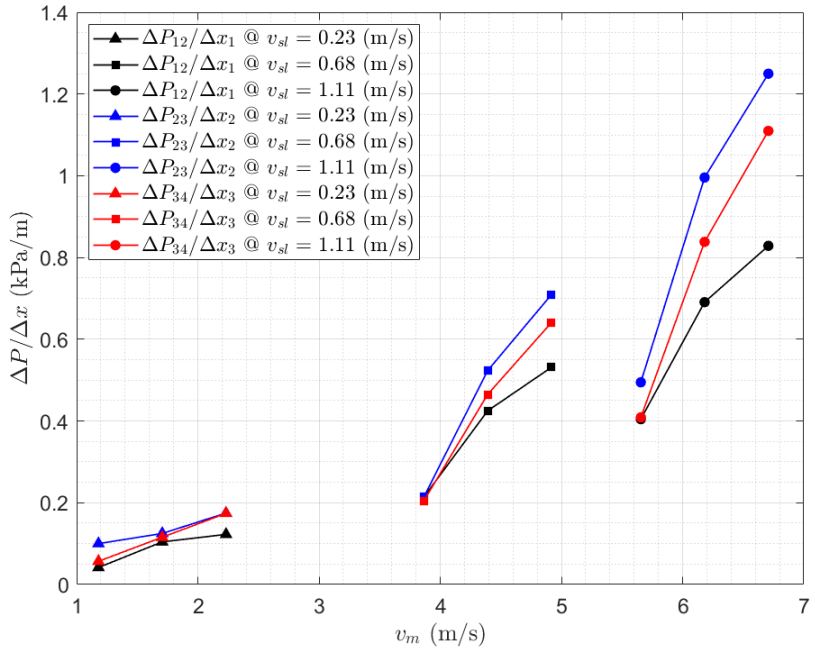

Fig. 3.13 Pressure gradients (mean)

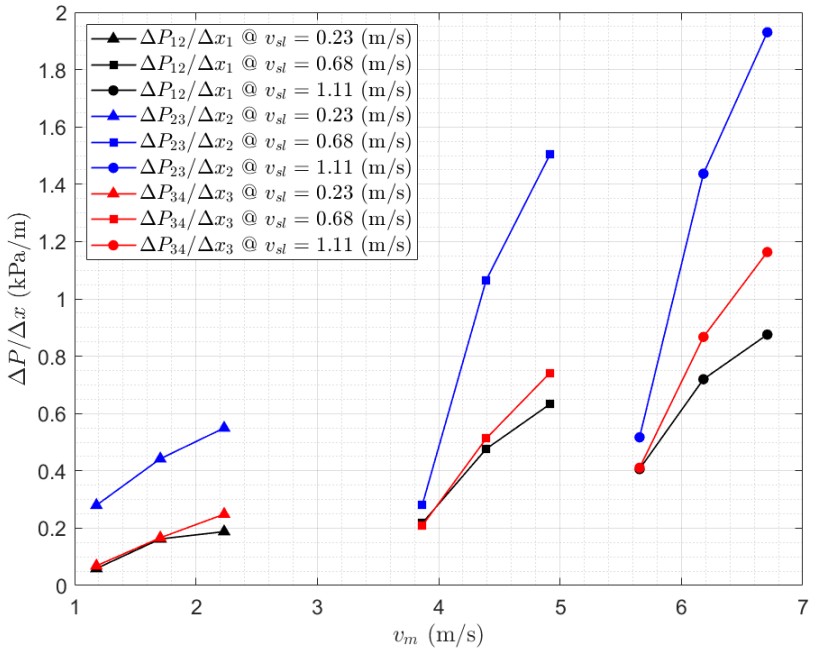

Fig. 3.14 Pressure gradients (rms)

Furthermore, since $\Delta P/\Delta x \sim \rho v^2/D$, an analogous scaling for the high-viscosity, two-phase flow can be defined as $(\Delta P_{ij}/\Delta x_i) \sim \overline{\rho_m} v_m^2/D$ (with $\overline{\rho_m}$ denoting the average mixture density). Thus the empirical correlation is:

$$\mathrm{Eu}_i = a\left(\frac{Q_l}{Q_g}\right)^b \tag{3.12}$$

where Eu_i represents the two-phase, RMS Euler number of the i-th section

$$\mathrm{Eu}_i \doteq \left(\frac{\Delta P_{ij}}{1/2\,\overline{\rho_m} v_m^2}\right)_{RMS} \tag{3.13}$$

The regression parameters a and b can be estimated employing the least square method. To consider the behavior of the pressure gradient explicitly, then equation (3.12) is rewrite in the following manner:

$$\left(\frac{\Delta P_{ij}}{\Delta x_i}\right)_{RMS} = a\left(\frac{Q_l}{Q_g}\right)^b \left(\frac{\overline{\rho_m}\, {v_m}^2}{2\,D}\right) \tag{3.14}$$

From the physical viewpoint, the right-hand side of equation (3.14) can be considered as the RMS interplay between the hydrodynamic head and the viscous losses. Thus, a serves as a kind of two-phase loss coefficient, weighted by some power of the ratio Q_l/Q_g. The estimated numerical values of the regression parameters a and b are summarized in Table 3.7 for the indicated mixture velocity (v_m). Accordingly, Figures 3.15(a) to 3.15(c) show the scaled pressure gradient (i.e. Eu_i) as a function of the ratio Q_l/Q_g.

Table 3.7 Regression parameters for the RMS Euler numbers at a given v_{sl} (from the data set of Exp. B).

v_{sl} (m/s)	Eu_1	Eu_2	Eu_3
0.2376 (m/s)	$a = 0.0053$ $b = 1$	$a = 6.0697 \times 10^{-4}$ $b = 1.4$	$a = 0.0072$ $b = 1$
0.6761 (m/s)	$a = 0.0070$ $b = 0.9$	$a = 0.0242$ $b = 0.5225$	$a = 0.0161$ $b = 0.7893$
1.1147 (m/s)	$a = 0.0051$ $b = 0.9$	$a = 0.0198$ $b = 0.5299$	$a = 0.0241$ $b = 0.7032$

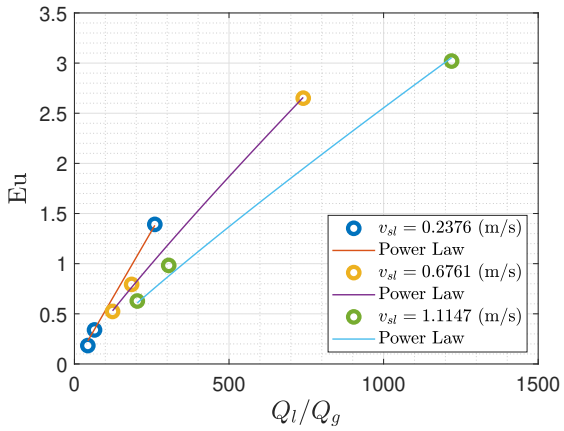

(a)

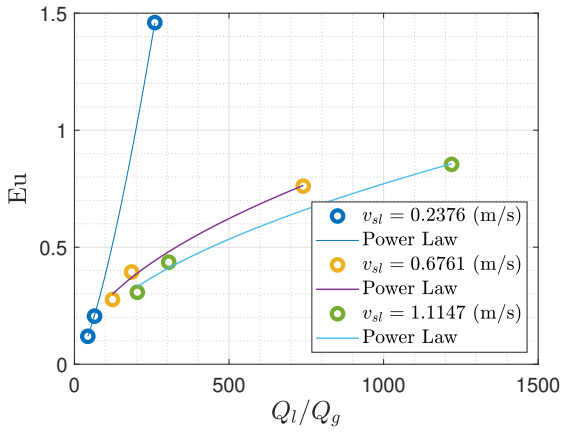

(b)

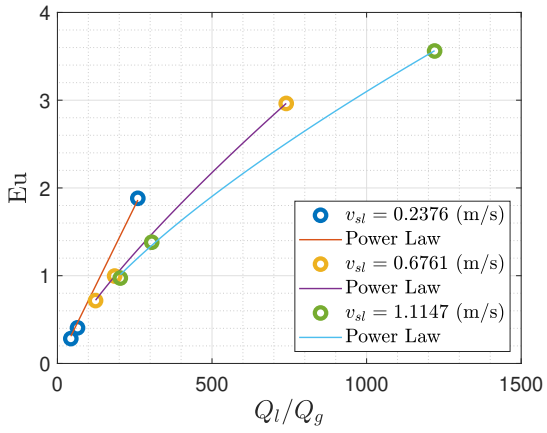

(c)

Fig. 3.15 Predictions for the Euler number obtained with equation (3.14) and the data set of Experiment B. Respectively, image (a) corresponds to the first column in Table 3.7, (b) corresponds to the second column, and (c) to the third column.

According to Figure 3.15(a), Eu_i exhibits a nearly linear dependence for the ratio Q_l/Q_g in the upstream section of the pipe. The low gas content in the mixture implies steeper pressure gradients because the liquid friction is dominant. In contrast, the linear dependence is lost in the U-section, except at low mixture velocities (Figure 3.15(b)). For moderate and intermediate v_m, the data are proportional to a near square root of Q_l/Q_g. In the downstream section of the pipe, Eu_i follows similar trends as those observed in the upstream section (Figure 3.15(c)). However, the overall values of Eu_i (hence of the pressure gradient) are higher in this section. Again, this is indicative of the effect produced by the slug ejection process at the outlet.

3.6 Conclusions

The work presents the calculation of the equivalent lengths and the pressure gradient for a curved pipe section for the monophasic glycerine flow. The importance of the work lies in its utility to improve the design of leak detection systems in curved sections based on the pressure gradient and to consider single-phase flow, as is the case in the oil sector, so there is an automatic tune factor (L_{eq}) to make the gradient and pressure correction in pipeline curved sections. The improvement of the leak detection and location systems is an important aspect for controlling damages caused by the hydrocarbon leak. Other researchers can use the analysis to validate models for describing glycerol flow in pressurized horizontal pipelines. The similarity of the viscosity of pure glycerol ($\approx$ 1.5 Pa.s) and extra-heavy crude ($\approx$ 1.0 Pa.s) provides the possibility to perform laboratory experiments for the research of extra-heavy oils safely.

The research of extra-heavy oils is critical in the petroleum industry because of the enormous increase in oil demand and the progressive exhaustion of low-viscosity oil reservoirs. Nevertheless, production, distribution, transport, blending, and the conditioning process of such crude oils are technological challenges due to their very high viscosity. This analysis can be used to validate pipeline dynamic models and improve the accuracy of leak detection systems. Model-based leak detection approaches are explained in detail in [82]. In particular, the transportation of heavy and extra-heavy crude oils through pipelines from the head-well to the refinery is difficult due to the low mobility and fluency of the crude, so this analysis can be used to compare the pressures and mass flow of the laboratory pipeline prototype with similar cases in the petroleum industry.

A series of high-viscosity, two-phase flow experiments were conducted in a flow loop with a length-to-diameter ratio $L/D \approx 700$. Because of this relatively high ratio, the flow developed for a longer time and revealed unique dynamical effects on pressure gradients. The mixtures

under consideration were produced with several mass-flow-rate combinations of air and glycerin.

The root means square (or RMS) values of the pressure gradients were calculated to adequately account for the pipe's pressure fluctuations. The corresponding plots show that some flow system elements (e.g., like the U-section) may significantly impact the pressure drop. To estimate the RMS pressure gradient in any section of the pipe, a simple correlation is proposed based on an RMS Euler number weighted with the flow rates ratio. The regression parameters are provided together with the corresponding computations for the experiments here reported.

Chapter 4

Slug prediction and statistical analysis for air-glycerol flow

4.1 Introduction

Highly viscous gas-liquid flows occur in regions where extra-heavy oils constitute a relevant share of the actual production [99]. According to recent estimates, nearly 50% of the technically recoverable heavy oil reserves have gravities below 15° API, while the fields producing them are observed to grow 5 times faster than the fields producing conventional (i.e., high API) crude oils [126, 103]. However, because of their particular composition and viscosity, flows of this type present challenging problems during the onshore and offshore pipelines [30, 114, 124].

Apart from the flow assurance problems caused by solid deposits and scaling, high viscosity flows entail an increased damaging potential to the transportation system. Chronic pipe fatigue and corrosion and erosion processes enhanced by high intermittent pressures may lead to failures with severe economic and environmental consequences (e.g. [156, 23, 132]). A recent survey indicates that much of the work has focused on improving models, measuring techniques, and control methods. Deepwater applications are particularly challenging [114]. This review's salient point is the lack of robustness of the flow control methods, ultimately related to the slugging processes.

Work carried out along these lines clearly shows that high-viscosity regimes are characterized by flow patterns that differ from those previously established for low viscosity mixtures. In fact, most of the available experimental evidence suggests that the predominant pattern is

intermittent in nature [162, 19, 64]. Under these circumstances, the relevant flow parameters exhibit a strong dependence on the viscosity of the mixture [56, 55, 24, 65].

For example, the liquid holdup in the slug body increases with increasing superficial liquid velocity but decreases with increasing superficial gas velocities [10]. This is valid at least in liquid viscosity interval from 0.189 to 8.0 Pa.s. The gaseous entrainment mechanisms have also been researched. To this end, the PIV measuring technique has been applied to analyze the bubble trajectories inside the slug body [85].

Another set of experiments carried out with oil-air mixtures, whose viscosities ranged from 1.0 to 5.5 Pa.s, showed that the slug length decreases with increasing viscosity [12]. The length was found to be sensitive to changes in the viscosity. Similarly, the bubble velocity and other slug properties have been the subject of dedicated analysis and modeling. In the high-viscosity interval from 0.1 to 1.0 Pa.s, the bubble velocity can still be predicted by the Nicklin et al. correlation with corrections for the radial distribution coefficient and drift velocity in terms of the Froude number [17]. The present work is concerned with the characteristic fluctuations of the pressure and the velocity fields produced by hydrodynamic slugging. The two-phase flow consists of a glycerin-air mixture with a viscosity of 0.9 Pa.s, which evolves in a horizontal pipe with a relatively large length-to-diameter ratio. The characterization is based on the statistical moments of the corresponding probability distributions obtained from the time-series for the pressure collected at three different sections along the pipe.

This chapter presents the experimental setup for the analysis of pressure signals (section 4.2). Algorithms for two-level waveforms are used for analyzing the intermittency of the pressure signals. From this analysis, three results are presented (section 4.3): (1) the characteristics of differential pressures time series, (2) the calibration of a well-known model for predicting the frequency of slugs and (3) Statistical characterization taking into account: descriptive statistics, normality tests and a gaussian mixture model

4.2 Experimental setup

Experimental tests were conducted in the same flow circuit described in the chapter 2, specially designed and constructed to study the long-term evolution of multi-phase flows.

The fluids used in this experiment were glycerin (dynamic viscosity $\mu = 1.1$ Pa.s (1,100 cP) at a room temperature of 25 °C, density $\rho = 1.2 \times 10^3$ kg/m^3 and interfacial tension $\sigma = 6.2 \times 10^{-2}$ N/m) and air (dynamic viscosity $\mu = 1.8 \times 10^{-5}$ Pa.s and density $\rho = 1.2$ kg/m^3). The glycerin was injected into the test section by a progressive cavity pump (Seepex

Mod. BN35-24), while the air was supplied by a twin-scroll Kaeser Aircenter SK.2 Compressor. The mass flow rate of air was tuned with a regulator and globe valves. The mixture was produced at the 3-way connection tube shown in Figure 2.4.

4.2.1 Measurement procedure

Both mass flow rates were measured at the inlet with Endress-Hauser Coriolis meters. The Promass 83F80 DN80 3" model used with the glycerine had an accuracy of 0.1% across the entire measuring range. Similarly, the Promass 83F50 DN50 2" model used with the air had an accuracy of 0.05% across the entire measuring range. Also, all the pressures were measured with an array of conventional MEAS U5300 transducers with a resolution of 0.1% across their measuring ranges.

The experiments were produced following the inlet mass flow rates indicated in Table 4.2, where Q_l denotes the mass flow rate of glycerin, whereas Q_g the mass flow rate of air. In total, nine different combinations of mass flow rate pairs (Q_g, Q_l) were considered, and several experiments were conducted for each one of them.

The quality ratio for each combination, which is the ratio of the gas mass flow rate to the total mass flow rate across a given area, are listed in Table 4.1.

Table 4.1 Quality ratio Q_g/Q_l

	Q_g: 0.005 (kg/s)	Q_g: 0.02 (kg/s)	Q_g: 0.03 (kg/s)
Q_l: 1.3 (kg/s)	0.0038	0.0076	0.0115
Q_l: 3.7 (kg/s)	0.0013	0.0027	0.0040
Q_l: 6.1 (kg/s)	0.0008	0.0016	0.0024

Table 4.2 Experiments set up

Q_g (kg/s)	Q_l (kg/s)
0.005	1.3
0.02	3.7
0.03	6.1

To characterize the two-phase flow, differential pressures were used, which were computed from different pressure time-series records. The pressure for measuring the ports was located at 0, 18, 22, and 43 m, downstream from the inlet. These ports were labeled with P_1, P_2, P_3, and P_4, respectively, in Figure 2.4. Here below, the nomenclature for the pressure drops and test sections is defined.

- $\Delta x_1 = 18$ (m): the length of the first section.
- $\Delta x_2 = 4$ (m): the length of the second section.
- $\Delta x_3 = 21$ (m): the length of the third section.
- $\Delta P_{12} = P_1 - P_2$ (kPa): pressure drop across Δx_1.
- $\Delta P_{23} = P_2 - P_3$ (kPa): pressure drop across Δx_2 (the curve).
- $\Delta P_{34} = P_3 - P_4$ (kPa): pressure drop across Δx_3.

4.3 Results

This section presents the characteristics of differential pressures time series across the three sections of pipe laboratory. Also, in this section a slug frequency prediction model is proposed taking into account the Manolis model and finally statistical analysis is developed based on descriptive statistics, normality tests and a gaussian mixture model to detect bimodality.

4.3.1 Singal's intermittency and flow characteristics

Everywhere along the pipeline, the pressure time series present a particular behavior known as *on-off intermittency*. The term is applied in this context to distinguish between the flat- and the spiky-time segments of the signal, rather than the properties of the flow itself [116]. The *off*-states correspond to fluctuation patterns with nearly constant low-amplitude bounds. Depending on the flow rates, these states may persist for prolonged periods of time. In contrast, the *on*-states correspond to short-duration bursts whereby the fluctuations undergo sharp departures' amplitude levels of the *off*-states [61]. The significance of the corresponding peak amplitudes deserves special consideration in certain situations (e.g., when modifications to a given system or its operating conditions are required).

For ($Q_l = 1.3$, $Q_g = 0.005$) kg/s the pressure drop shows the unsteady bursts (*on*-states) occurring between quiescent periods of time (*off*-states), as can be seen in upper row images of Figure 4.1. From the flow's point of view, the signal is related to the alternate passage of elongated bubbles and liquid slugs. The discussion on the occurrence of the pressure peaks caused by slug and plug flows is well known [91], [90]. When a slug moves to a certain position, the local pressure at that point increases sharply because the liquid body obstructs

the cross-section. Thus, the upstream section of the pipe remains pressurized until the liquid slugs' ejection relieves some of the excess pressure. If it is assumed that the frictional losses are mostly due to the liquid phase, then the pressure rises from the mixing front of the slug's body to its tail, where it reaches a maximum that tends to remain constant. This summary embodies the slug blockage concept and its effect on the local pressure [91].

While the foregoing description gives a valid account of the basic processes, the high-viscosity regime calls for further consideration of the observed phenomena. For instance, the wide variation of the pressures must be understood in terms of the slugs units' system (i.e., slug bodies and bubbles) and the phases' local volume fractions.

Furthermore, because the frictional effects are exacerbated in the high viscosity regime, the pipe pressure must build up accordingly to overcome the total head loss. This entails an effective increase of the energy distributed throughout the system of slug units. Under these circumstances, an unsteady process is triggered by the liquid bodies' ejection through the pipeline's discharge plane. As soon as the slug leaves the test section, the trailing bubble depressurizes rapidly to acquire (approximately) the outlet pressure. This results in the generation of a rarefaction wave that propagates upstream, forcing the remaining slug units to recoil successively. With the shortening of the separations between slugs, the bubbles' gas undergoes further compression, and the energy ceases to remain uniformly distributed. To restore the uniformity of the energy distribution, the remaining slug units are accelerated towards the outlet. However, their accelerating motions cannot occur as expeditiously as they would with low viscosity mixtures, so the entire motion enters a highly coupled, nonlinear regime.

Moreover, the actual height, width, and several peaks in the signal strongly depend on the flow's local properties. For concreteness consider the inlet mass flow rates ($Q_l = 1.3$, $Q_g = 0.02$) kg/s. The images in the middle row of Figure 4.1 clearly show that significant amplification of the pressure fluctuations occur when more air is injected into the transport system. From the physical point of view, the much richer structure of the pressure fluctuations (which manifests as a tendency of the *off*-states to disappear) indicates higher void fractions in the slugs and a more complex liquid film structure trailing bubbles. With high-viscosity mixtures, the gas entrained in the liquid phase has much higher residence times. Therefore, the void fraction increases continuously as the flow progresses downstream from the inlet. The liquid film wraps around the gas bubble, creating a considerable thickness layer (see Figure 4.4 below). When Q_g is further increased to 0.03 kg/s, the pressure bursts acquire greater amplitudes but become narrower (see the last row of images in Figure 4.1). The slugs' velocities and the radial distribution of the glycerin around the bubbles are significantly higher in this regime. Because the liquid phase

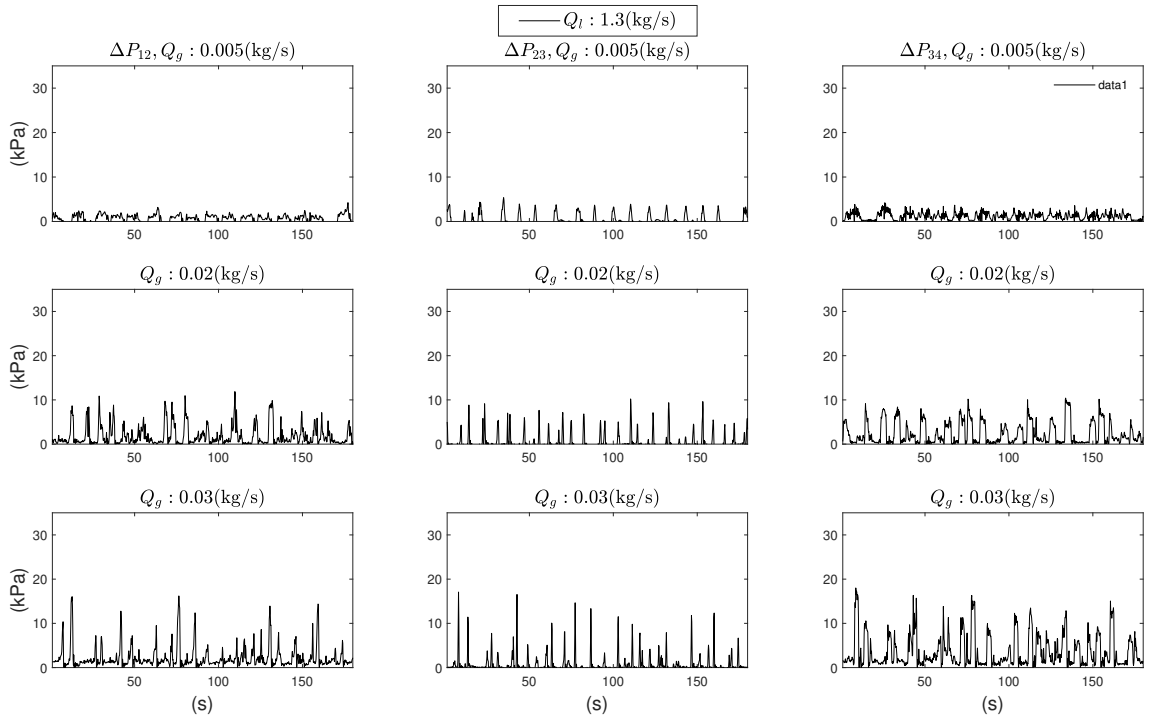

Fig. 4.1 Time series of the differential pressure ΔP_{12}, ΔP_{23} and ΔP_{34} for the flow rate $Q_l = 1.3$(kg/s).

occupies a much larger portion of the cross-sectional area of the pipeline at any given time, the pressure drop produced by the frictional losses is more pronounced.

Consider next the cases with glycerin mass flow rates of 3.7 kg/s and 6.1 kg/s. At high Q_l, the ensuing pressure signals exhibit a far more complex fluctuation pattern (as the time-series of Figure 4.2 and 4.3 show). Here, well-defined intermittency ceases to exist because the *off*-states are no longer discernible. This is because a much larger amount of air bubbles is entrained in the high-viscosity liquid. Despite the apparent similarities of the signals collected in a given (Q_l, Q_g) combination (Figure 4.3), the flow properties differ substantially.

Another aspect to highlight is that the *off*-states of some pressure drop signals are negative, which means that the pressure downstream of the section is greater than the upstream pressure, which means that the flow changes direction during the *off*-states. This flow is glycerin that flows in reverse in a laminar regime.

Finally, from the time series of the pressure drops, notice that the width of the bursts is greater for ΔP_{12} and ΔP_{34} than for ΔP_{23}. This is because ΔP_{12} and ΔP_{34} are the pressure drops

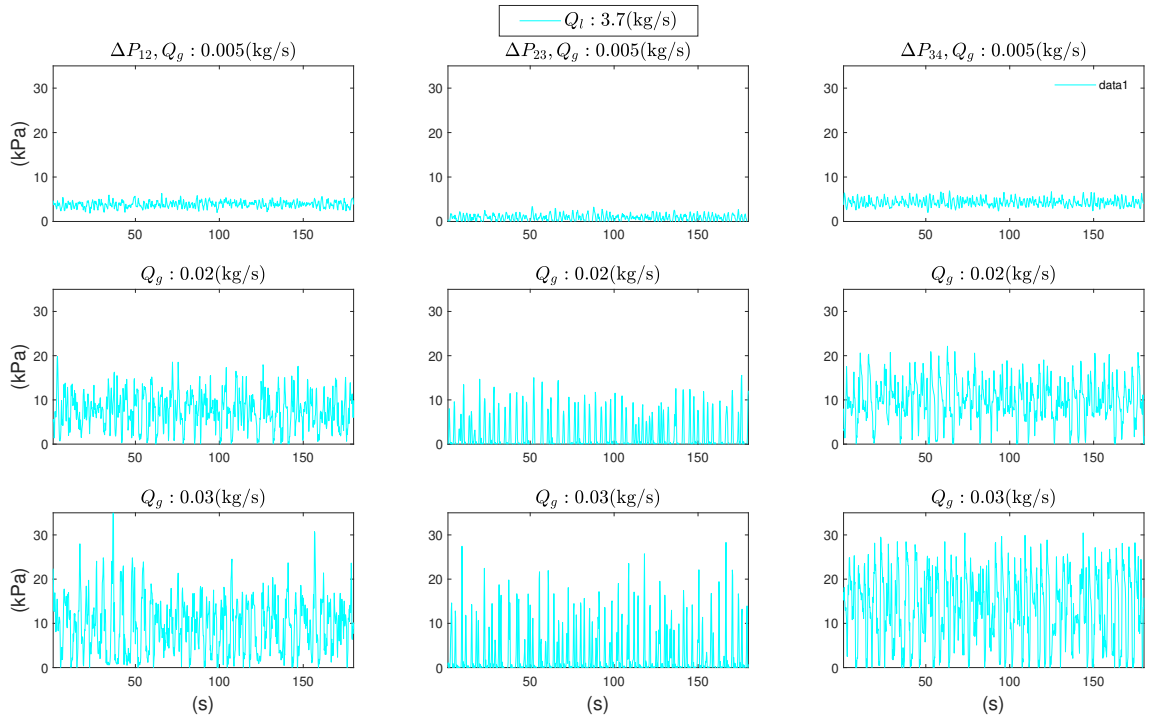

Fig. 4.2 Time series of the differential pressure ΔP_{12}, ΔP_{23} and ΔP_{34} for the flow rate $Q_l = 3.7$(kg/s).

corresponding to sections Δz_1 and Δz_2, which are longer. For this reason, the front of a slug takes longer to reach from the sensor upstream of the section to the sensor downstream of it.

The snapshots of Figure 4.4 illustrate the underlying physical processes discussed above.

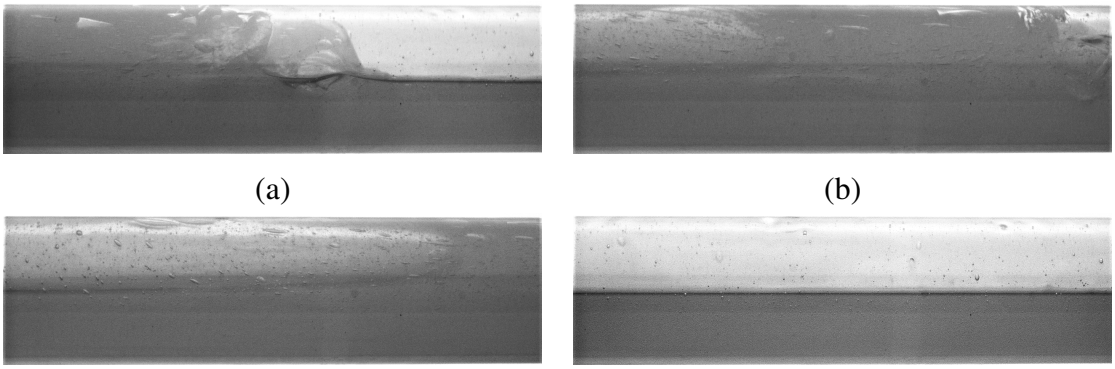

Fig. 4.4 Gaseous entrapment and liquid film behavior in the high-viscosity regime. It must be noted that, only, in this case, the mixture's viscosity was reduced to $\mu \approx 0.5$ Pa.s to enhance the visualization of the described effects.

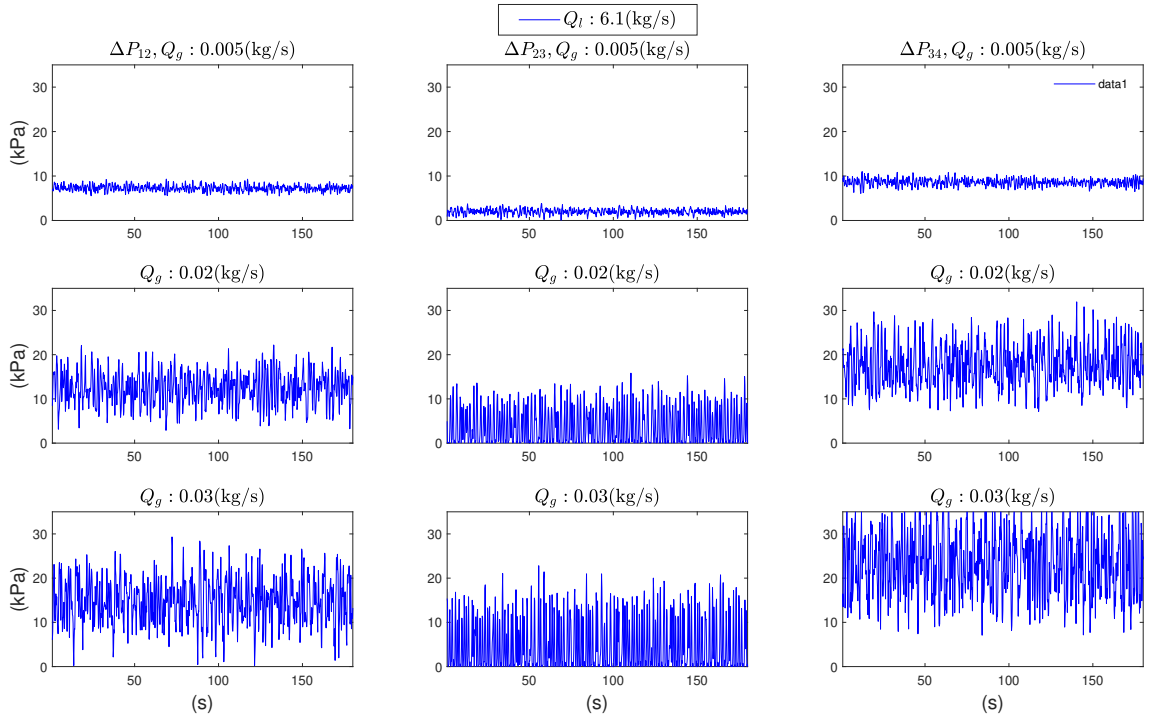

Fig. 4.3 Time series of the differential pressure ΔP_{12}, ΔP_{23} and ΔP_{34} for the flow rate $Q_l = 6.1$(kg/s).

Both the effects of the gaseous entrapment (Figure 4.4a) and the persistence of a thick liquid film wrapping around the gas bubble (Figure 4.4d) are discernible in the photographs' sequence. Only after a sufficiently long time, the liquid film region resembles a typical stratified flow (this is especially true in long gas bubbles). Nonetheless, small air bubbles persist immersed in the thick layer of fluid attached to the pipe's wall. One may have a rough idea of the viscous time-scale by observing the pipe's upper wall's gas pockets. These air pockets are severely stretched as they are dragged along by the liquid (Figure 4.4a and 4.4b) and eventually become a mixture of round and elongated bubbles (Figure 4.4c), depending on their location.

4.3.2 Slugs prediction

According to [5], the slug frequency is the number of slugs passing a specific point along the pipeline over a certain period of time. Slugs that occur during a certain time interval (or time window) can be counted from the number of *on*-states detected in the pressure drop signal within such an interval. *On*-states can be detected by employing metrics and algorithms for two-level waveforms. Specifically, the detection was performed by counting the number of times the two-level signal crossed the reference level twice. In this manner, the number of slugs in a time window equals the number of *on*-states. Figure 4.5 shows the time series of ΔP_{23} for a given flow rate combination. Notice that the crossings indicate the *on*-states. The slugs' frequency in a given pipeline section can then be calculated from the slug count in a given time window. To this end, it suffices to divide the number of *on*-states by the time window in which the number of slugs was counted, as showed in the following equation:

$$f_s = \frac{N_s}{\Delta t_{sw}} \tag{4.1}$$

Where N_s denotes the total number of slugs, and Δt_{ws} is the duration of the analyzed time window.

Several studies suggest that the slugging characteristics influence the erosion and corrosion rates of the pipelines' inner walls (e.g., it [97, 132, 89, 163, 150, 49]). Because similar processes occur at higher pressure levels in the high-viscosity regimes, an accurate prediction of the slug frequencies becomes crucial to the correct assessment of the mechanical integrity of conduit. Various models have been proposed that depend on measurable quantities, such as mass flow rates, pressures and densities [13, 9]. The particularly popular model developed by Gregory and Scott [58] was conveniently adapted to the SI system of units by Manolis et al. [98], as it was pointed out by Al-Safran [5]. In this model the frequency is estimated with:

$$f_s = 0.0037 \frac{v_l}{gD} \left(\frac{25 + v_m^2}{v_m} \right)^{1.8} \tag{4.2}$$

where v_m is the mixture (or no-slip) velocity, v_l is the actual liquid velocity, g the gravitational acceleration, and D the inner diameter of the pipeline. Figure 4.6 compares the slug frequency predicted by the equation (4.2) with the slug frequency obtained by directly counting the *on*-states in the data experiments A and B. The uncertainties caused by slugs overcounting, or undercounting, are due to the preselected threshold levels. Figure 4.6 shows that, within an error of 10%, the experiments' frequencies do not agree with the predicted values. Certainly, the model accounts for uncertainties in the mass flow rates, temperatures, and densities, in the low viscosity regime.

To improve the prediction of the frequencies, the Manolis equation (4.2) was calibrated with the experiment A data. After applying an optimization algorithm, the modified equation is:

$$f_s = 0.0057 \frac{v_l}{gD} \left(\frac{20 + v_m^2}{v_m} \right)^{1.9} \tag{4.3}$$

The predicted values produced by this newly calibrated model are shown in Figure 4.7. It is noted that the frequencies were determined from experiment A and experiment B, respectively.

4.3.3 Statistical characterization

The reader can check the particular features of Figures (4.8 - 4.10). It is interesting to notice general patterns, for example, [4] states that for a slug flow differential pressure distribution depends on the distance of differential pressure section, then ΔP_{12} and ΔP_{34} have approximately the same behavior inside Figures (4.8 - 4.10) because Δx_1 and Δx_3 have almost the same distance. However, Figures (4.9, 4.10) show that for greater flow rates, particularly, for $Q_l = 3.7$kg/s with $Q_g = 0.03$kg/s and $Q_l = 6.1$kg/s with $Q_g = 0.03$kg/s, the behavior tends to be the same in ΔP_{23}.

Table 4.3 shows the calculated mean for the pressure drops associated with the three test sections. It is interesting to note that the mean increases when either of the two mass flow rates increases. This is somewhat expected since the pressure drop is directly proportional to the fluid velocities.

As for the standard deviation, it increases when Q_g increases. But it diminishes when Q_l becomes greater. This means that the pressure drop fluctuates more when air is injected into the pipe with higher velocity, something that doesn't happen when more glycerin is injected at a

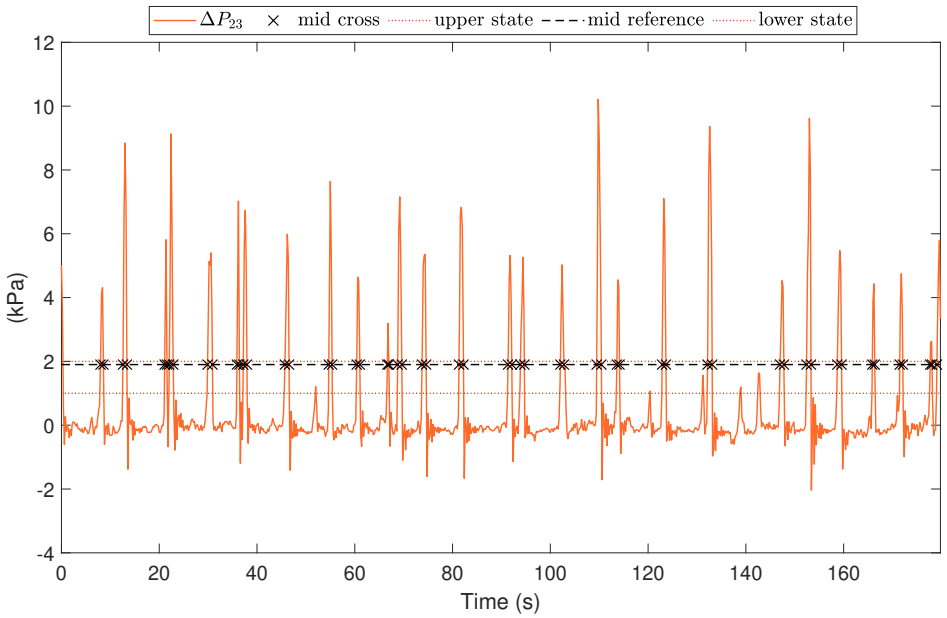

Fig. 4.5 Detection of slugs in the ΔP_{23} time series for Q_l: 1.3 (kg/s) and Q_g: 0.02 (kg/s)

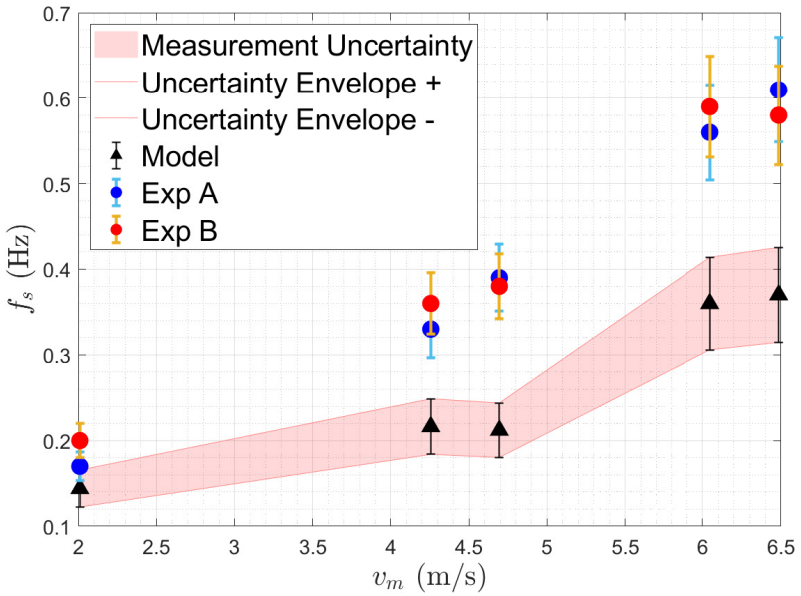

Fig. 4.6 Predicted and measured frequencies

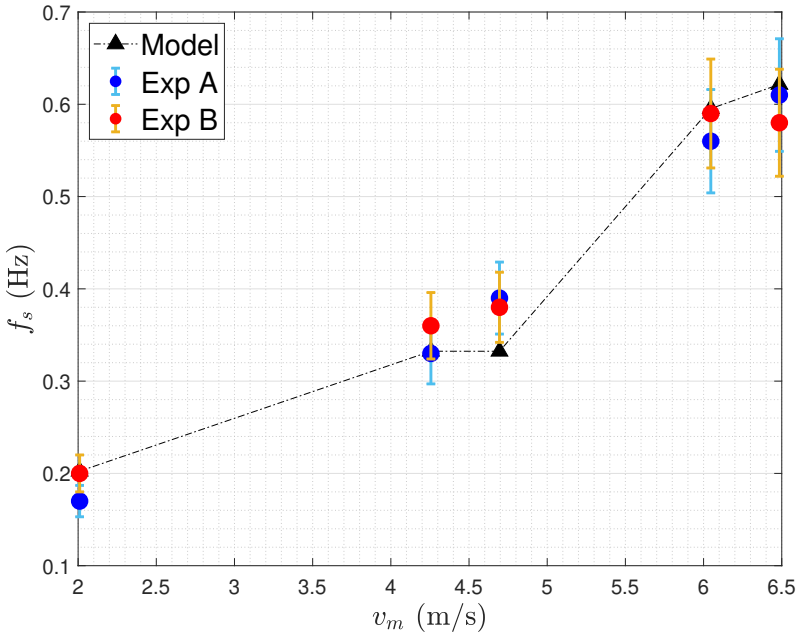

Fig. 4.7 Predicted frequencies by the proposed model

Table 4.3 Mean (kPa)

	ΔP_{12}			ΔP_{23}			ΔP_{34}		
q_l/q_g	**0.005**	**0.02**	**0.03**	**0.005**	**0.02**	**0.03**	**0.005**	**0.02**	**0.03**
1.3	0.75	1.88	2.21	0.40	0.5	0.7	1.19	2.43	3.66
3.7	3.85	7.65	9.56	0.86	2.09	2.84	4.30	9.77	13.46
6.1	7.28	12.44	14.91	1.98	3.98	5	8.59	17.6	23.3

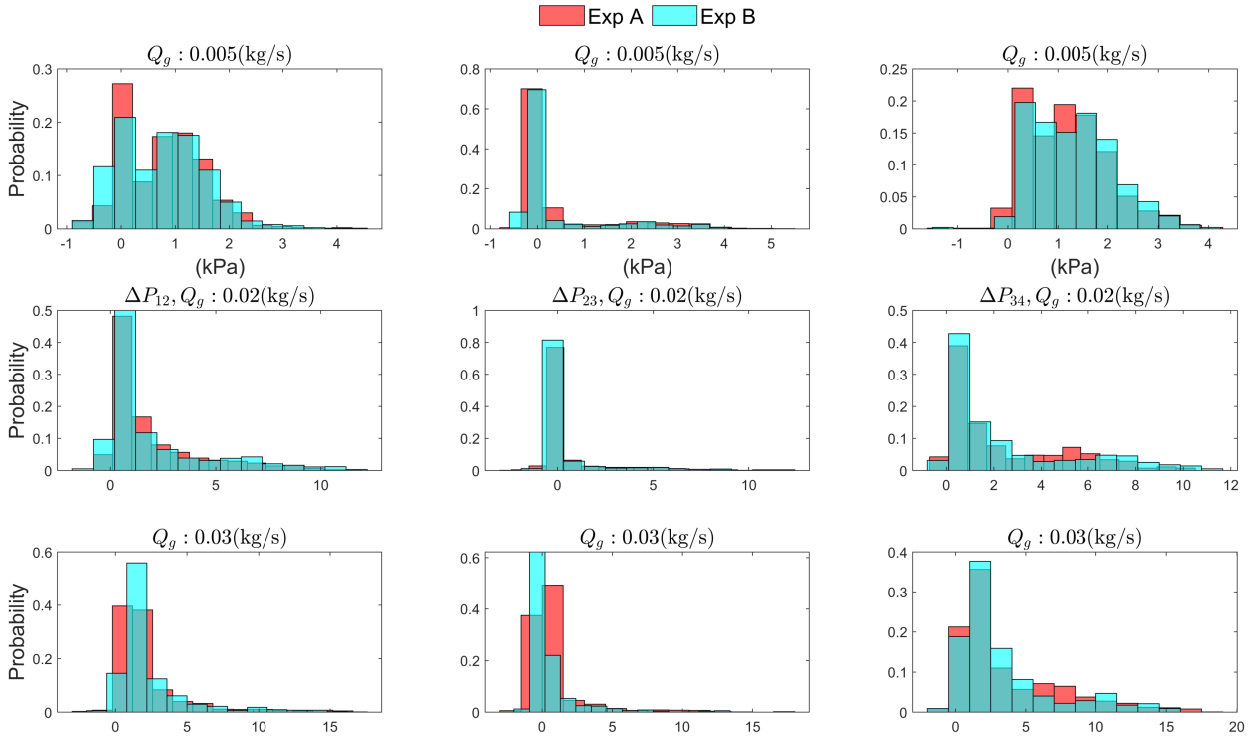

Fig. 4.8 Histograms of $\Delta P_{12}, \Delta P_{23}, \Delta P_{34}$ for a liquid mass flow rate 1.3 kg/s with 0.005, 0.02 and 0.03 kg/s of gas mass flow rate. Data from two experiments are presented.

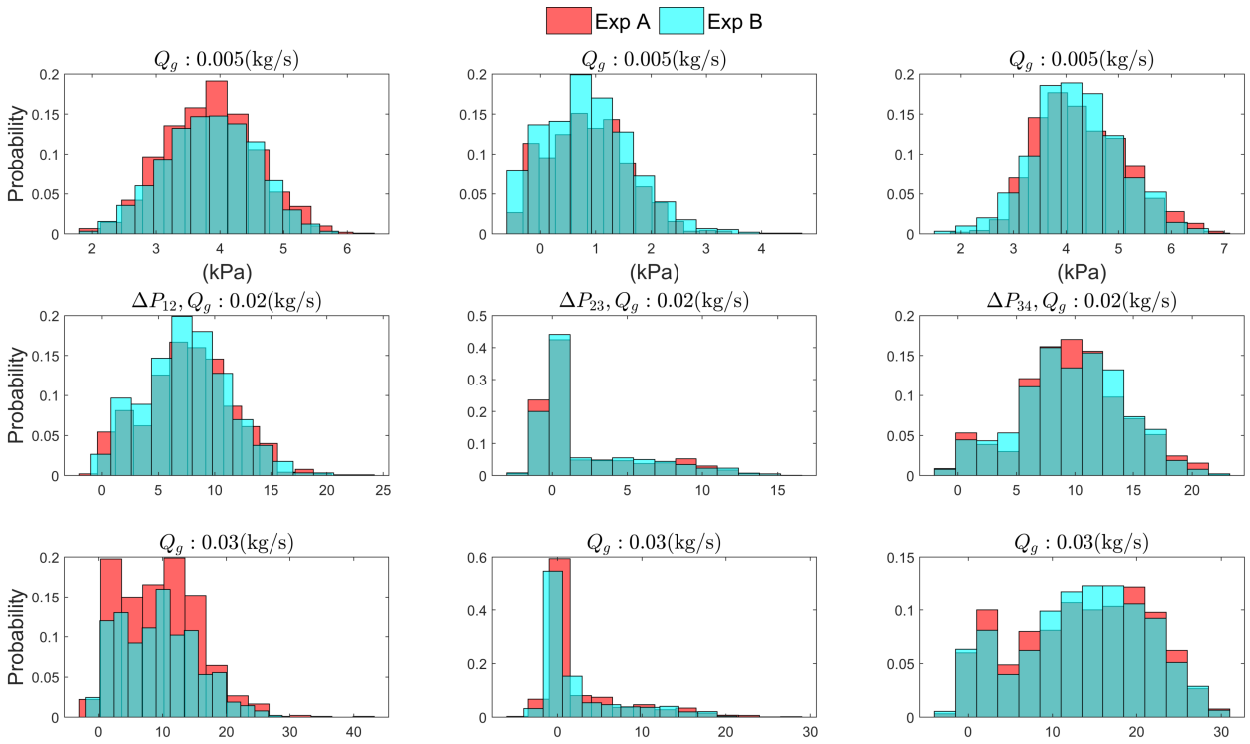

Fig. 4.9 Histograms of $\Delta P_{12}, \Delta P_{23}, \Delta P_{34}$ for a liquid mass flow rate 3.7 kg/s with 0.005, 0.02 and 0.03 kg/s of gas mass flow rate. Data from two experiments are presented.

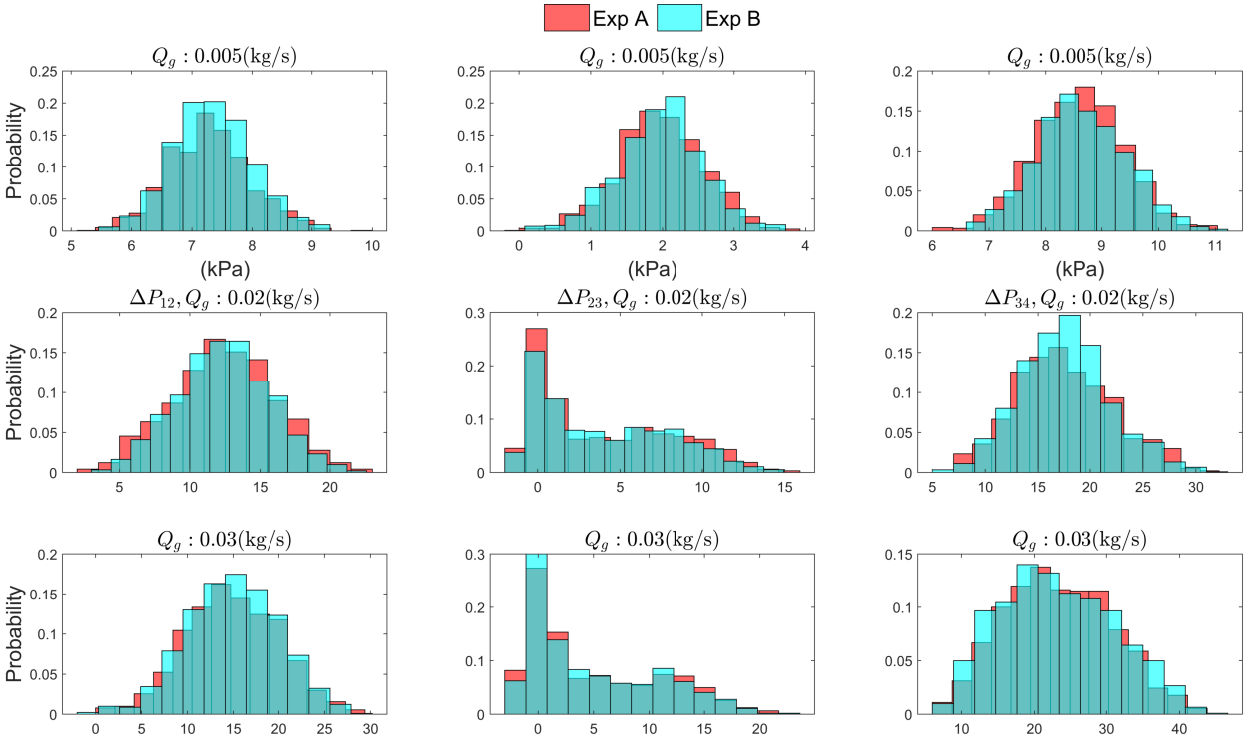

Fig. 4.10 Histograms of $\Delta P_{12}, \Delta P_{23}, \Delta P_{34}$ for a liquid mass flow rate 6.1 kg/s with 0.005, 0.02 and 0.03 kg/s of gas mass flow rate. Data from two experiments are presented.

Table 4.4 Standard deviation (kPa)

	ΔP_{12}			ΔP_{23}			ΔP_{34}		
q_l/q_g	**0.005**	**0.02**	**0.03**	**0.005**	**0.02**	**0.03**	**0.005**	**0.02**	**0.03**
1.3	0.76	2.24	2.56	1.05	1.70	2.09	0.81	2.52	3.73
3.7	0.72	3.88	6.19	0.73	3.71	5.31	0.85	4.54	7.86
6.1	0.68	3.63	5.09	0.60	4.15	5.89	0.79	4.67	7.33

Table 4.5 Kurtosis

	ΔP_{12}			ΔP_{23}			ΔP_{34}		
q_l/q_g	**0.005**	**0.02**	**0.03**	**0.005**	**0.02**	**0.03**	**0.005**	**0.02**	**0.03**
1.3	3.26	5.81	12.97	6.48	11.59	22.27	3.19	3.1	4.54
3.7	2.86	2.7	3.63	2.73	4.04	6.03	2.75	2.84	2.03
6.1	2.91	2.64	2.75	3.04	2.08	2.36	3.03	2.66	2.37

higher rate. In such a case, the effect is the regularization of the flow unsteadiness condition. This situation can be verified in Table 4.4.

A literary review shows no statistical analysis to verify the bimodality in the two-phase flow data. This is important because it is known the presence of two phases in the flow and determine the type of flow in the pipe leads to developing a more efficient system operation, as previously stated. For this reason, a statistical flow analysis could be used to implement online flow identification techniques to determine the flow pattern at a given moment and thus modify, for example, the operation of the pumping system to optimize product transport. That is the main reason to compare a few statistical tests. The principle would be to test the null hypothesis H_0 to verify if the data comes from a normal distribution, which indicates an almost total mix

Table 4.6 Skewness

	ΔP_{12}			ΔP_{23}			ΔP_{34}		
q_l/q_g	**0.005**	**0.02**	**0.03**	**0.005**	**0.02**	**0.03**	**0.005**	**0.02**	**0.03**
1.3	0.52	1.8	2.98	2.12	2.91	4.05	0.58	1.08	1.48
3.7	0.07	0.09	0.56	0.33	1.47	1.86	0.37	-0.05	-0.14
6.1	0.18	-0.03	-0.03	-0.03	0.57	0.75	-0.04	0.27	0.13

Table 4.7 Anderson-Darling normality test, experiment A

	ΔP_{12}			ΔP_{23}			ΔP_{34}		
q_l/q_g	**0.005**	**0.02**	**0.03**	**0.005**	**0.02**	**0.03**	**0.005**	**0.02**	**0.03**
1.3	1	1	1	1	1	1	1	1	1
3.7	0	1	1	1	1	1	1	1	1
6.1	1	0	0	0	1	1	0	1	1

of the two phases. If the null hypothesis H_0 is rejected, then the flow will behave due to the two separate phases, such as a slug flow pattern.

The tests were calculated using Matlab with a 5% level of the goodness of fit to normal distribution. The Kolmogorov-Smirnov test states that all data does not come from a normal distribution, the Anderson test (Table 4.7) instead says for ΔP_{12}(0.005-3.7, 0.02-6.1, 0.03-6.1), ΔP_{23}(0.005-6.1) and ΔP_{34}(0.005-6.1), the data come from a normal distribution in experiment A (the number "0" in the Table indicates normal distribution) and is very similar to experiment B except ΔP_{12}(0.005-6.1, 0.03-3.7). The reader can see the normal distribution similarity in the decision of Anderson test comparing with Figures (8,9,10) except ΔP_{12}(0.02-6.1) in experiment A where the tests seem to fail to reject the null hypothesis. The author in [36] shows the tests percentages of the correct decision in the assessment at 5% level of the goodness of fit to a normal distribution for several empirical distributions, and with the bimodal case is very difficult to achieve a good decision (16% the best correct decision for lilliefors test at 200 samples and 92% of correct decision for Shapiro-Wilk test at 40 samples). In this way, it is necessary to use a specific unimodality test. So, the author in [15] proposes a sufficient condition for unimodality;

$$|\mu_1 - \mu_2| \leq 2\min(\sigma_1, \sigma_2) \tag{4.4}$$

To implement equation (4.4) it is necessary to find $(\mu_1, \mu_2, \sigma_1, \sigma_2)$, so for automatic recognition of this values inside the data can be implemented a Gaussian Mixture Model.

The Gaussian Mixture Model (GMM) uses a mixture of Gaussian random variables to fit the real-world data. The principle of maximum likelihood and EM algorithm is used for parameter estimation of GMM. Then, a scalar continuous random variable x has a Gaussian-mixture distribution if its PDF is specified by the sum of Normal or Gaussian distributions;

Table 4.8 Anderson-Darling normality test, experiment B

	ΔP_{12}			ΔP_{23}			ΔP_{34}		
q_l/q_g	**0.005**	**0.02**	**0.03**	**0.005**	**0.02**	**0.03**	**0.005**	**0.02**	**0.03**
1.3	1	1	1	1	1	1	1	1	1
3.7	0	1	0	1	1	1	1	1	1
6.1	0	1	0	0	1	1	0	1	1

$$P(x) = \sum_{m=1}^{M} \frac{c_m}{((2\pi)^{1/2}\sigma_m)} \exp\left[-\frac{1}{2}\left(\frac{x-\mu_m}{\sigma_m}\right)^2\right] \tag{4.5}$$

where $-\infty < x < \infty$, $\sigma > 0$, $c_m > 0$, and the positive mixture weights sum to unity: $\sum_{m=1}^{M} c_m = 1$. The Gaussian mixture distribution is multimodal, with $M > 1$, unlike a normal/Gaussian distribution where $M = 1$. A Gaussian distribution mixture can adequately describe many physical data types exhibiting multimodality instead of a single Normal/Gaussian distribution with data poorly suited. The multimodality in data may come from multiple underlying causes (in this case, the two-phase flow air-glycerin). It is responsible for the particular mixture components in the distribution. In this way, the mixture distribution can be decomposed into a set of cause-dependent or context-dependent component distributions [38].

The Gaussian-mixture distributions contain a set of parameters (c_m, μ_m, σ_m). The parameter estimation can be viewed as a missing data problem. So, It is possible to consider that data points have a "membership" or "mixture component", in one of the individual Gaussian distributions used to model the data. First, the "membership" is unknown. The parameter estimation work is to learn adequate parameters for the distribution, connected to data points represented as their membership in the individual Gaussian distributions. Next, the solution relies on the maximum likelihood methods for parameter estimation of the Gaussian-mixture distribution, specifically, the expectation-maximization (EM) algorithm. This algorithm is a popular technique used to estimate the mixture parameters given a fixed number of mixture components. In this way, this algorithm can be used for computing parameters of any parametric mixture distribution. The algorithm includes two steps: an Expectation step (E-step) and a Maximization step (M-step)[38].

The multivariate generalization of the mixture Gaussian distribution can be described by;

$$P(x) = \sum_{m=1}^{M} \frac{c_m}{(2\pi)^{D/2}\,|\Sigma_m|^{1/2}} \exp\left[-\frac{1}{2}[x-\mu_m]^T \Sigma_m^{-1}[x-\mu_m]\right] \tag{4.6}$$

$$P(x) = \sum_{m=1}^{M} c_m \mathcal{N}(x : \mu_m, \Sigma_m), (c_m > 0) \tag{4.7}$$

Next, the iterative form of E-step;

$$h_m^{(j)}(t) = \frac{c_m^{(j)} \mathcal{N}(x^{(t)} : \mu_m^{(j)}, \Sigma_m^{(j)})}{\sum_{i=1}^{n} c_i^{(j)} \mathcal{N}(x^{(t)} : \mu_m^{(j)}, \Sigma_m^{(j)})} \tag{4.8}$$

and the iterative form of M-step;

$$c_m^{(j+1)} = \frac{1}{N} \sum_{t=1}^{N} h_m^{(j)}(t) \tag{4.9}$$

$$\mu_m^{(j+1)} = \frac{\sum_{t=1}^{N} h_m^{(j)}(t) x(t)}{\sum_{t=1}^{N} h_m^{(j)}(t)} \tag{4.10}$$

$$\Sigma_m^{(j+1)} = \frac{\sum_{t=1}^{N} h_m^{(j)}(t)[x(t)-\mu_m^{(j)}][x(t)-\mu_m^{(j)}]^T}{\sum_{t=1}^{N} h_m^{(j)}(t)} \tag{4.11}$$

Where m is the mixture component, N is the sample size, $x(t)$ is the observation at time t and Σ_m the covariance matrix [38]. Then, the Matlab function "fitgmdist(x,k)" fits a Gaussian mixture model to data x with k Gaussian components, in this way it is possible to extract $(\mu_1, \mu_2, \sigma_1, \sigma_2)$ from two Gaussian components and implementing the equation (4.4). The Figure 4.3.3 shows the automatic two components (yellow and blue circles) and the GMM automatic fit to data (red circles). The Figures (4.12,4.13,4.14) show all the GMM fits data from experiment A (red "*") and experiment B (blue "*"). The Table 4.9 and Table 4.10 show the results for applying the unimodality test, equation (4.4), with the two Gaussian components from GMM without any modification. But, it is possible to make a manual fit to data from the initial GMM hint of parameter $(\mu_1, \mu_2, \sigma_1, \sigma_2)$ values. The algorithm would then be like the flow chart in Figure 4.15 setting "yes=0" for the unimodality case and "no=1" for no data unimodality. In this way, the results depend on subject fit and there is no automatic bimodality identification from data. Analyzing the results in Tables (4.9, 4.10) there is concordance generally with Figures (4.12,4.13,4.14) but in specific some cases by example ΔP_{12}, $Q_g = 0.03$kg/s, $Q_l = 3.7$kg/s there

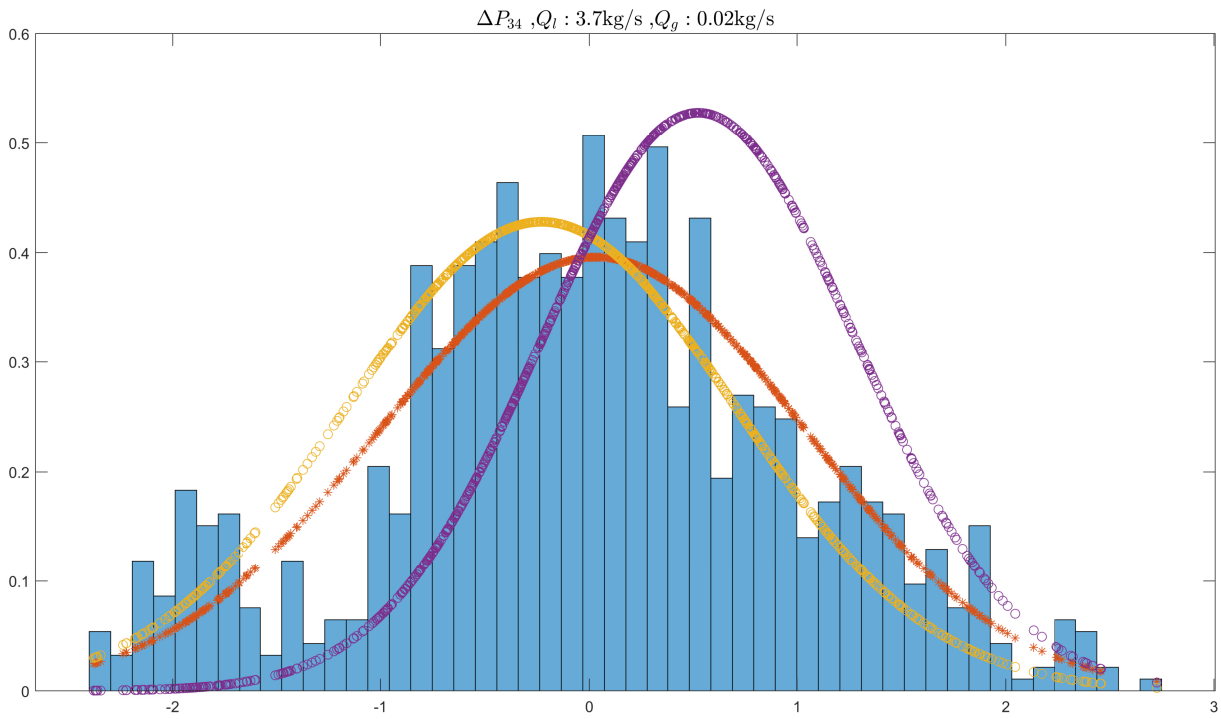

Fig. 4.11 Two components GMM fit to Histogram of ΔP_{34} for a liquid mass flow rate of 3.7 kg/s with 0.02 kg/s of gas mass flow rate. Data from experiment A.

is a little difference in the "Gaussians that leads to the umbral from one decision to other. The Figure also proposes an issue: if the GMM proposes two Gaussians (yellow and blue), then the little peak to the left could be the real another mode. In this way, a three-component GMM was implemented using a modification to equation (4.4);

$$|\max(\mu_1,\mu_2,\mu_3) - \min(\mu_1,\mu_2,\mu_3)| \leq 2\min(\mu_1,\mu_2,\mu_3) \tag{4.12}$$

The automatic three components GMM fit is showed in Figures (4.16 - 4.18), there is no Table because the equation (4.12) states that all results are not unimodal. Generally, the results show that more research is required on automatic bimodality data identification from two-phase flow in future work. This is an interesting problem not reported in the literature for two-phase flow and deserves to be investigated to lead better pipeline operation systems.

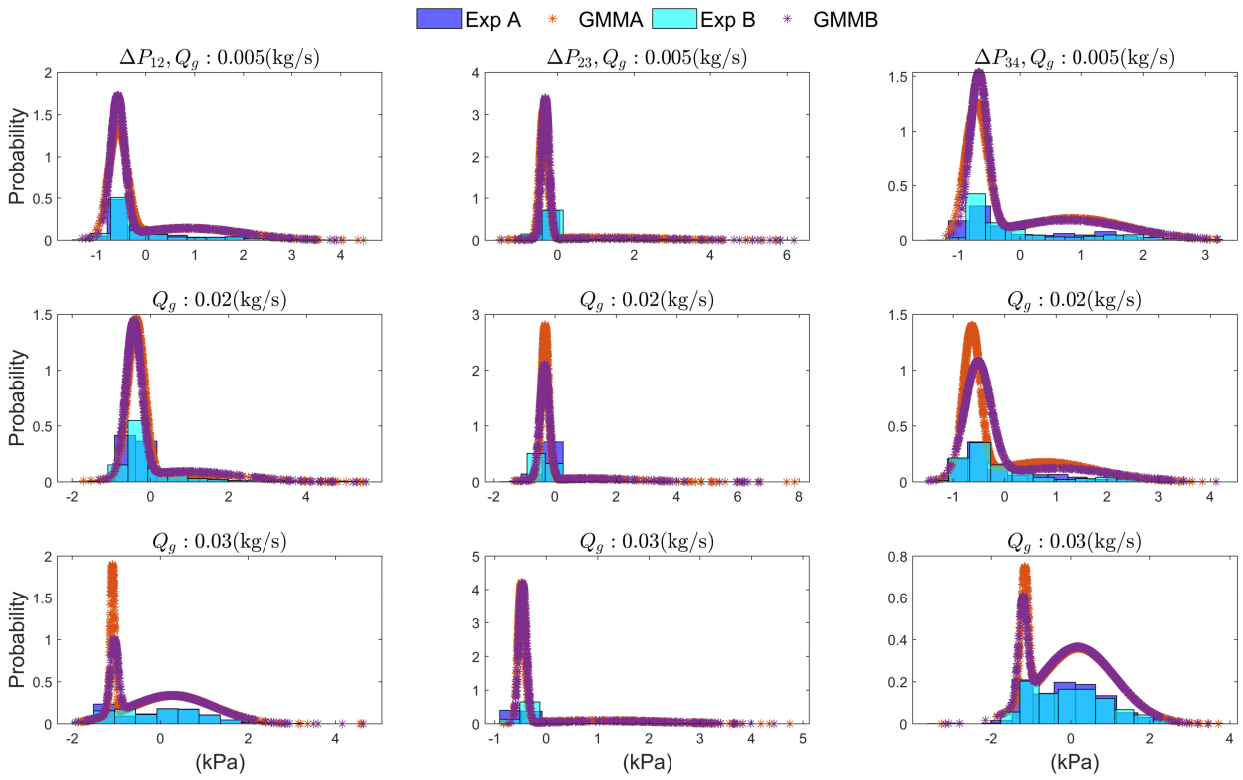

Fig. 4.12 Two components GMM fit to Histograms of $\Delta P_{12}, \Delta P_{23}, \Delta P_{34}$ for a liquid mass flow rate 1.3 kg/s with 0.005, 0.02 and 0.03 kg/s of gas mass flow rate. Data from two experiments are presented.

Table 4.9 Automatic fit from two components GMM for behboodian unimodality test, experiment A

	ΔP_{12}			ΔP_{23}			ΔP_{34}		
q_l/q_g	**0.005**	**0.02**	**0.03**	**0.005**	**0.02**	**0.03**	**0.005**	**0.02**	**0.03**
1.3	1	1	1	1	1	1	1	1	1
3.7	1	1	0	1	1	1	0	1	1
6.1	0	0	0	1	1	0	1	1	0

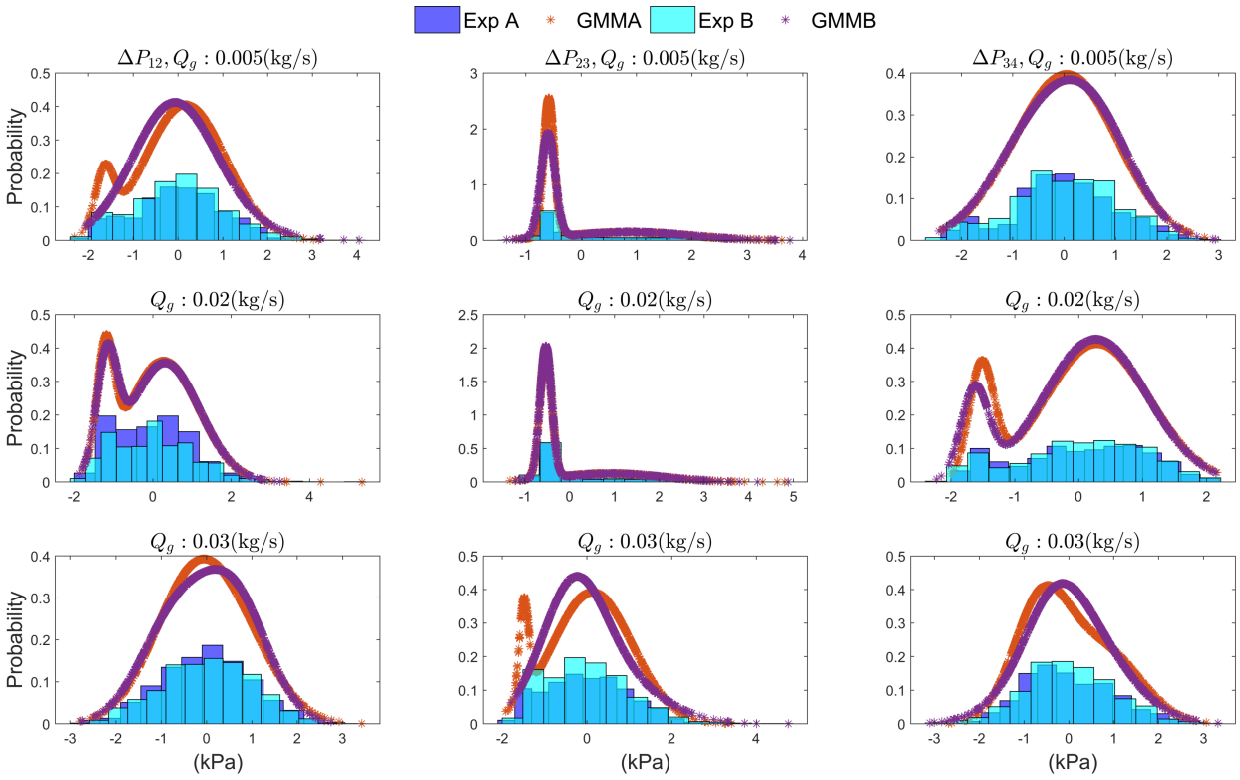

Fig. 4.13 Two components GMM fit to Histograms of $\Delta P_{12}, \Delta P_{23}, \Delta P_{34}$ for a liquid mass flow rate 3.7 kg/s with 0.005, 0.02 and 0.03 kg/s of gas mass flow rate. Data from two experiments are presented.

Table 4.10 Automatic fit from two components GMM for behboodian unimodality test, experiment B

	ΔP_{12}			ΔP_{23}			ΔP_{34}		
q_l/q_g	**0.005**	**0.02**	**0.03**	**0.005**	**0.02**	**0.03**	**0.005**	**0.02**	**0.03**
1.3	1	1	1	1	1	1	1	1	1
3.7	0	1	1	1	1	0	1	1	0
6.1	0	0	0	1	1	1	0	1	0

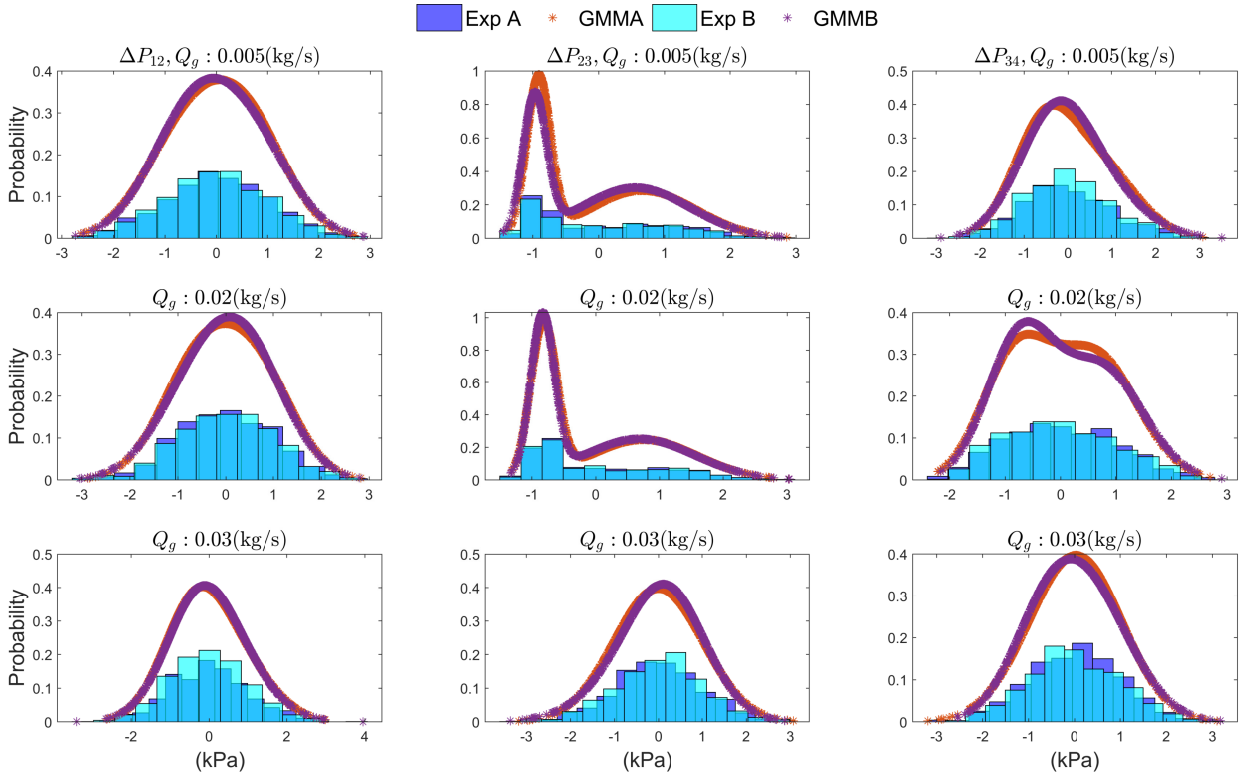

Fig. 4.14 Two components GMM fit to Histograms of $\Delta P_{12}, \Delta P_{23}, \Delta P_{34}$ for a liquid mass flow rate 6.1 kg/s with 0.005, 0.02 and 0.03 kg/s of gas mass flow rate. Data from two experiments are presented.

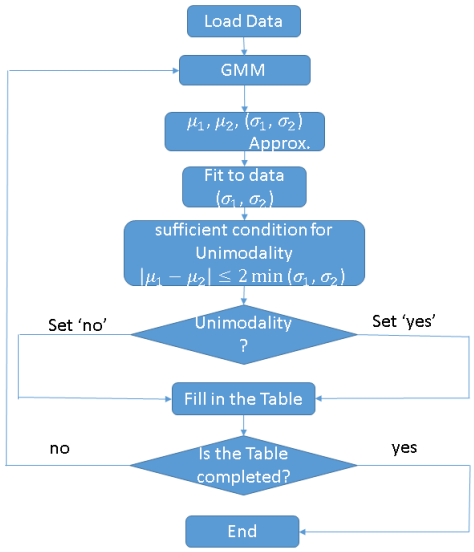

Fig. 4.15 Flow chart

4.4 Conclusions

A series of high-viscosity, two-phase flow experiments were conducted in a flow loop. The mixtures under consideration were produced with several mass-flow-rate combinations of air and glycerin and the time series pressure data revealed unique dynamical effects.

Regarding the spatial distribution of the phases, it is first noted that their evolution in the high-viscosity regime differs substantially from their low-viscosity counterparts. For instance, it appears that stratified flow patterns cannot be produced when the liquid-phase viscosity is of order ~ 1.0 Pa.s, regardless of the air and glycerin flow rates. It follows that the transition from the stratified to the intermittent flow pattern is not possible within the experimental intervals considered in this study.

According to the experimental observations, all intermittent flow patterns were directly produced at the test section's inlet plane due to the liquid phase's accumulation effect. Depending on the flow rates, the flow structure varied from very short to relatively long slug units. Each kind of flow was represented by a distinctive intermittent signal with specific mean and fluctuating pressure values. Thus, the *on*- and *off*-states of these signals were analyzed to determine the respective frequencies. As a result, the correlation proposed by Gregory and

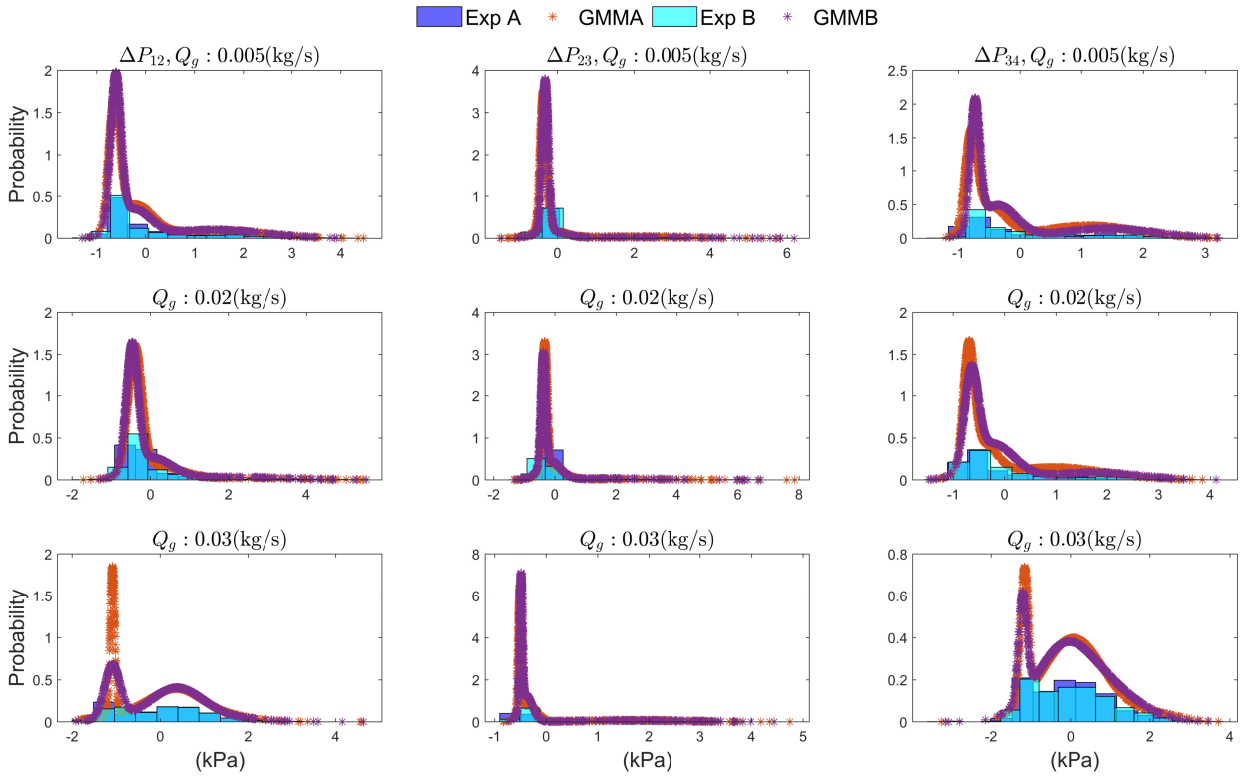

Fig. 4.16 Three components GMM fit to Histograms of $\Delta P_{12}, \Delta P_{23}, \Delta P_{34}$ for a liquid mass flow rate 1.3 kg/s with 0.005, 0.02 and 0.03 kg/s of gas mass flow rate. Data from two experiments are presented.

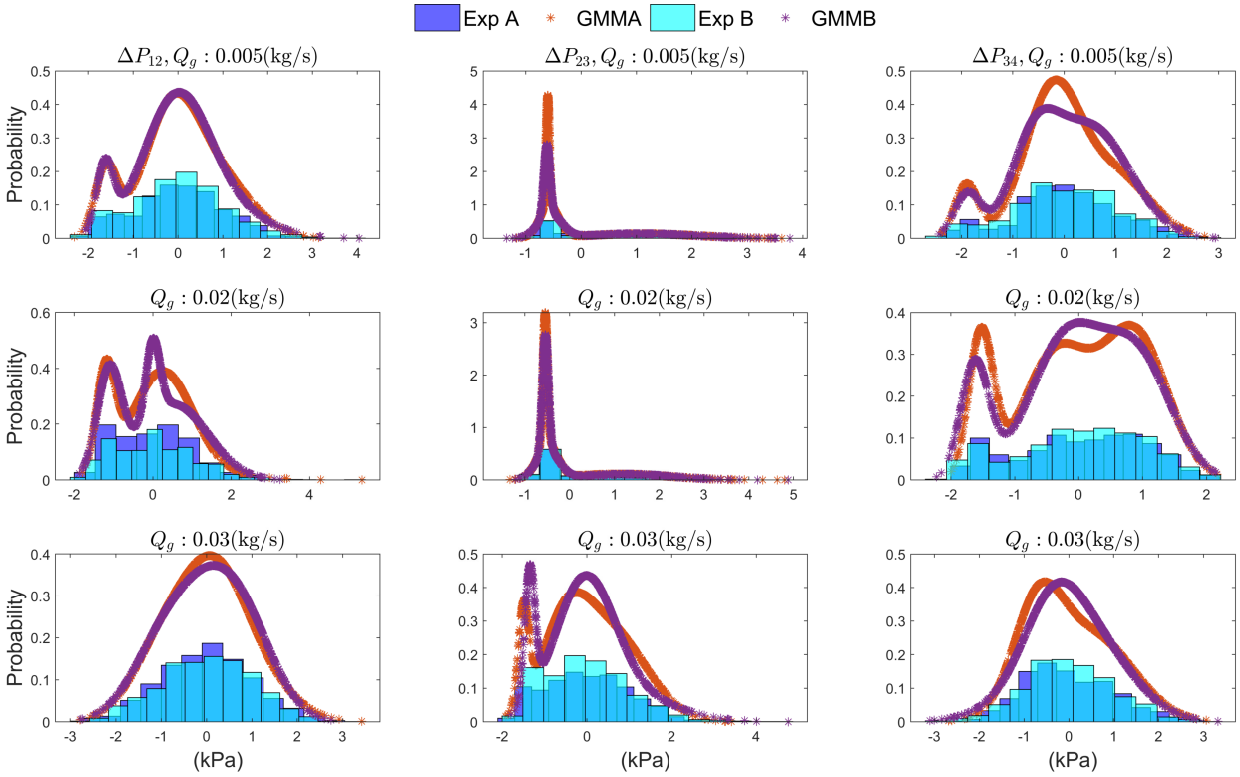

Fig. 4.17 Three components GMM fit to Histograms of $\Delta P_{12}, \Delta P_{23}, \Delta P_{34}$ for a liquid mass flow rate 3.7 kg/s with 0.005, 0.02 and 0.03 kg/s of gas mass flow rate. Data from two experiments are presented.

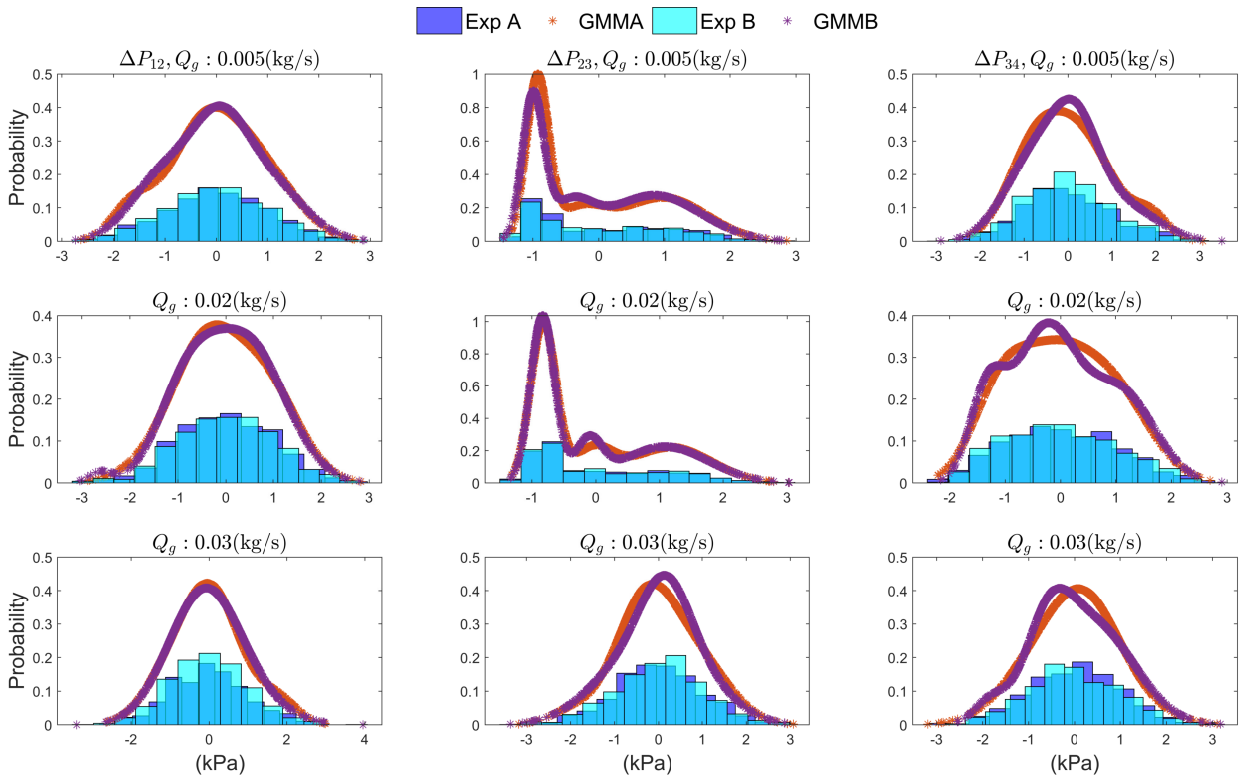

Fig. 4.18 Three components GMM fit to Histograms of $\Delta P_{12}, \Delta P_{23}, \Delta P_{34}$ for a liquid mass flow rate 6.1 kg/s with 0.005, 0.02 and 0.03 kg/s of gas mass flow rate. Data from two experiments are presented.

Scott was adjusted to determine the type of intermittency generated in the high-viscosity regime.

Furthermore, the flow was statistically characterized from the time-series to analyze the pressure itself. The resulting pressure distributions showed sensitivity concerning the flow rates and the appearance of secondary flows (in the U-section), and the slug ejection effects. Nonetheless, the pressure drop in all three sections exhibited an almost linear dependence on the gas and liquid flow rates, here were showed normality tests and a gaussian mixture model to detect bimodality, this is important because bimodality may reveals the two phase flow and to determine the type of flow in the pipe leads to developing a more efficient system operation like pumping system to optimize product transport.

Chapter 5

Leak diagnosis algorithms for water-glycerol flow

5.1 Introduction

Based on the context information presented in Chapter 1, pipelines are the preferred mean of transporting products because they have a low cost of transport, they are not affected by the weather, low energy consumption, do not produce road congestion, do not produce noise, do not produce atmospheric pollution and they are safe for humans. Transporting fluids in pipelines has a high degree of reliability and automation because it represents a continuous operation [94]. Also, it is well known that pipeline networks go through mountains, deserts, forests, neighborhoods, and cities. The petroleum industry collects crude oil from many places throughout the world to deliver it to refineries. This petroleum is converted into several products such as: diesel oil, gasoline, kerosene, heating fuel oils, lubricating oils, and liquefied petroleum gas. However, not only products that come from petroleum are transported through pipelines but also other substances, including water, slurry, sewage, hydrogen, and beverages [79]. In [47] it is reported that there are more than 3.650.000 km of pipelines in about 120 countries throughout the world. In [141] the survey shows that 134.866 km of pipelines are planned and under construction throughout the world. From this data, 61.782 km are projects at the design phase, and 73.083 km are projects in the construction phase. Also, in South/Central America and the Caribbean, there are about 2930 km of pipelines under construction and 4601 km of new and planned pipelines.

From the perspective of safety and environment, the main drawback in pipeline transportation operations are hydrocarbon leaks. Most of this transportation activity occurs safely, efficiently, and quietly. But accidents happen, like leaks, breaks, and spills. Detecting these events as quickly as possible provides a mean to minimize the negative consequences of these events. Leak detection is accomplished using a wide range of approaches with various strengths, weaknesses, and costs, and literature review shows numerous works on pipeline leak detection methods. This chapter will present a brief review and taxonomy organization of these approaches (section 5.2), the development of a new method for leak location taking into account pressure levels and gradient angles (section 5.3). Finally, a Kalman-based algorithm to detect the leaks is showed (section 5.4).

5.2 Leak detection systems

Different detection principles and different technologies cover leak detection systems (LDS). They can be categorized into two major types according to the author [79]: internal leak detection systems and external leak detection systems. In internal type methods, typical pipeline instrumentation is used to monitor pipeline parameters (i.e., temperature, flow or pressure sensors). In external type methods, observation and field instrumentation are used for pipeline parameters monitoring (i.e., visual inspection, fiber-optic cables, thermal cameras, acoustic microphones or infrared radiometers). As it was mentioned in chapter 1, section 1.3, there is a possible combination of internal and external methods (mixed or hybrid approach) according to [121], [143]. This section (5.2) is developed preferring the ideas from [79] for the simplicity of leak detection methods organization as shown in Figure 5.1. The literature collected by [62] offers a similar taxonomy as in Figure 5.2, but the external type proposed by [79] can include the incidental observation inside visual inspection category. In this way, a more compact organization is presented.

5.2.1 External methods

External methods look for fluid spills near or surroundings pipelines. The external methods are also divided into two branches: non-continuous methods in blue color dashed lines and continuous methods in red color dashed lines. External continuous methods have better functionality in shorter pipelines because there is an extra cost associated with installing additional sensors through the pipeline. These methods are:

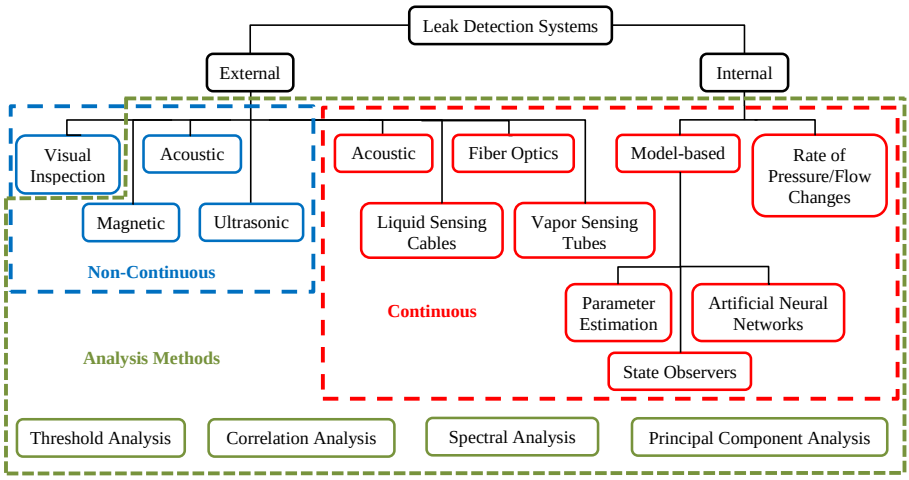

Fig. 5.1 Leak detection methods categorization from [79]

- **Acoustic leak detection:** acoustic sensors can detect internal noise levels when there is a leak in the pipeline [52, 53, 107]. An alarm will then be activated if the leak's acoustic frequency signal is different from the baseline, and localization of the leak takes into account the nearest stronger noise signal.

- **Fiber optics cables:** light propagation through fiber optic cables is sensitive to temperature changes in the pipeline. These temperature changes are possible because when the pipe suffers a leak, the product inside the pipeline change its temperature. It gets in touch with the fiber cable, causing an increment of the cable temperature [129, 87, 110, 67]. The sensors are placed through the pipeline to detect tiny cracks, corrosion, and metal loss [109].

- **Liquid sensing cables:** electrochemical cables produce changes in their impedance when it enters in contact with hydrocarbons. They are buried in touch with the pipeline [159, 122].

- **Vapor sensing tubes:** There are vapor sensing tubes through the pipeline. These tubes are full of air. When the leak occurs, the product inside the pipeline enters the tube, causing an increment in gas concentration that gas sensors may detect. Also, the level of the gas concentration can show the leak size [54].

Non-continuous methods are organized as follows:

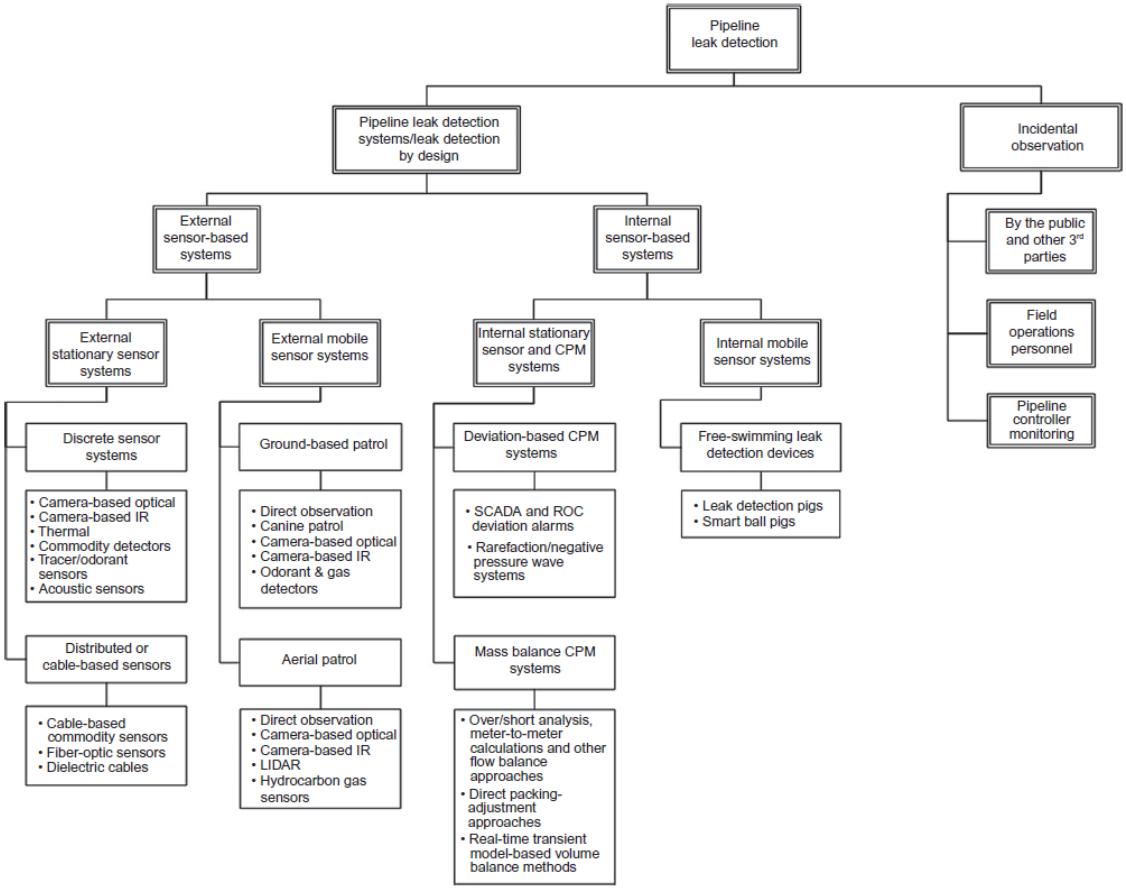

Fig. 5.2 Pipeline leak detection taxonomy from [62]

- **Magnetic and ultrasonic methods:** these methods are used in smart pigs. Magnetic flux leak detection systems consist of a magnetized pipeline with a permanent magnet. When there is a leak, the smart pig can detect it by sensing probes attached to the pig. These sensors detect the magnetic flux line changes. [130, 46]. Also, the pig has an ultrasonic sensor that sends an ultrasonic pulse to the pipeline wall. When a leak occurs, the pig receives and processes the reflected signals, and then the leak is located [146].

- **Visual inspection methods:** these methods consist of periodic pipeline right-of-way inspection. These methods can include the incidental observation developed by the public and other third parties, field operations personnel, and pipeline controller like state by the author in [62]. Pipeline surface conditions are inspected to look for leaks and some other conditions like corrosion or land stability, which put at risk the pipeline's integrity.

5.2.2 Internal methods

Internal methods are based on sensors to monitor the pipeline integrity taking into account internal pipe conditions like pressures, flow, and temperature. These methods consider measurements under normal operating conditions, and when these measurements are different, an alarm is activated. It is essential to reasonable accuracy in the measures to develop a suitable leak detection method. Examples of the internal methods are:

- **Rate of pressure/flow change method:** this method considers the sudden changes in pressure or flow or the difference between them. This behavior can detect the presence of a leak. Nevertheless, it is necessary to turn off this method for pump start-up or operation pipeline transients to avoid false alarms [100].
- **Model-based methods:** these methods depend on mathematical models. They use non-measurable quantities found by estimation methods. Some techniques inside these methods are:
  - **Artificial neural networks (ANNs):** the ANNs develop a processing routine considering the pipeline measurements. Then ANNS can be used for leak detection because there is a pipeline characterization with and without a leak. This characterization is used to train the ANNs to learn to detect signal conditions when there is a leak. For example, in [16] training, data were generated by a computer code because it is not usual or easy to find real data for simulating flow in pipelines with and without leaks. The main reason is the data are classified as private information of companies.
  - **State observer:** this technique uses a state estimator to reconstruct the non-measurable variables from measurable signals like pressures, temperatures, flows, among others. [71, 54].
  - **Parameter estimation:** by mean of model parameters (physical process coefficients) is possible to find leaks in the pipeline, so when there is a change in the process model parameters, a non-measurable leak can be detected or localized because there is a relation between pressures, flows and coefficients like the friction or the pipe length [71], [79].
  - **Continuity, momentum and energy equations-based:** this method uses the physical principles of momentum, mass, and energy conservation [21]. So, the flow rates,

pressures, or even temperature measurements are essential to developing leak detection systems considering estimated and measured variables [135, 148, 137, 111]. Also, state observer algorithms are based on momentum, mass, and energy conservation physical principles [134–136, 133, 20, 148, 149].

– **Mass balance-based method:** this method focuses on the mass conservation principle. Taking into account that pipeline is considered a closed system. The mass inlet flow must be approximately equal to outlet mass flow. If there is a significant difference between them, this can be interpreted as an alarm to detect a leak, but the leak location is unknown [93].

In data analysis, several techniques can use the data obtained from the previous methods of leak detection. These are; threshold analysis [71], correlation analysis [66, 77], spectral analysis [128], principal component analysis [118], among others.

5.3 Angle-based diagnostic algorithm

The present proposal takes into account the pressure gradient angle to detect the leak location. First, let's consider three pipe sections like showed in Figure 3.2. These three sections are: (1) pipe linear section, (2) curved pipe section, and (3) linear pipe section. The bottom of Figure 5.3 shows the linear version of the three previous pipe sections (Δz_1, Δz_2, Δz_3) to compare each pipe section's gradient behavior. This configuration can show a typical gradient behavior like the upper section of Figure 5.3 in the black dotted line (without a leak). In this way, when a leak occurs, there is a pressure drop (solid blue line in Figure 5.3). Thus, to locate the leak must follow the steps:

- Pressures levels and gradient angles should be recorded and monitored.
- When a variation in the gradients and pressure levels is detected, the rate of change of each value must be calculated since the leak will be close to the maximum values of change, which shows which pair of sensors should be analyzed.

Based on the previous information, sensor P_2 presents the significant variation in his pressure level. Analyzing the gradient change in P_1, P_2 and P_3 noticed a significant change in the gradient angles between P_1 and P_2. So, analyzed the pressure level changes and gradient changes are selected the pressure signal sensors P_1 and P_2. Thus, Figure 5.4 shows the segment of Figure

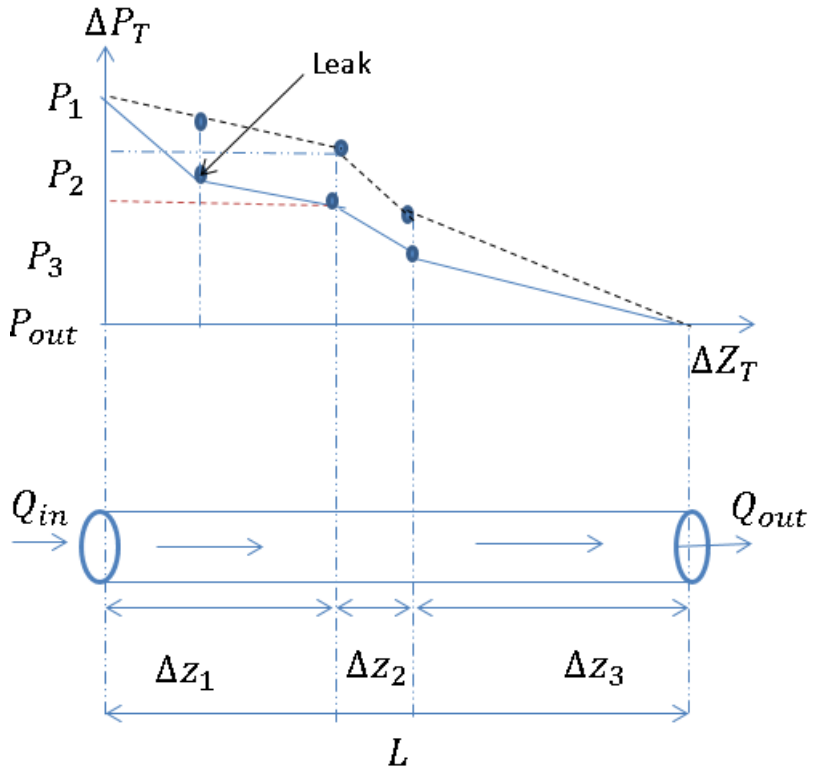

Fig. 5.3 Gradient pipeline behavior

5.3 where the leak occurs (Between P_1 and P_2); this is Δz_1. The dotted lines are the imaginary lines for trigonometric calculations. The ideal gradient angles (without a leak) are α', and β', but instead of these, new angles are α and β. Then, there is a triangle formed by the angles A, B, and H with opposite sides a (solid green line), b (solid red line), and h (black dashed line), respectively. Pressure levels of P_1 and P_{out} are fixed pressure values because they are the input (due to pump pressure) and the output (due to atmospheric pressure) of the pipeline.

Looking at Figure 5.4,

$$h = \sqrt{(P_1 - P_2)^2 + (\Delta Z_1)^2} \tag{5.1}$$

Applying the following trigonometric relationships to find $\beta^{'}$ from the hicks $P_1 - P_2$ and ΔZ_1 (see Figure 5.4):

$$\beta^{'} = \tan^{-1}\left(\frac{P_1 - P_2}{\Delta Z_1}\right) \tag{5.2}$$

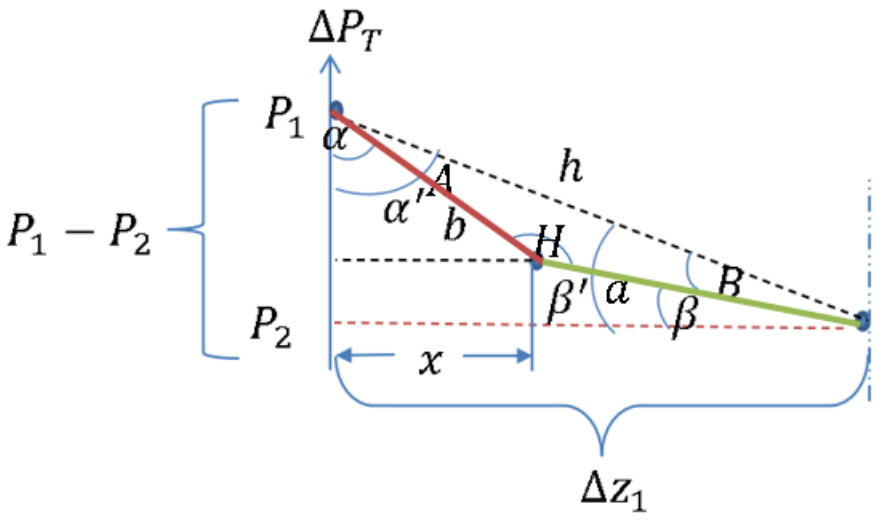

Fig. 5.4 Leak location analysis

In the same way, from equation (5.2) it is obtained α'. Pressure sensors P_1 and P_2 can be differential pressure sensors to obtain the gradient. Also, sensors P_1 and P_2 can be a combination of two very closely located pressure sensors; thus, α and β can be found, and with these values it is possible to calculate the angles between the ideal gradient h and the new gradients of P_1 and P_2:

$$B = \beta^{'} - \beta \tag{5.3}$$

$$A = \alpha^{'} - \alpha \tag{5.4}$$

$$H = 180 - (A + B) \tag{5.5}$$

now, applying the sine theorem:

$$\frac{h}{\sin H} = \frac{b}{\sin B} \tag{5.6}$$

Next:

$$\frac{h \sin B}{\sin H} = b \tag{5.7}$$

Now, the leak location is:

$$x = b \sin \alpha \tag{5.8}$$

Then, x defines the leak location measured from the location of sensor P_1. This method can be easily implemented in any low-cost process controller, which makes it field-implementable. The next section presents a more complex method for calculating the location of the leak.

5.4 Kalman-based leak diagnosis algorithm

The Kalman filter's theoretical concepts in this section was developed based on the work reported in [138] and references in [83, 95, 125, 59, 72]. The Kalman filter is an algorithm developed by Rudolf Emil Kalman [83, 88, 92]. These algorithm is used to solve linear-quadratic problems; this can identify a linear system's hidden non-measurable state even who an affected by white noise. Therefore, it is a linear quadratic estimator (LQE), which becomes a statistically optimal estimator for any quadratic function of the estimation error. This section presents the discrete Kalman filter basics, key concepts from the extended Kalman filter theory and the continuous Kalman filter with a prescribed degree of stability. Finally, an example of how a Kalman filter can detect and localize a leak in a straight horizontal pipe.

5.4.1 The discrete Kalman filter

Considering a linear dynamic system state-space representation:

$$\begin{aligned} x(k+1) &= Ax(k) + Bu(k) + w(k) \\ y(k) &= Cx(k) + v(k) \end{aligned} \tag{5.9}$$

Here $w(k)$ and $v(k)$ represent uncorrelated white noise with mean $\mu = 0$ with covariances $Q(k)$ and $R(k)$.

Then, the associated cost function is the squared prediction error expected value:

$$\begin{aligned} J &= E\left\{ \| \hat{x}(k+1) - x(k+1) \|_2^2 \right\} \\ &= E\left\{ \left(\hat{x}(k+1) - x(k+1)\right)^T \left(\hat{x}(k+1) - x(k+1)\right) \right\} \end{aligned} \tag{5.10}$$

The Kalman filter is based on two steps, prediction, and correction. The first step uses the estimated state from the previous time step to estimate the state at time $t = k+1$ (the *a priori*

estimated state $\hat{x}(k+1|k)$). In the second step, the *a priori* estimated state is corrected, taking into account the output measurements $y(k+1)$ and producing a new term knowing as the *a posteriori* estimated state ($\hat{x}(k+1|k+1)$). Next, the states covariance matrix (the measure of the estimated state accuracy) is calculated as:

$$P(k) = E\left\{(\hat{x}(k) - x(k))^T (\hat{x}(k) - x(k))\right\} \tag{5.11}$$

Prediction step

If the noise $w(k)$ is assumed equal to zero (its mean), then the *a priori* state estimation follows:

$$\hat{x}(k+1|k) = A\hat{x}(k) + Bu(k) \tag{5.12}$$

Considering the measurements up to k time step, the equation (5.12) and some algebraic manipulation [72], the covariance matrix is found as:

$$P(k+1|k) = AP(k)A^T + Q(k) \tag{5.13}$$

Correction step

When there is a new measurement $y(k+1)$, the estimated states are corrected as:

$$\begin{aligned}\hat{x}(k+1|k+1) &= \hat{x}(k+1|k) + \\ &+ K(k+1)\left(y(k+1) - C\hat{x}(k+1|k)\right)\end{aligned} \tag{5.14}$$

In this way, the selection of $K(k+1)$ determines if the states prediction $K(k+1)$ or present measurements $y(k+1)$ has a major weight in updating the estimated states $\hat{x}(k+1|k)$. So, after some simplifications (see [72]) the optimal choice of $K(k+1)$ (feedback gain) is found as:

$$K(k+1) = P(k+1|k)C^T\left(CP(k+1|k)C^T + Q\right)^{-1} \tag{5.15}$$

Thus, considering the *a posteriori* state estimation in the equation (5.14), the covariance matrix can be found as:

$$P(k+1|k+1) = (I - K(k+1)C)P(k+1|k) \tag{5.16}$$

Figure 5.5 shows the block diagram for the Kalman filter.

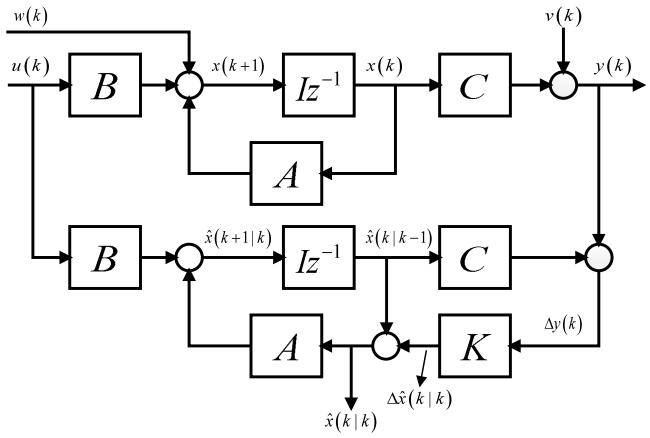

Fig. 5.5 Kalman filter block diagram, from [138]

5.4.2 Extended Kalman filter

The extended Kalman filter (EKF) is the non-linear version of the Kalman Filter. Then, there is a non-linear system as:

$$\begin{aligned} x(k+1) &= f_k(x(k), u(k)) + w(k) \\ y(k) &= g_k(x(k)) + v(k) \end{aligned} \tag{5.17}$$

with $w(k)$ and $v(k)$ as uncorrelated white noise with mean $\mu = 0$ and covariances $Q(k)$ and $R(k)$.

Thus, the predicted state and the predicted measurement are computed from the previously estimated state by mean of the functions f_k and g_k, and a first-order Taylor series expansion of (5.17) is used to update the covariance matrix $P(k)$. First, the non-linear system is linearized around the current estimate, and the Jacobian is evaluated each time step taking into account the current predicted states. Hence, the EKF is also calculated in two steps:

Prediction step

$$\hat{x}(k+1|k) = f_k(x(k), u(k)) \tag{5.18}$$

$$F(k) = \left.\frac{\partial f_k(x,u)}{\partial x}\right|_{x=\hat{x}(k),u=u(k)} \tag{5.19}$$

$$P(k+1|k) = F(k)P(k)F^T(k) + Q(k) \tag{5.20}$$

Correction step

$$G(k+1) = \left.\frac{\partial g_{k+1}(x)}{\partial x}\right| x = \hat{x}(k+1|k) \tag{5.21}$$

$$K(k+1) = P(k+1|k)G^T(k+1) \times \left(G(k+1)P(k+1|k)G^T(k+1) + Q(k+1)\right)^{-1} \tag{5.22}$$

$$\hat{x}(k+1|k+1) = \hat{x}(k+1|k) + K(k+1)\left(y(k+1) - g_{k+1}(\hat{x}(k+1|k))\right) \tag{5.23}$$

$$P(k+1|k+1) = (I - K(k+1)G(k+1))P(k+1|k) \tag{5.24}$$

5.4.3 Continuous extended Kalman filter with a prescribed degree of stability

In this topic, first consider a continuous non-linear system as:

$$\begin{aligned} \dot{x}(t) &= f(x(t),u(t)) \\ y(t) &= h(x(t)) \end{aligned} \tag{5.25}$$

where the input is $u(t) \in \mathbb{R}^p$, the output is $y(t) \in \mathbb{R}^m$, and the state is $x(t) \in \mathbb{R}^q$. Thus, the observer is found as [138]:

$$\dot{\hat{x}}(t) = f(\hat{x}(t),u(t)) + K(t)[y(t) - h(\hat{x}(t))] \tag{5.26}$$

with $\hat{x}(t)$ as the estimated state estimate and $K(t)$ is the observer gain which is a time-varying $q \times m$ found as:

$$K(t) = \mathbf{P}(t)\mathbf{C}^{\mathrm{T}}(t)\mathbf{W}^{-1} \tag{5.27}$$

The previous equation needs the differential Ricatti equation calculation as:

$$\dot{\mathbf{P}}(t) = (\mathbf{A}(t) + \alpha\mathbf{I})\mathbf{P}(t) + \mathbf{P}(t)(\mathbf{A}^{\mathrm{T}}(t) + \alpha\mathbf{I}) - \mathbf{P}(t)\mathbf{C}^{\mathrm{T}}(t)\mathbf{W}^{-1}\mathbf{C}(t)\mathbf{P}(t) + \mathbf{Q} \tag{5.28}$$

Where $\alpha > 0$ (estimation stability degree) can be tuned for the convergence time (estimation rate) and with the calculus of Jacobians:

$$\mathbf{A}(t) = \frac{\partial f}{\partial x}(\hat{x}(t), u(t)),\ \mathbf{C}(t) = \frac{\partial h}{\partial x}(\hat{x}(t))$$

$$\mathbf{P}(0) = \mathbf{P}(0)^{\mathrm{T}} > \mathbf{0}, \mathbf{Q} = \mathbf{Q}^{\mathrm{T}} \geq \mathbf{0}, \mathbf{W} = \mathbf{W}^{\mathrm{T}} > \mathbf{0}$$

Finally, It is worth mention this has a significant computational cost for implementing the discrete version because it requires the solution of the matrix Ricatti differential equation 5.28.

5.4.4 Design of a Kalman filter: an example

The main purpose of the following example is to show how a Kalman filter can be designed to detect and localize a leak in a straight pipe without branches.

This example involves an extended Kalman filter with a prescribed degree of stability.

Step 1: *Identify the available information (observations, data, measurements, records) for performing the estimation.*

In this step, the available information for performing the estimation must be analyzed and characterized. It must also be defined how the information will be processed before being injected into the state observer. Some data features that should be considered during the analysis are the sample time, the existence of delays, and the information's synchronization. In this step, it is essential to define which measured variables will calculate the estimation error.

For this example, the following information (time series data) is required: the inlet flow rate (Q_{in}), the upstream pressure head (H_{in}), the outlet flow rate (Q_{out}), and the downstream pressure head (H_{out}).

Step 2: *Formulate a model assuming convenient assumptions and constraints.*

In the present example, the model used for the design of the Kalman filter is the so-called rigid water column model (RWC model) [27], which describes the flow in a pipeline by taking into account the assumptions (A1)-(A5) given in chapter 2 section 2.3 together with the following assumptions:

(A7) the pipeline wall is rigid, and

(A8) the liquid fluid is incompressible.

The RWC model for a pipeline section Δz is expressed by the following equation [73, 108]:

$$\dot{Q}(t) = \theta \frac{\Delta H(t)}{\Delta z} - \alpha(Q)|Q(t)|Q(t) \tag{5.29}$$

where Q is the flow rate in the pipeline section, ΔH is the pressure head loss along Δz, $\theta = gA_r$, g is the gravity acceleration, A_r is the cross-sectional area and $\alpha(Q) = f(Q)/2\phi A_r$, where $f(Q)$ is the friction factor, which can be computed with any of the equations presented in [25]. By assuming that the flow rate is unidirectional, equation (5.29) becomes:

$$\dot{Q}(t) = \theta \frac{\Delta H(t)}{\Delta z} - \alpha(Q)Q^2(t) \tag{5.30}$$

which is the model used in this example for the conception of the Kalman filter.

Step 3: *Set the model in state-space representation.*

The starting point for executing this step is the formulation of the two following equations that describe the flow in two different sections of the pipeline as in Figure 5.6: the section to the left of the leak (namely $\Delta z = z_L - z_0$) where the head loss is $\Delta H = H_{in} - H_L$ and the section to the right of the leak (namely $\Delta z = L - z_L$) where the head loss is $\Delta H = H_L - H_{out}$. Both equations are obtained from the RWC model, equation (5.30), by substituting Δz and ΔH by the corresponding values:

$$\dot{Q}_{in}(t) = \frac{\theta}{z_L - z_0}(H_{in}(t) - H_L(t)) - \alpha(Q_{in}(t))Q_{in}^2(t) \tag{5.31}$$

$$\dot{Q}_{out}(t) = \frac{\theta}{L - z_L}(H_L(t) - H_{out}(t)) - \alpha(Q_{out}(t))Q_{out}^2(t) \tag{5.32}$$

where $z_0 = 0$ is the origin coordinate (the upstream end) of the pipeline, z_L is the leak coordinate (position) and H_L is the branch junction's pressure head.

If any of the equations replaces H_L:

$$\frac{H_{in}(t) - H_L(t)}{z_L} = \frac{\alpha(Q_{in}(t))}{\theta}Q_{in}^2(t), \quad \frac{H_L(t) - H_{out}(t)}{L - z_L} = \frac{\alpha(Q_{out}(t))}{\theta}Q_{out}^2(t) \tag{5.33}$$

and if the new state variables are defined as $x_1(t) = Q_{in}(t) - Q_{out}(t)$ and $x_2(t) = 1/z_L(t)$, then the following second-order system results from equation (5.31) and equation (5.32):

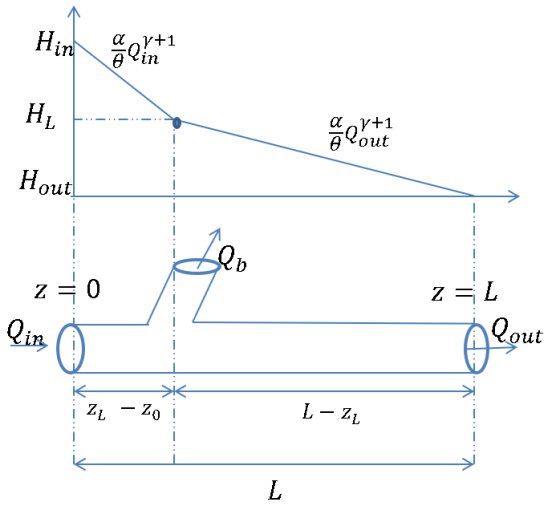

Fig. 5.6 Hydraulic gradient in a pipeline with a leak.

$$\dot{x}_1(t) = x_2(t)\underbrace{\left[\theta(H_{in}(t) - H_{out}(t)) - L\left(\alpha(Q_{out}(t))Q_{out}^2(t)\right)\right]}_{u(t)} - \alpha(Q_{in}(t))Q_{in}^2(t) + \alpha(Q_{out}(t))Q_{out}^2(t)$$

$$\dot{x}_2(t) = 0 \tag{5.34}$$

Step 4: *Set the equations of the Kalman filter.*

$$\begin{aligned}\dot{\hat{x}}_1(t) &= \hat{x}_2(t)u(t) - \alpha(Q_{in}(t))Q_{in}^2(t) + \alpha(Q_{out}(t))Q_{out}^2(t) + K_1(t)e(t)\\ \dot{\hat{x}}_2(t) &= K_2(t)e(t)\end{aligned} \tag{5.35}$$

where

$$e(t) = Q_{in}(t) - Q_{out}(t) - \hat{x}_1(t) \tag{5.36}$$

Step 5: *Compute the gain of the state observer.* To calculate $K_1(t)$ and $K_2(t)$, equation (5.27) can be used together with equation (5.28). Notice that for this example $\mathbf{P}(t), \mathbf{Q} \in \mathbb{R}^{2\times 2}$ and W$\in \mathbb{R}$.

The Kalman filter described by equations (5.35)-(5.36) was numerically implemented in MATLAB to test its performance with real data coming from a laboratory pipeline.

Table 5.1 Pipeline parameters

Parameter	**Value**
Diameter, ϕ	0.0486 (m)
Length, L	84.58 (m)
Leak position, z_ℓ	39.99 (m)
Relative roughness,ε	3.47×10^{-4}
Area, A_r	0.001855 (m)
Gravity acceleration, g	9.81 (m/s^2)
Fluid viscosity, ν	8.03×10^{-7} (m^2/s)
Fluid density, δ	996.59 (kg/m^3)

The pipeline parameters located at the Instituto Tecnológico de Tuxtla Gutiérrez, are listed on Table 5.1 [123]. The factor friction $f(Q)$ was calculated by using the Swamee-Jain equation. The observer´s parameters were chosen $\mathbf{P}(0) = \mathbf{Q} = \mathbf{I}$, where $\mathbf{I}$ is the identity matrix, and $\mathbf{W} = 1$. The observer's states were initialized with the following initial conditions: $\hat{x}_1(0) = 0.0002$ and $\hat{x}_2(0) = 10$.

Figure 5.7 shows the Kalman filter flow rate and pressure head for the estimation of the leak position.

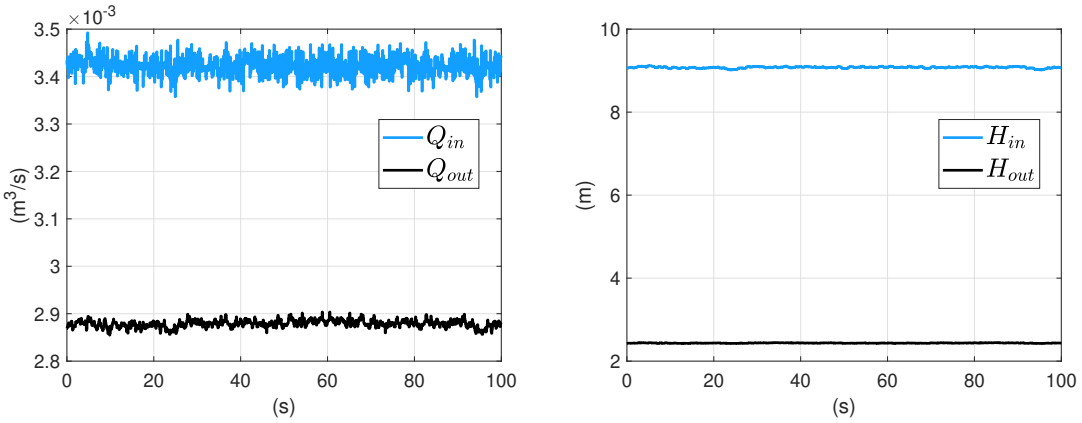

Fig. 5.7 Flow rates and pressure heads.

Figure 5.8 shows the estimation of the leak position performed by the Kalman filter and the values of $K_1(t)$ and $K_2(t)$. Notice that the leak position estimation is very close to the real leak value given in Table 5.1, with a relative error of less than 0.1 %.

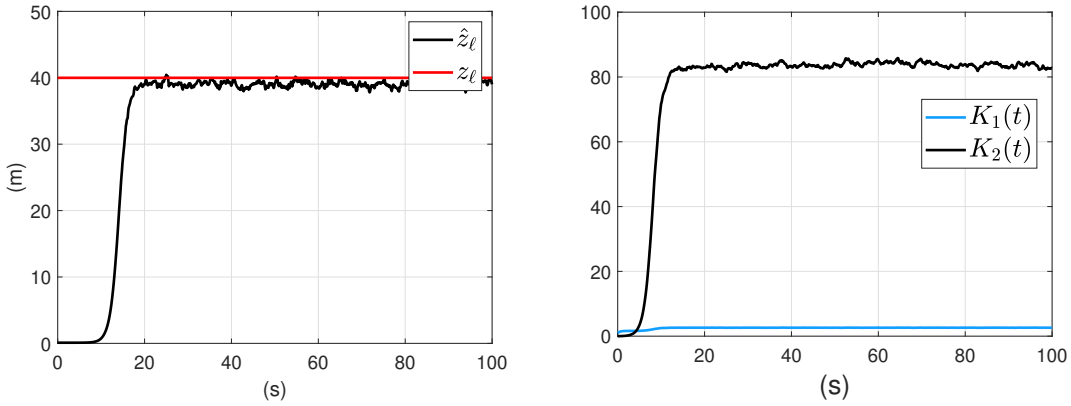

Fig. 5.8 (left) Real leak position and estimation of the leak position. (right) Evolution of the observer gain.

5.5 Conclusions

This chapter presented a brief review of the leak detection methods organization (section 5.2), which gives us a better understanding of how different methods can detect and locate pipeline leaks. For further details on this topic, the reader can consult [79] and [62]. This chapter also develops a new method for calculating the leak location using pressure levels and gradient angles measurements of the pipeline's sensors (section 5.3). This method uses essential trigonometric functions to find the distance of the leak from a given sensor. For this method's correct operation, it is necessary to have a differential pressure sensors or a combination of two pressure sensors with close distance to obtain the pressure gradient angles. It is worth mentioning that this method needs to be validated in real experiments. Finally, a Kalman-based algorithm to detect the leaks was showed (section 5.4). This algorithm uses only four steps to estimate the leak's actual position with less than 0.1% of relative error. However, this method has higher memory requirements and computing costs than the angle-based method (section 5.3).

Chapter 6

Conclusions and future work

6.1 Summary

This doctoral thesis presented the context and problems associated with hydrocarbons transport using pipelines with a particular interest in pipeline leaks. A mathematical model was then proposed to describe the flow of a mixture of water and glycerol in pressurized horizontal pipelines, which emulates the mixture of heavy oil and a viscosity reducer. The model was based on the mass and momentum conservation principles and empirical correlations for the mixture's density and viscosity. The set of partial differential equations was solved using finite differences. This simulation platform is a tool to simulate leak cases for different fractions of water and glycerol to evaluate algorithms for leak detection and localization in a simulation environment before their implementation in a laboratory setting. This work presented an experimental methodology to calculate the pressure gradient for a glycerin-water flow in a pipe with curved sections. Experimental data with defined boundary conditions show an agreement with model predictions. The pressure gradient correction described in this work improved the model's prediction for a pipeline with a U-shaped segment.

A high-viscosity two-phase flow was analyzed through a statistical characterization of the corresponding pressure signals. The flow of a glycerin-air mixture moving through a horizontal pipeline with a U-turn section installed midway along the pipe was investigated. Different combinations of liquid and air mass flow rates were experimentally tested. Then, the moments of the statistical distributions obtained from the resulting pressure time series were examined to highlight the flow's significant dynamical traits. Distinctive variations of the pressure gradients were observed in each section of the pipeline, which suggests that the

flow dynamics' local perspective must not be disregarded in favor of global considerations. It proposed a slug prediction model based on liquid mixture velocity, actual fluid velocity, gravitational acceleration, and the pipeline's diameter.

Finally, the literature on leak diagnosis algorithms briefly shows the taxonomy organization of different leak detection systems methods. Also, two leak diagnosis algorithms based on pressure gradients and Kalman filter were proposed. The first proposed method needs experimental validation as future work. This method can be implemented to reduce the associated risk (human and environmental) due to leaks in pipelines transporting hydrocarbons and increasing the percentage of automatic pipeline leak detection and localization.

6.2 Future work

Future works derived from this research could address the following issues:

- Employ statistical design of experiments to obtain a model more adjusted to the different operating conditions.
- Use the remaining data in Figure 2.5 to develop leak detection algorithms in the presence of Drag Reducing Agent's dynamical values (DRA).
- Validate the mathematical model at different pump speeds and with a more significant number of experimental runs.

As part of the research and data validation work, the development of the following activities are proposed:

1. Two pressure transducers should be located at the beginning of the loop and two at the end of the loop to verify a location method based on pressure gradients.
2. Two flow sensors should be located, one at the beginning of the loop and another at the end, together with the pressure sensors indicated in point 1. This configuration will allow the verification of a location method based on state observers (Kalman).
3. An experimental run should be carried out without leakage. The flow, pressure, viscosity, and temperature measurements should be recorded.
4. One-inch diameter tubing should have a quarter-inch leak in the first few meters of the pipe.

5. The flow and pressure measurements with the leak from point 4 should be recorded.
6. A second quarter-inch leak should be caused differently from the leak at point 4, preserving the instrumentation configuration of points 1 and 2. Furthermore, this second leak must be in the first few meters of the pipe. It is recommended 2 or 3 meters of difference concerning the 1st leak.
7. The flow and pressure measurements will be recorded with the leak from point 6.
8. Degrade the glycerin with water and repeat the execution of points 1-7. Record the percentage ratio of water and glycerin.
9. Degrade the glycerin further with water and repeat the execution of points 1-7. Record the percentage ratio of water and glycerin.
10. Degrade the glycerin further with water and repeat the execution of steps 1-7. Record the percentage ratio of water and glycerin.

References

[1] A. Concha, Quiroga, H., and Benjumea, P. (2007). Modelamiento de la propagación de los frentes de contaminación generados por el transporte de combustibles por poliducto. *Dyna*, 74(152):89–96.

[2] Adams, F. V., Niyomugabo, A., and Sylvester, O. P. (2017). Bioremediation of Crude Oil Contaminated Soil Using Agricultural Wastes. *Procedia Manufacturing*, 7:459–464.

[3] Ahmed, S. A. and John, B. (2018). Liquid-liquid horizontal pipe flow-a review. *Journal of Petroleum Science and Engineering*, 168:426–447.

[4] Akagawa, K., Hamaguchi, H., Sakaguchi, T., and Ikari, T. (1971). Studies on the Fluctuation of pressure Drop in Two-Phase Slug Flow : 1 st Report, Experimental Study. *Bulletin of JSME*, 14(71):447–454.

[5] Al-Safran, E. (2009). Investigation and prediction of slug frequency in gas/liquid horizontal pipe flow. *Journal of Petroleum Science and Engineering*, 69(1-2):143–155.

[6] Al-Sarkhi, A., Sarica, C., et al. (2010). Power-law correlation for two-phase pressure drop of gas/liquid flows in horizontal pipelines. *SPE Projects, Facilities & Construction*, 5(04):176–182.

[7] Angeli, P. and Hewitt, G. (1999). Pressure gradient in horizontal liquid–liquid flows. *International Journal of Multiphase Flow*, 24(7):1183–1203.

[8] Apraiz, I., Leoni, G., Lindenstrand, D., Persson, J. O., and Cristobal, S. (2009). Proteomic analysis of mussels exposed to fresh and weathered Prestige's oil. *Journal of Proteomics and Bioinformatics*, 2:255–261.

[9] Arabi, A., Salhi, Y., Zenati, Y., Si-Ahmed, E. K., and Legrand, J. (2020). On gas-liquid intermittent flow in a horizontal pipe: Influence of sub-regime on slug frequency. *Chemical Engineering Science*, 211:115–251.

[10] Archibong-Eso, A., Okeke, N., Baba, Y., Aliyu, A., Lao, L., and Yeung, H. (2019). Estimating slug liquid holdup in high viscosity oil-gas two-phase flow. *Flow Measurement and Instrumentation*, 65:22 – 32.

[11] Arirachakaran, S., Oglesby, K., Malinowsky, M., Shoham, O., and Brill, J. (1989). An Analysis of Oil/Water Flow Phenomena in Horizontal Pipes. In *SPE Production Operations Symposium*.

[12] Baba, Y. D., Aliyu, A. M., Archibong, A. E., Abdulkadir, M., Lao, L., and Yeung, H. (2018). Slug length for high viscosity oil-gas flow in horizontal pipes: Experiments and prediction. *Journal of Petroleum Science and Engineering*, 165:397 – 411.

[13] Baba, Y. D., Archibong, A. E., Aliyu, A. M., and Ameen, A. I. (2017). Slug frequency in high viscosity oil-gas two-phase flow: Experiment and prediction. *Flow Measurement and Instrumentation*, 54:109–123.

[14] Becerra, J. A. (2018). Como el pozo Lizama 158, habría otros 38 en mal estado. accessed: 29 August 2018. http://www.elcolombiano.com/colombia/como-el-pozo-lizama-158-habria-otros-38-con-un-mal-abandono-ED8454240.

[15] Behboodian, J. (1970). On the Modes of a Mixture of Two Normal Distributions. *Technometrics*, 12(1):131–139.

[16] Belsito, S., Lombardi, P., Andreussi, P., and Banerjee, S. (1998). Leak detection in liquefied gas pipelines by artificial neural networks. *AIChE Journal*, 44(12):2675–2688.

[17] Bendiksen, K. H., Langsholt, M., and Liu, L. (2018). An experimental investigation of the motion of long bubbles in high viscosity slug flow in horizontal pipes. *International Journal of Multiphase Flow*, 104:60 – 73.

[18] Beretta, A., Ferrari, P., Galbiati, L., and Andreini, P. (1997). Horizontal oil-water flow in small diameter tubes. pressure drop. *International Communications in Heat and Mass Transfer*, 24(2):231–239.

[19] Bertola, V. (2003). Experimental characterization of gas–liquid intermittent subregimes by phase density function measurements. *Experiments in fluids*, 34(1):122–129.

[20] Besançon, G. (2007). *Nonlinear observers and applications*, volume 363. Springer, Berlin, Heidelberg.

[21] Besançon, G., Bornard, G., and Hammouri, H. (1996). Observer synthesis for a class of nonlinear control systems. *European Journal of control*, 2(3):176–192.

[22] Blažič, S., Matko, D., and Geiger, G. (2004). Simple model of a multi-batch driven pipeline. *Mathematics and Computers in Simulation*, 64(6):617–630.

[23] Bordalo, S. N. and Morooka, C. K. (2018). Slug flow induced oscillations on subsea petroleum pipelines. *Journal of Petroleum Science and Engineering*, 165:535 – 549.

[24] Brito, R. (2012). *Effect of medium oil viscosity on two-phase oil-gas flow behavior in horizontal pipes*. PhD thesis, University of Tulsa.

[25] Brkić, D. (2011). Review of explicit approximations to the Colebrook relation for flow friction. *Journal of Petroleum Science and Engineering*, 77(1):34–48.

[26] C. A. García, Rodríguez, O. C., Hernández, F. E., Afanador, L. E., Rodríguez, L., Casallas, P. A., and Cruz, G. (2010). Optimización del transporte por oleoducto de crudo pesado castilla. *Revista Fuentes. El Reventón Energético*, 8(1):17–28.

[27] Cabrera, E., Garcia-Serra, J., and Iglesias, P. L. (1995). Modelling Water Distribution Networks: From Steady Flow to Water Hammer. In Cabrera, E. and Vela, A. F., editors, *Improving Efficiency and Reliability in Water Distribution Systems*, pages 3–32. Springer, Dordrecht.

[28] Capuano, L. (2018). International Energy Outlook 2018 (IEO2018). accessed: 1 September 2018. https://www.eia.gov/pressroom/presentations/capuano_07242018.pdf.

[29] Chakrabarti, D. P., Das, G., and Ray, S. (2005). Pressure drop in liquid-liquid two phase horizontal flow: Experiment and prediction. *Chemical Engineering & Technology*, 28(9):1003–1009.

[30] Chala, G., Sulaiman, S., and Japper-Jaafar, A. (2018). Flow start-up and transportation of waxy crude oil in pipelines: a review. *Journal of Non-Newtonian Fluid Mechanics*, 1(251):69–87.

[31] Chaudhry, M. H. (2013). *Applied hydraulic transients*. Springer, New York, NY.

[32] Cheng, N. S. (2008). Formula for the viscosity of a glycerol-water mixture. *Industrial and Engineering Chemistry Research*, 47(9):3285–3288.

[33] CICERM Centro de Investigación de Crudo Extra pesado y Recuperación Mejorada (2017). Infraestructura del IIUNAM en el Centro de Investigación de Crudos Extra pesados y Recuperación Mejorada. accessed: 29 August 2018. http://cicerm.geoestratos.info/.

[34] Crawford, R. L. and Crawford, D. L. (2005). *Bioremediation: Principles and Applications*. Biotechnology Research. Cambridge University Press, New York.

[35] de la Cruz, J. L. M., Alvarez-Badillo, S., Ram\'\irez-Jaramillo, E., Aquino-Olivos, M. A., and Orea, P. (2013). Measurements and correlation of Mexican heavy dead crude oil viscosities. *Journal of Petroleum Science and Engineering*, 110:184–192.

[36] de Sá, J. P. (2007). *Applied Statistics Using SPSS, STATISTICA, MATLAB and R*. Springer-Verlag.

[37] de Sousa, J. V. N., Sodré, C. H., de Lima, A. G. B., and Neto, S. R. d. F. (2013). Numerical Analysis of Heavy Oil-Water Flow and Leak Detection in Vertical Pipeline. *Advances in Chemical Engineering and Science*, 03(01):9–15.

[38] Dong Y., L. D. (2015). *Automatic Speech Recognition, A Deep Learning Aproach*. Springer-Verlag.

[39] Dulhoste, J. F., Guillén, M., Besançon, G., and Santos, R. (2017). One-dimensional modeling of pipeline transients. In *Modeling and Monitoring of Pipelines and Networks*, pages 63–81. Springer.

[40] Ecopetrol S. A. (2014). Mapa Infraestructura Petrolera. accessed: 4 September 2018. https://www.ecopetrol.com.co/especiales/mapa_infraestructura.htm.

[41] Ecopetrol S. A. (2015). El petroleo y su mundo. accessed: 29 August 2018. https://www.ecopetrol.com.co/wps/portal/es/ecopetrol-web/nuestra-empresa/sala-de-prensa/publicaciones/el-petroleo-y-su-mundo.

[42] Eghorieta, R. A., Afolabi, T. A., and Panacharoensawad, E. (2018). Drift flux modeling of transient high-viscosity-liquid and gas two-phase flow in horizontal pipes. *Journal of Petroleum Science and Engineering*, 171:605–617.

[43] El TIEMPO (1997). Contaminación por derrames de petróleo. accessed: 29 August 2018. https://www.eltiempo.com/archivo/documento/MAM-555907.

[44] EL TIEMPO (2012). Atribuyen a omisión de Ecopetrol la tragedia de Dosquebradas. accessed: 29 August 2018. https://www.eltiempo.com/archivo/documento/CMS-11277187.

[45] Elseth, G. (2001). *An Experimental Study of Oil / Water Flow in Horizontal Pipes*. PhD thesis, Telemark University College.

[46] Eze, J., Nwagboso, C., and Georgakis, P. (2017). Framework for integrated oil pipeline monitoring and incident mitigation systems. *Robotics and Computer-Integrated Manufacturing*, 47:44–52.

[47] Factbook, C. I. A. (2017). The world factbook. accessed: 29 August 2018. https://www.cia.gov/library/publications/the-world-factbook/fields/2117.html.

[48] Farrington, J. W. (2014). Oil pollution in the marine environment II: Fates and effects of oil spills. *Environment: Science and Policy for Sustainable Development*, 56(4):16–31.

[49] Feng, Z. and Cui, M. (2020). Influence of slug flow on local corrosion of pipelines. *Surface Review and Letters*, 27(5):1–8.

[50] Foletti, C., Farisè, S., Grassi, B., Strazza, D., Lancini, M., and Poesio, P. (2011). Experimental investigation on two-phase air/high-viscosity-oil flow in a horizontal pipe. *Chemical engineering science*, 66(23):5968–5975.

[51] Forbes Media LLC (2020). Global 2000-The World´s Largest Public Companies 2020. accessed: 7 January 2021. https://www.ecopetrol.com.co/especiales/mapa_infraestructura.htm.

[52] Fuchs, H. and Riehle, R. (1991). Ten years of experience with leak detection by acoustic signal analysis. *Applied acoustics*, 33(1):1–19.

[53] Gao, Y., Brennan, M. J., Liu, Y., Almeida, F. C., and Joseph, P. F. (2017). Improving the shape of the cross-correlation function for leak detection in a plastic water distribution pipe using acoustic signals. *Applied Acoustics*, 127:24–33.

[54] Geiger, G., Werner, T., Matko, D., et al. (2003). Leak detection and locating-a survey. In *PSIG Annual Meeting*, pages 1–11. Pipeline Simulation Interest Group.

[55] Gokcal, B. (2008). *An experimental and theoretical investigation of slug flow for high oil viscosity in horizontal pipes*. PhD thesis, University of Tulsa.

[56] Gokcal, B., Wang, Q., Zhang, H.-Q., Sarica, C., and Others (2008). Effects of high oil viscosity on oil/gas flow behavior in horizontal pipes. *SPE Projects, Facilities & Construction*, 3(02):1–11.

[57] Greenpeace (2012). Impactos ambientales del petróleo. accessed: 29 August 2018. https://storage.googleapis.com/planet4-mexico-stateless/2018/11/cd1362c6-cd1362c6-impactos_ambientales_petroleo.pdf.

[58] Gregory, G. A. and Scott, D. S. (1969). Correlation of liquid slug velocity and frequency in horizontal cocurrent gas-liquid slug flow. *AIChE Journal*, 15(6):933–935.

[59] Grewal, M. S. and Andrews, A. P. (2002). *Kalman Filtering*. John Wiley & Sons, Inc., New York, USA.

[60] Guzmán Vázquez, J. E. (2009). *Análisis de un flujo bifásico con tapones hidrodinámicos largos en un sistema de producción costa-afuera*. PhD thesis, Universidad Nacional Autónoma de México.

[61] Heagy, J. F., Platt, N., and Hammel, S. M. (1994). Characterization of on-off intermittency. *Physical Review E*, 49(2):1140.

[62] Henrie, M., Carpenter, P., and Nicholas, R. E. (2016). *Pipeline leak detection handbook*. Gulf Professional Publishing, Chennai, India.

[63] Herm Stapelberg, H. and Mewes, D. (1994). The pressure loss and slug frequency of liquid-liquid-gas slug flow in horizontal pipes. *International Journal of Multiphase Flow*, 20(2):285–303.

[64] Hernandez, J., Montiel, J. C., Palacio-Pérez, A., Rodríguez-Valdés, A., and Guzmán, J. E. V. (2018). Horizontal Evolution of Intermittent Gas-Liquid Flows With Highly Viscous Phases. *Multiphase Flow: Theory and Applications*, 6(1):152 – 161.

[65] Hernández, J., Galaviz, D. F., Torres, L., Palacio-Pérez, A., Rodríguez-Valdés, A., and Guzmán, J. E. V. (2019). Evolution of high-viscosity gas–liquid flows as viewed through a detrended fluctuation characterization. *Processes*, 7(11):1–16.

[66] Hord, J. (1967). *Correlations for predicting leakage through closed valves*, volume 355. US National Bureau of Standards: for sale by the Supt. of Docs., US Govt. Print. Off.

[67] Huang, S.-C., Lin, W.-W., Tsai, M.-T., and Chen, M.-H. (2007). Fiber optic in-line distributed sensor for detection and localization of the pipeline leaks. *Sensors and Actuators A: Physical*, 135(2):570–579.

[68] Ibarra, R., Zadrazil, I., Matar, O. K., and Markides, C. N. (2018). Dynamics of liquid–liquid flows in horizontal pipes using simultaneous two–line planar laser–induced fluorescence and particle velocimetry. *International Journal of Multiphase Flow*, 101:47–63.

[69] Ibarra, T. P. and EL-TIEMPO (2018). En Colombia se han derramado 3,7 millones de barriles de crudo. accessed: 29 August 2018. https://www.eltiempo.com/vida/medio-ambiente/cifras-de-derrames-de-crudo-en-colombia-en-los-ultimos-anos-207664.

[70] Institute, P. M. (2017). *A Guide to the Project Management Body of Knowledge (PMBOK® Guide)-Sixth Edition*.

[71] Isermann, R. (1982). Process fault detection based on modeling and estimation methods. *IFAC Proceedings Volumes*, 15(4):7–30.

[72] Isermann, R. and Münchhof, M. (2010). *Identification of Dynamic Systems: An Introduction with Applications*. Springer-Verlag Berlin Heidelberg.

[73] Islam, M. R. and Chaudhry, M. H. (1998). Modeling of Constituent Transport in Unsteady Flows in Pipe Networks. *Journal of Hydraulic Engineering*, 124(11):1115–1124.

[74] J. S. Lead, J. Herd, L. Marcus, E. Terrell, A. W. y. J. S. (2017). The Oil & Gas Industry Transportation & Storage. accessed: 29 August 2018. http://www.loc.gov/rr/business/BERA/issue5/transportation.html.

[75] Jelali, M. and Kroll, A. (2006). *Hydraulic Servo-systems: Modelling, Identification and Control*. Springer-Verlag London Surrey.

[76] Jewett, S. C., Dean, T. A., Woodin, B. R., Hoberg, M. K., and Stegeman, J. J. (2002). Exposure to hydrocarbons 10 years after the Exxon Valdez oil spill: Evidence from cytochrome P4501A expression and biliary FACs in nearshore demersal fishes. *Marine Environmental Research*, 54(1):21–48.

[77] Jiang, B. and Braatz, R. D. (2017). Fault detection of process correlation structure using canonical variate analysis-based correlation features. *Journal of Process Control*, 58:131–138.

[78] Jiménez, J., Torres, L., Verde, C., and Sanjuán, M. (2017). Friction estimation of pipelines with extractions by using state observers. *IFAC-PapersOnLine*, 50(1):5361–5366.

[79] Jimenez-Cabas, J. (2018). *Liquid Transport Pipeline Monitoring Architecture Based on State Estimators for Leak Detection and Location*. PhD thesis, Universidad del Norte.

[80] Jiménez-Cabas, J., Romero-Fandiño, E., Torres, L., Sanjuan, M., and López-Estrada, F. R. (2018). Localization of Leaks in Water Distribution Networks using Flow Readings. *IFAC-PapersOnLine*, 51(24):922–928.

[81] Jimenez Cabas, J. and Ruiz Ariza, J. D. (2018). Modeling and simulation of a pipeline transportation process. *Journal of Engineering and Applied Sciences*, 13(9):2614 – 2621.

[82] Jiménez-Cabas, J., Torres, L., López-Estrada, F. R., and Sanjuan, M. (2017). Leak diagnosis in pipelines by only using flow measurements. In *2017 IEEE 3rd Colombian Conference on Automatic Control (CCAC)*, pages 1–6. IEEE.

[83] Kalman, R. E. et al. (1960). A new approach to linear filtering and prediction problems. *Journal of basic Engineering*, 82(1):35–45.

[84] Kam, S. I. (2010). Mechanistic modeling of pipeline leak detection at fixed inlet rate. *Journal of Petroleum Science and Engineering*, 70(3-4):145–156.

[85] Kim, T.-W., Al-Safran, E., Pereyra, E., and Sarica, C. (2020). Experimental study using advanced diagnostics to investigate slug aeration and bubble behavior in high liquid viscosity horizontal slug flow. *Journal of Petroleum Science and Engineering*, 191:107–202.

[86] Kowalczuk, Z. and Tatara, M. (2017). Numerical issues and approximated models for the diagnosis of transmission pipelines. In *Modeling and Monitoring of Pipelines and Networks*, pages 39–62. Springer International Publishing AG, Switzerland.

[87] Kurmer, J. P., Kingsley, S. A., Laudo, J. S., and Krak, S. J. (1992). Distributed fiber optic acoustic sensor for leak detection. In *Distributed and Multiplexed Fiber Optic Sensors*, pages 117–128. International Society for Optics and Photonics.

[88] Lauritzen, S. L. (1981). Time Series Analysis in 1880: A Discussion of Contributions Made by T.N. Thiele. *International Statistical Review / Revue Internationale de Statistique*, 49(3):319.

[89] Li, W., Pots, B., Brown, B., Kee, K., and Nesic, S. (2016). A direct measurement of wall shear stress in multiphase flow - is it an important parameter in co2 corrosion of carbon steel pipelines. *Corrosion Science*, 110(1):35–45.

[90] Liejin, G., Bofeng, B., Liang, Z., Xin, W., and Hanyang, G. (2009). Online recognition of the multiphase flow regime and study of slug flow in pipeline. In *Journal of Physics: Conference Series*, volume 147, page 12047. IOP Publishing.

[91] Lin, P. Y. and Hanratty, T. J. (1987). Detection of slug flow from pressure measurements. *International Journal of Multiphase Flow*, 13(1):13–21.

[92] Lindley, D. V. (2004). Thiele: pioneer in statistics, by Steffen L. Lauritzen. Pp. 264. £65. 2002. ISBN 0 19 850972 3 (hbk) (Oxford University Press). *The Mathematical Gazette*, 88(512):382–383.

[93] Lion, J. C. P. (1995). Leak Detection: A Transient Flow Simulation Approach. In *Pipeline Engineering AME Petroleum Division Publication PD V60, 1994 Proceedings of the Energy Source Technology Conference*.

[94] Liu, H. (2003). *Pipeline Engineering*. CRC Press, Florida.

[95] Ljung, L. (1979). Asymptotic behavior of the extended Kalman filter as a parameter estimator for linear systems. *IEEE Transactions on Automatic Control*, 24(1):36–50.

[96] Lurie, M. V. (2009). *Modeling of Oil Product and Gas Pipeline Transportation*. WILEY-VCH Verlag GmbH Co. KGaA, Weinheim.

[97] Lv, W., Ou, G., Liu, X., and Gong, C. (2020). Experimental and numerical studies on the corrosion properties of aisi 316l stainless steeel in two-phase upward slug flows. *Engineering Applications of Computational Fluid Mechanics*, 14(1):897–909.

[98] Manolis, I. G., Mendes-Tatsis, M. A., and Hewitt, G. F. (1995). The effect of pressure on slug frequency in two-phase horizontal flow. In *Multiphase Flow 1995*, pages 347–354. Elsevier.

[99] Martínez-Palou, R., Mosqueira, M., Zapata-Rendón, B., Mar-Juárez, E., Bernal-Huicochea, C., Clavel-López, J. C., and Aburto, J. (2011). Transportation of heavy and extra-heavy crude oil by pipeline: a review. *Journal of Petroleum Science and Engineering*, 1(75):274–282.

[100] Mashford, J., De Silva, D., Marney, D., and Burn, S. (2009). An approach to leak detection in pipe networks using analysis of monitored pressure values by support vector machine. In *Network and System Security, 2009. NSS'09. Third International Conference on*, pages 534–539. IEEE.

[101] Matko, D., Geiger, G., and Gregoritza, W. (2000). Pipeline simulation techniques. *Mathematics and Computers in Simulation*, 52(3-4):211–230.

[102] McIntyre, A. D. (1978). Marine ecology and oil pollution. *Journal of Animal Ecology*, 47(3):1018–1018.

[103] Meyer, R., Attanasi, E. D., and Freeman, P. (2007). Heavy oil and natural bitumen resources in geological basins of the world. *US Geological Survey*, 1(1):1–42.

[104] Miesner, T. O. and Leffler, W. L. (2006). *Oil & Gas Pipelines in Nontechnical Language*. PennWell Corporation, Tulsa.

[105] Molina-Espinosa, L., Aguilar-Madera, C. G., Herrera-Hernández, E. C., and Verde, C. (2017). Numerical modeling of pseudo-homogeneous fluid flow in a pipe with leaks. *Computers and Mathematics with Applications*, 74(1):64–73.

[106] Mota, C. J., Pinto, B. P., and De Lima, A. L. (2017). *Glycerol: A Versatile Renewable Feedstock for the Chemical Industry*. Springer International Publishing AG, Cham.

[107] Muntakim, A. H., Dhar, A. S., and Dey, R. (2017). Interpretation of acoustic field data for leak detection in ductile iron and copper water-distribution pipes. *Journal of Pipeline Systems Engineering and Practice*, 8(3):05017001.

[108] Nault, J. D. and Karney, B. W. (2016). Improved Rigid Water Column Formulation for Simulating Slow Transients and Controlled Operations. *Journal of Hydraulic Engineering*, 142(9):04016025.

[109] Newman, N. (2015). New integrity solutions facing many same old problems. *Pipeline & Gas Journal*, 242(10).

[110] Niklès, M., Vogel, B. H., Briffod, F., Grosswig, S., Sauser, F., Luebbecke, S., Bals, A., and Pfeiffer, T. (2004). Leakage detection using fiber optics distributed temperature monitoring. In *Smart Structures and Materials*, pages 18–25. International Society for Optics and Photonics.

[111] Noguera, J. F., Torres, L., Verde, C., Guzman, E., and Sanjuan, M. (2019). Model for the flow of a water-glycerol mixture in horizontal pipelines. In *Conference on Control and Fault-Tolerant Systems, SysTol*.

[112] Noguera-Polania, J. F., Hernández-García, J., Gálaviz-López, D. F., Torres, L., Guzmán, J. E. V., Sanjuán-Mejía, M. E., and Jiménez-Cabas, J. (2020). Dataset on water-glycerol flow in a horizontal pipeline with and without leaks. *Data in Brief*, page 105950.

[113] Noguera Polania, J. F., Robles Algarín, C., and Guillot Fula, J. (2015). Control predictivo-cooperativo para operar una red de bombas centrífugas en un sistema serial de poliductos. *Ingeniare. Revista chilena de ingeniería*, 23(1):38–49.

[114] Pedersen, S., Durdevic, P., and Yang, Z. (2017). Challenges in slug modeling and control for offshore oil and gas productions: A review study. *International Journal of Multiphase Flow*, 88:270 – 284.

[115] Pereira Pérez, Z. (2011). Los diseños de método mixto en la investigación en educación: Una experiencia concreta. *Revista Electrónica Educare*, xv(1):15–29.

[116] Platt, N., Spiegel, E. A., and Tresser, C. (1993). On-off intermittency: A mechanism for bursting. *Physical Review Letters*, 70(3):279.

[117] Plitt, L. (2010). ¿Cuál es el verdadero impacto de un derrame de petróleo? accessed: 29 August 2018. https://www.bbc.com/mundo/internacional/2010/04/100428_derrame_petroleo_claves_lp.shtml.

[118] Portnoy, I., Melendez, K., Pinzon, H., and Sanjuan, M. (2016). An improved weighted recursive pca algorithm for adaptive fault detection. *Control Engineering Practice*, 50:69–83.

[119] Publicaciones SEMANA S.A. (2020). Ecopetrol, entre las mejores del mundo. accessed: 7 January 2021. https://www.dinero.com/empresas/articulo/ecopetrol-entre-mejores-del-mundo/162635.

[120] Rahmati, M., Yazdizadeh, H., and Yazdizadeh, A. (2017a). Leakage detection in a gas pipeline using artificial neural networks based on wireless sensor network and Internet of Things. In *Proceedings - 2017 IEEE 15th International Conference on Industrial Informatics, INDIN 2017*.

[121] Rahmati, M., Yazdizadeh, H., and Yazdizadeh, A. (2017b). Leakage detection in a gas pipeline using artificial neural networks based on wireless sensor network and Internet of Things. In *Proceedings - 2017 IEEE 15th International Conference on Industrial Informatics, INDIN 2017*.

[122] Raymond, D. M. (2017). Twisted leak detection cable. US Patent 9,755,389.

[123] Santos-Ruiz, I., Bermúdez, J., López-Estrada, F., Puig, V., Torres, L., and Delgado-Aguiñaga, J. (2018). Online leak diagnosis in pipelines using an EKF-based and steady-state mixed approach. *Control Engineering Practice*, 81:55–64.

[124] Sivakumar, P., Sircar, A., Deka, B., Anumegalai, A., Moorthi, P., and Yasvanthrajan, N. (2018). Flow improvers for assured flow of crude oil in midstream pipeline - a review. *Journal of Petroleum Science and Engineering*, 1(164):24–30.

[125] Song, Y. and Grizzle, J. W. (1992). The Extended Kalman Filter as a Local Asymptotic Observer for Nonlinear Discrete-Time Systems. In *1992 American Control Conference*, pages 3365–3369. IEEE.

[126] Sorrel, S., Speirs, J., Bentley, R., Miller, R., and Thompson, E. (2012). Shaping the global oil peak: a review of the evidence on field sizes, reserve growth, decline rates and depletion rates. *Energy*, 1(37):709–724.

[127] Soto-Cortes, G., Pereyra, E., Sarica, C., Rivera-Trejo, F., and Torres, C. (2019). Effects of high oil viscosity on oil-gas upward flow behavior in deviated pipes. *Experimental Thermal and Fluid Science*, 109:109896.

[128] Souza, A., Cruz, S., and Pereira, J. (2000). Leak detection in pipelines through spectral analysis of pressure signals. *Brazilian Journal of Chemical Engineering*, 17(4-7):557–564.

[129] Spirin, V. V., Shlyagin, M. G., Miridonov, S. V., Jimenez, F. J. M., and Gutierrez, R. M. L. (1999). Fiber Bragg grating sensor for petroleum hydrocarbon leak detection. *Optics and Lasers in Engineering*, 32(5):497–503.

[130] Swarz, R. S. (2017). The trans-alaska pipeline system: A systems engineering case study. In *Complex Systems Design & Management*, pages 17–27. Springer, Cham.

[131] Tavares, D. P. S. d. A., Vasconcellos, M. A., de Farias Neto, S. R., and de Lima, A. G. B. (2014). Evaluation of multiphase flow in the presence of leak in oil pipelines: modeling and simulation. In *Defect and Diffusion Forum*, volume 348, pages 64–70. Trans Tech Publ.

[132] Thaker, J. and Banerjee, J. (2006). Influence of intermittent flow sub-patterns on erosion-corrosion in horizontal pipe. *Corrosion Science*, 48(1):2363–2379.

[133] Torres, L. (2011). *Modèles et observateurs pour les systèmes d'écoulement sous pression. Extension aux systèmes chaotiques*. PhD thesis, Université de Grenoble.

[134] Torres, L., Astorga, C. M., Targui, B., and Quintero-Marmol, E. (2004). On-line monitoring and modelling of multivariable nonlinear systems : methanol/ethanol distillation. In *2nd IFAC Symposium on System, Structure and Control*, Oaxaca, Mexico.

[135] Torres, L., Besançon, G., and Georges, D. (2008). A collocation model for water-hammer dynamics with application to leak detection. In *Proceedings of the 47th IEEE Conference on Decision and Control*, Cancun, Mexico.

[136] Torres, L., Besançon, G., and Georges, D. (2009a). Collocation modeling with experimental validation for pipeline dynamics and application to transient data estimations. In *European Control Conference*, Budapest, Hungary.

[137] Torres, L., Besançon, G., and Georges, D. (2009b). Multi-leak estimator for pipelines based on an orthogonal collocation model. In *Proceedings of the 48th IEEE Conference on Decision and Control*, Shanghai, China.

[138] Torres, L., Jiménez-Cabas, J., González, O., Molina, L., and López-Estrada, F.-R. (2020). Kalman Filters for Leak Diagnosis in Pipelines: Brief History and Future Research. *Journal of Marine Science and Engineering*, 8(3):173.

[139] Torres, L., Verde, C., and Rojas, J. (2019). Minimal-order observers for locating leaks in a pipeline with a branch. In *IFAC-PapersOnLine*.

[140] Trallero, J. L., Sarica, C., and Brill, J. P. (1997). A study of oil/water flow patterns in horizontal pipes. *SPE Production and Facilities*, 12(3):165–172.

[141] Tubb, R. (2017). P&gj's 2017 worldwide pipeline construction report. *Pipeline & Gas Journal*, 244(1):16–20.

[142] U.S. Department of Health and Human Services (2016). Resúmenes de Salud Pública - Hidrocarburos aromáticos policíclicos (HAP) [Polycyclic Aromatic Hydrocarbons (PAH)]. accessed: 4 September 2018. https://www.atsdr.cdc.gov/es/phs/es_phs69.html.

[143] U.S. Department of Transportation Pipeline and Hazardous Materials Safety Administration (PHMSA) (2012). Final Report: Leak Detection Study. accessed: 4 September 2018. https://www.phmsa.dot.gov/sites/phmsa.dot.gov/files/docs/technical-resources/pipeline/16691/leak-detection-study.pdf.

[144] U.S. Department of Transportation Pipeline and Hazardous Materials Safety Administration (PHMSA) (2021). Serious Pipeline Incidents Report. accessed: 4 September 2018. https://hip.phmsa.dot.gov/analyticsSOAP/saw.dll?Portalpages.

[145] Valle, A. (2000). *Three phase gas-oil-water pipe flow*. PhD thesis, Imperial College London (University of London).

[146] Vanaei, H., Eslami, A., and Egbewande, A. (2017). A review on pipeline corrosion, in-line inspection (ili), and corrosion growth rate models. *International Journal of Pressure Vessels and Piping*, 149:43–54.

[147] Velásquez Arias, J. A. (2017). Contaminación de suelos y aguas por hidrocarburos en Colombia. Análisis de la fitorremediación como estrategia biotecnológica de recuperación. *Revista de Investigación Agraria y Ambiental*, 8(1):151 – 167.

[148] Verde, C., Molina, L., and Torres, L. (2014). Parameterized transient model of a pipeline for multiple leaks location. *Journal of Loss Prevention in the Process Industries*, 29:177–185.

[149] Verde, C., Torres, L., and González, O. (2016). Decentralized scheme for leaks' location in a branched pipeline. *Journal of Loss Prevention in the Process Industries*, 43:18–28.

[150] Villarreal, J., Laverde, D., and Fuentes, C. (2006). Carbon-steel corrosion in multiphase slug flow and co2. *Corrosion Science*, 48(1):2363–2379.

[151] Volk, A. and Kähler, C. J. (2018). Density model for aqueous glycerol solutions. *Experiments in Fluids*, 59(5):1–4.

[152] Wambsganss, M. W., Jendrzejczyk, J. A., and France, D. M. (1994). Determination and characteristics of the transition to two-phase slug flow in small horizontal channels. *ASME. Journal of Fluids Engineering*, 116(1):140–146.

[153] Wang, S. and Shoji, M. (2002). Fluctuation characteristics of two-phase flow splitting at a vertical impacting T-junction. *International journal of multiphase flow*, 28(12):2007–2016.

[154] Wang, Y., Liu, Z., Chang, Y., Zhao, X., and Guo, L. (2019). Experimental study of gas-liquid two-phase wavy stratified flow in horizontal pipe at high pressure. *International Journal of Heat and Mass Transfer*, 143:118537.

[155] Wendt, J. F., Anderson, J. D., Degroote, J., Degrez, G., Dick, E., Grundmann, R., and Vierendeels, J. (2009). *Computational Fluid Dynamics*. Springer Berlin Heidelberg, Berlin, Heidelberg.

[156] Wood, M., Vetere Arellano, A., and Van Wijk, L. (2013). Corrosion related accidents in petroleum refineries. *JRC Scientific and Policy Reports*, 1(1):1–100.

[157] Wu, B., Firouzi, M., Mitchell, T., Rufford, T. E., Leonardi, C., and Towler, B. (2017). A critical review of flow maps for gas-liquid flows in vertical pipes and annuli. *Chemical Engineering Journal*, 326:350 – 377.

[158] Wylie, E. B. and Streeter, V. L. (1993). Fluid Transients in Systems. *PrenticeHall Upper Saddle River NJ*.

[159] Xu, S., Ma, Q., Yang, X.-F., and Wang, S.-D. (2017). Design and fabrication of a flexible woven smart fabric based highly sensitive sensor for conductive liquid leakage detection. *RSC Advances*, 7(65):41117–41126.

[160] Yang, Z. (2014). A study of viscous oil and water pipe flow. In *BHR Group - 9th North American Conference on Multiphase Technology 2014*.

[161] Yusuf, N., Al-Wahaibi, Y., Al-Wahaibi, T., Al-Ajmi, A., Olawale, A., and Mohammed, I. (2012). Effect of oil viscosity on the flow structure and pressure gradient in horizontal oil–water flow. *Chemical Engineering Research and Design*, 90(8):1019–1030.

[162] Zhang, H., Sarica, C., and Pereyra, E. (2012). Review of high-viscosity oil multiphase pipe flow. *Energy and Fuels*, 1(26):3979–3985.

[163] Zheng, D., Che, D., and Liu, Y. (2008). Experimental investigation on gas-liquid two-phase slug flow enhanced carbon dioxide corrosion in vertical upward pipeline. *Corrosion Science*, 50(1):3005–3020.